

DISS. ETH NO. 26876

**ADVANCED BIOFABRICATION METHODS FOR  
CARTILAGE TISSUE ENGINEERING**

A thesis submitted to attain the degree of  
DOCTOR OF SCIENCES of ETH ZURICH  
(Dr. sc. ETH Zurich)

presented by  
BENJAMIN KESSEL

M.Sc. in Molecular Bioengineering,  
Technische Universität Dresden

born on 28.06.1988  
citizen of Germany

accepted on the recommendation of

Prof. Dr. Marcy Zenobi-Wong

Dr. Martin Ehrbar

Dr. Steffen Zeisberger

2020



## Abstract

The aim of this thesis was to develop and utilize novel approaches for biofabrication of cartilage tissue. Until now, tissue engineering could not provide a potent and effective strategy to create *de novo* cartilage tissue for regenerative medicine. The presented work is targeted towards advancing the methods of biofabrication, in an attempt to ultimately let this vision become true. On the search for a successful solution for cartilage tissue engineering, diverse approaches were pursued. A clinically translatable bioink, formulated from a range of minimally modified natural polymers, was developed and used for extrusion 3D bioprinting. Bioprinted constructs were characterized regarding their chondrogenic maturation *in vitro* and *in vivo*. Additionally, methods were devised to evaluate the clinical relevance of this bioink as well as bioprinted constructs in general. In a second study, a new and facile fabrication method using elongated, micron sized hydrogels was developed. Bulk hydrogels were mechanically deconstructed into a new microgel material named “entangled microstrands”. This simple but powerful strategy is applicable to a wide range of hydrogels. The resulting, microporous material excels as bioink and can be 3D bioprinted into biological relevant shapes. Biocompatibility is outstanding and microstrands can be flow-aligned to direct orientation and development of embedded cells. In a third study, a novel biofabrication method for weakly crosslinked gels, non-annealed microgels and fluid materials was devised. By utilizing a sacrificial hydrogel mold and semi-permeable hydrogel shell, it was possible to confine cell-laden infill materials within a custom shape. Highly viscous polymer solutions and commercially available tissue fillers were, for the first time, successfully cultured *in vitro* and screened for their chondrogenic potential. In conclusion, advanced biofabrication strategies were conceptualized and implemented. These methods have relevance for an extensive range of materials and are sophisticated, but not unnecessary complicated. This has far-reaching significance, as entangled microstrands and semi-permeable hydrogel shells

can be deployed as a platform to tackle the problems and challenges in today's tissue engineering. Their accessibility will give the biofabrication community tools to employ and utilize traditional, as well as novel materials in an exciting, new setup.



## Kurzfassung

Die Zielsetzung dieser Arbeit war die Entwicklung und Anwendung neuer Strategien für die Biofabrikation von Knorpelgewebe. Bis heute konnte mit Hilfe von Tissue Engineering (*engl.* für Gewebekonstruktion) noch kein effektiver und wirksamer Ansatz gefunden werden, um *de novo* Knorpelgewebe für den Einsatz in der regenerativen Medizin zu erzeugen. Die vorgestellte Arbeit beabsichtigt dabei verschiedene Verfahren im Feld der Biofabrikation voranzubringen, damit das immense theoretische Potenzial dieses Gebietes zukünftig auch praktisch voll ausgeschöpft werden kann. Auf der Suche nach einem erfolgreichen Konzept für das Tissue Engineering von Knorpel wurden hierbei unterschiedliche Strategien verfolgt. Zunächst wurde für den klinischen Einsatz geeigneter Bioink (*engl.* Biotinte), zusammengesetzt aus mehreren minimal modifizierten, natürlichen Polymeren, entwickelt und mit einem Bioprinter (*engl.* Biodrucker) extrudiert. Die auf diese Art hergestellten Proben wurden auf ihr Entwicklungspotenzial hin zu Knorpelgewebe untersucht und bewertet. Zusätzlich wurden Methoden entworfen, um die klinische Relevanz von Bioinks als auch generell von Arbeitsstücken aus dem Bioprinter zu evaluieren. In einer zweiten Studie wurde eine neue und einfache Biofabrikationsmethode auf Basis von länglichen, mikrometergroßen Hydrogelen entwickelt. Dafür wurde ein Hydrogel-Block mechanisch in einzelne Mikrogele zerlegt, um ein Hydrogel Material von „verwobenen Mikrosträngen“ zu erzeugen. Diese einfache, aber wirkungsvolle Methode ist auf eine umfangreiche Auswahl von Hydrogelen anwendbar. Das daraus resultierende, mikroporöse Material eignet sich hervorragend als Bioink and konnte unter Verwendung eines Bioprinters in biologisch relevante Formen (z.B. in der Form eines menschlichen Ohres) gedruckt werden. Die Biokompatibilität erwies sich dabei als ausgezeichnet. Da sich die einzelnen Mikrostränge des Materials beim Extrudieren an der Fließrichtung ausrichten, kann die Orientierung von eingebetteten Zellen entsprechend

gesteuert werden. In einer dritten Studie wurde eine neue Biofabrikationsmethode für schwach vernetzte Gele, nicht stabilisierte Mikrogele und flüssige Materialien entwickelt. Durch den Einsatz einer Hydrogel-Gussform und einer semipermeablen Hydrogelhülle, war es möglich mit Zellen beladenes Füllmaterial in einer frei wählbaren Form einzugrenzen. Hochviskose Polymerlösungen und kommerziell verfügbare Substanzen zur Faltenunterspritzung (sogenannte Dermalfiller) wurden erfolgreich *in vitro* kultiviert und auf ihr Transformationspotenzial zu Knorpelgewebe hin untersucht. Zusammenfassend lässt sich sagen, dass in dieser Arbeit fortgeschrittene Möglichkeiten der Biofabrikation konzipiert und praktisch etabliert werden konnten. Die vorgestellten Verfahren sind auf ein breites Spektrum von Ausgangsmaterialien anwendbar und dabei zur gleichen Zeit hochentwickelt, aber nicht unnötig kompliziert. Hieraus ergibt sich eine weitreichende Bedeutung für die vorgestellten Methoden. Verwobene Mikrostränge und semipermeable Hydrogelhüllen können zukünftig als Plattform eingesetzt werden, um Lösungen für die Probleme und Herausforderungen im Tissue Engineering zu finden. Da diese Methoden leicht zugänglich sind, können sie Wissenschaftlern als Hilfsmittel dienen, Materialien für die Biofabrikation auf eine ganze neue Art zu nutzen und der modernen Medizin zur Verfügung zu stellen.

---

# Table of Contents

<b>Abstract</b> .....	<b>i</b>
<b>Kurzfassung</b> .....	<b>iii</b>
<b>Table of Contents</b> .....	<b>v</b>
<b>Chapter I - Introduction</b> .....	<b>1</b>
1.1 Tissue Engineering .....	3
1.2 Cells for Tissue Engineering .....	4
1.3 Cartilage Tissue Engineering .....	6
1.4 The Rise of Biofabrication.....	8
1.5 Materials in Tissue Engineering.....	12
1.6 Evolution of Hydrogels.....	12
1.7 Microgels – a Next Step? .....	15
1.8 Tissue Engineering Liquids.....	19
<b>Scope of the Thesis</b> .....	<b>21</b>
<b>Chapter II - Clinically Relevant Bioinks for Cartilage Tissue Engineering</b> .....	<b>25</b>
Abstract.....	26
2.1 Introduction .....	27
2.2 Materials and Methods.....	31
2.3 Results.....	37
2.4 Discussion.....	49
2.5 Acknowledgments .....	53
2.6 Supporting Information.....	54

<b>Chapter III - 3D Bioprinting of Macroporous Materials Based on Entangled Hydrogel Microstrands .....</b>	<b>59</b>
Abstract.....	60
3.1 Introduction .....	61
3.2 Materials and Methods .....	65
3.3 Results .....	74
3.4 Discussion .....	85
3.5 Acknowledgments.....	88
3.6 Supporting Information.....	89
<b>Chapter IV - Shape Defining, semi-permeable Hydrogel Shells as Culture Chambers for Tissue Engineering.....</b>	<b>93</b>
Abstract.....	94
4.1 Introduction .....	95
4.2 Materials and Methods .....	98
4.3 Results .....	104
4.4 Discussion .....	113
4.5 Supporting Information.....	116
<b>Chapter V - Conclusions and Outlook.....</b>	<b>119</b>
5.1 Keep it simple .....	123
5.2 Polymer Concentrations.....	124
5.3 Architected Hydrogels .....	126
<b>Appendix .....</b>	<b>129</b>
Cell-compatible Surface Modification.....	130

<b>Oxygen Tolerant and Cytocompatible Iron(0)-Mediated ATRP Enables the Controlled Growth of Polymer Brushes from Mammalian Cell Cultures .....</b>	<b>133</b>
Abstract.....	134
6.2 Introduction.....	135
6.3 Results and Discussion .....	137
6.4 Conclusions .....	148
<b>Bibliography .....</b>	<b>149</b>
<b>Acknowledgments.....</b>	<b>167</b>
<b>Curriculum Vitae .....</b>	<b>173</b>



# **Chapter I - Introduction**

The human body can recover from deep wounds and regenerate broken bones and torn skin. Still, possibilities are limited and not every damage can be healed. Biological recovery from severe trauma is possible though, as several examples from the animal kingdom prove. One of the most prominent, the axolotl *Ambystoma mexicanum* can heal without scarring and possesses the power to fully regenerate lost limbs (**Figure 1.1**)<sup>[1-2]</sup>. It can even integrate organs transplanted from other individuals to restore full function<sup>[3]</sup>. Though humanity might never reach complete control over these biological processes to exploit such potent regeneration capabilities, tissue engineering as a scientific field aims at providing solutions when healing and regeneration of tissue reaches its limit.

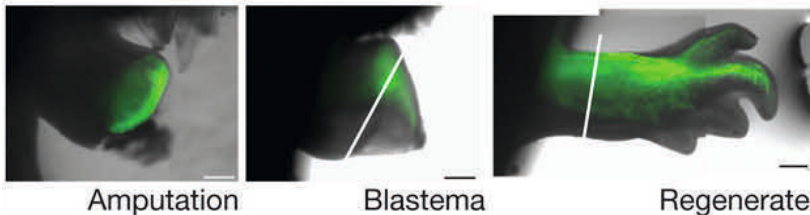


**Figure 1.1** Amputated limbs of the axolotl show full regeneration. Adapted from M. Kragl, D. Knapp, E. Nacu, S. Khattak, M. Maden, H. H. Epperlein, E. M. Tanaka, *Nature* **2009**, 460, 60, © (2009), with permission from Springer Nature.

Medical sciences have long been trying to engineer tissue to transplant into the human body and as a second mission, to create realistic models for development of therapeutics. The challenges that come with this task, however, are tremendous. Even though the last two decades of research deepened our knowledge and helped improve patient's life, traditional cell-culture and biofabrication techniques did not live up to the vision of enabling us to create readily available laboratory grown tissue replacements<sup>[4-5]</sup>. This chapter will introduce the concept of tissue engineering and illustrate the relevance for advanced tissue engineering strategies using the specific example of cartilage tissue. Developments in methodology as well as availability of materials, with a focus on microgel based approaches will be elucidated.



Finally, a novel idea for a tissue engineering approach for liquids and extremely weak or unstable hydrogel materials will be illustrated.

## 1.1 Tissue Engineering

A broadly accepted definition of tissue engineering describes it as “an interdisciplinary field that applies the principles of engineering and life sciences to the development of biological substitutes that restore, maintain, or improve tissue function or a whole organ”<sup>[6]</sup>. Severe damage to tissues through trauma, often referred to critical size defects or congenital disorders are often beyond the body’s own capabilities for repair. In such cases, tissue engineering, as a branch of regenerative medicine, attempts to restore or establish normal function<sup>[7]</sup>. General strategies pursued are: acellular scaffolds, cells only and cellularized matrices<sup>[8-9]</sup>.

Acellular scaffolds are meant to stimulate and guide the body’s natural repair mechanism. Matrices are usually slowly degraded over time and replaced by extracellular matrix (ECM) and regenerated tissue<sup>[10]</sup>. Cell integration is solely achieved by migration of cells from the nearby tissue, which can be achieved with or without integrated bioactive cue molecules<sup>[11-12]</sup>. A steady refinement in the design of scaffolds happened over the last decades. Initially, designs could be described as sponges that did merely replicate the defect shape, but since have evolved into highly sophisticated materials<sup>[13]</sup>. Porosity of these scaffolds is crucial as cell-infiltration and subsequently nutrient and gas-exchange must be ensured. Different methods such as gas-foaming or freeze drying enabled the creation of highly porous scaffolds<sup>[14-15]</sup>. Tuning of pore size and void fraction also plays a critical role in cellular development and maturation inside a tissue graft<sup>[16-17]</sup>. Besides control over microstructural, chemical and mechanical properties a trend emerged towards presentation of bioactive molecules to directly interact with the cellular processes<sup>[13, 18-19]</sup>. Initial attempts to administer growth factors or cytokines in unbound form or directly bound to the scaffold resulted in nonphysiological responses<sup>[13, 20]</sup>. More advanced designs use spatiotemporal

patterning of drug carriers and natural binding motifs to create gradients that better replicate physiological processes <sup>[19, 21]</sup>. However, acellular scaffolds do not possess any actively regenerating component (cells), and after all, rely on the body's own ability to transform implanted scaffolds into functional tissue. There also lies the limit of acellular approaches. Since the potential and speed of regeneration declines with age, acellular approaches, which only support and guide the inherent regeneration potential decline in their power as well <sup>[22-23]</sup>. Further restrictions apply for tissues with limited capabilities for self-repair or full organ failures. Advanced concepts of acellular scaffolds envision programmable materials that precisely replicate the spatiotemporal cellular cues and signals that are displayed during tissue regeneration or creation <sup>[13]</sup>. However, such tight control over chemical, physical and structural architecture of a scaffold still has to be demonstrated.

Cell-derived constructs or cellularized scaffolds can be deployed to administer an active, biological component to regenerate damaged or lost tissue. To obtain cells for tissue engineering, a piece of donor tissue is harvested and processed to isolate individual cells that can be further processed. Cells are combined with a support material, often similar or identical to that used for acellular scaffolds, and cultured *in vitro* to start tissue formation before implantation into the host <sup>[24]</sup>.

## 1.2 Cells for Tissue Engineering

Finding an appropriate cell source is critical for successful tissue engineered constructs. Similar to organ transplants, the immune system responds and attacks 'foreign' cells, which reduces the effectiveness of cells received from a different species (xenogenic) or when cells originate from different individual from the same species (allogenic) <sup>[25]</sup>. Cells, derived from host tissue (autologous) are considered superior in terms of compatibility, but come with other drawbacks. Autologous cell numbers isolated from a biopsy are often insufficient for proper cellularization of engineered matrices and expansion

of cells is necessary. However, many cell types only show limited growth, or can lose their phenotype during expansion <sup>[26-28]</sup>. Further, differences between hosts and their specific cell populations can impact the effectiveness of tissue engineered constructs. An engineered tissue with autologous cells from a young host can be significantly more effective than a similar tissue, engineered with autologous cells of an old host <sup>[29-32]</sup>. To overcome this high variance, stem-cell derived tissue engineered products has attracted a lot of attention in recent years <sup>[33-34]</sup>. Stem-cells possess the power to proliferate in a nearly unlimited manner and differentiate into a wide range of specific cell types. This makes them a strong candidate for better cell-laden matrices for regenerative medicine <sup>[35]</sup>.

Harvesting stem cells comes with its own set of problems to overcome <sup>[35]</sup>. Embryonic stem cells can be derived from the inner cell mass of a blastocyst, but the isolation raises ethical issues <sup>[36]</sup>. Induced pluripotent stem cells (iPS), however, can be generated from somatic cells. iPS hold the promise to be an unlimited cell source that can propagate into any other cell type, even when this specific cell type lost its potential to fulfill its function due to trauma, disease or mutational load. Major regulatory concerns, mainly regarding tumorigenicity of iPS dampened the progress in this field <sup>[37]</sup>. An alternative to pluripotent stem cells for tissue engineering are a less potent, stem-cell derived cell type, called progenitor cells. Compared to stem cells, progenitors have a more limited self-renewal potential. Proliferation, however, is adequate to reach a relevant cell population in culture and to populate engineered scaffolds. Since progenitor cells are already more determined towards a specific cell type, they need to match the desired tissue type. Adult progenitor cells have been isolated from a wide range of tissues including, besides many others, bone marrow, peripheral blood, skeletal muscle and cartilage <sup>[38-41]</sup>. Access to stem cell and progenitor populations provided an important tool for tissue engineering. But, successful applications will need to take a holistic approach, combining suitable materials with potent cells and appropriate fabrication methods <sup>[42]</sup>.

### 1.3 Cartilage Tissue Engineering

Cartilage is a resilient, elastic connective tissue that forms the lubricated, sliding surface inside joints and gives structural support as well as shape to many body components including the ear, rib cage and intervertebral discs. The architecture of the tissue is considered to be relatively simple, with only one specific cell type, chondrocytes, embedded in abundantly deposited extracellular matrix [43-44]. ECM consists mainly of collagens and glycosaminoglycans and no blood vessels or nerves are present, which limits nutrient supply and gas exchange to diffusion mechanisms only [31,43-44]. These characteristics lead to a very slow turnover of cartilage ECM and result in very limited capabilities for self-repair [45-46]. Articular cartilage injuries, though, are widespread, often impair severe restrictions on patients and are expected to even increase in prevalence [47-49].

Traditional methods for treatment of cartilage lesions, like microfracture of the underlying subchondral bone aim at activating and stimulating the body's own regenerative capabilities (**Figure 1.2A**) [50-52]. Commonly, such treatment only results in formation of transient fibrocartilaginous tissue [31, 53]. Alternatively, transplantation of autologous healthy cartilage can be employed, which can be effective short term, but comes with problems due to donor site morbidity and highly questionable long term outcome (**Figure 1.2B**) [31, 54-58]. The poor clinical outcome of conventional treatment options paired with the inability for spontaneous self-repair spotlights cartilage as an ideal candidate for an tissue engineering approach, more specifically for cellular tissue engineered grafts [59].

Production of *de novo* cartilage tissue remains a challenge, though. Simple strategies in which autologous chondrocytes are harvested from a biopsy punch, expanded *in vitro* and re-introduced into the defect raised high expectations of a reliable and effective treatment for cartilage lesions (**Figure 1.2C**). However, this autologous chondrocyte implantations (ACI)

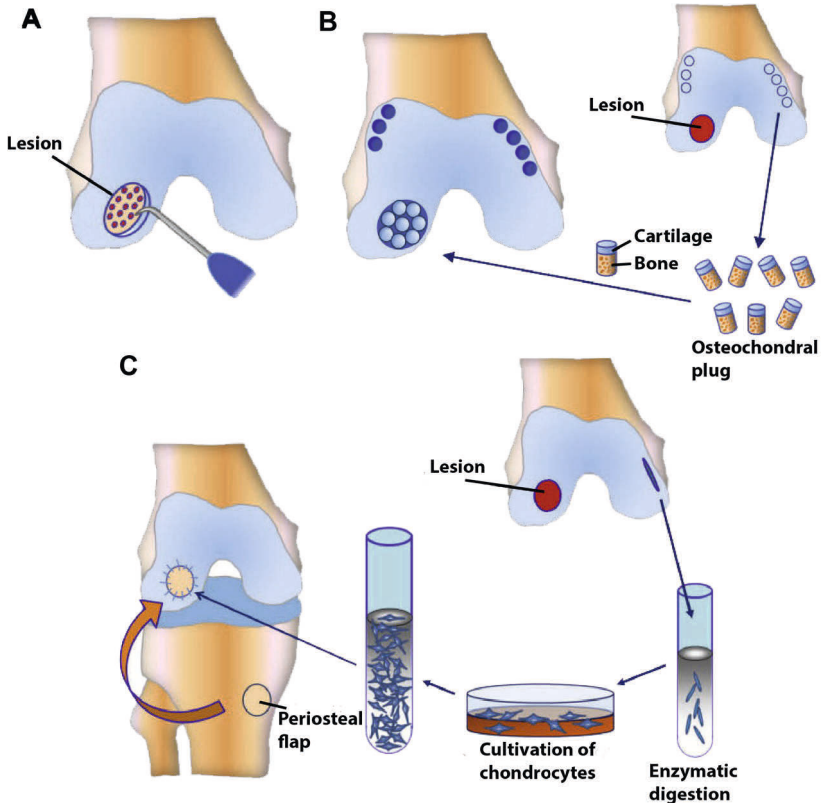


**Figure 1.2** Current treatments for articular cartilage lesions. (A) Microfracture (B) Chondroplasty (C) Autologous chondrocyte implantation. Adapted from E. B. Hunziker, K. Lippuner, M. Keel, N. Shintani, *Osteoarthritis and cartilage* **2015**, 23, 334 © (2015), with permission from Elsevier.

did not perform different from traditional techniques in a long term study<sup>[46, 58]</sup>. An advanced version of this technique, in which a carrier matrix is used to stabilize and fix the expanded chondrocytes in the defect termed MACI was introduced more recently<sup>[60]</sup>. Clinical evaluation report promising results, but more controlled studies are needed to find exact parameters<sup>[61]</sup>. Especially, a consensus on the specific type and composition of the matrix has not been

found yet, since implantation of foreign material can result in inflammation and degradation [31, 46, 62-63]. Advanced tissue engineering strategies are therefore required and developed by the scientific community.

## 1.4 The Rise of Biofabrication

3D printing revolutionized the way we think about manufacturing today. Continuous innovations in the last decades have led to more and more control over the production process. Today, 3D printing has evolved into a powerful tool for manufacturing. For life-science, and tissue engineering in particular, 3D printing turned out to be an ideal method to create personalized scaffolds and improve the spatial control of materials and cells in tissue engineered constructs. First attempts to incorporate additive manufacturing into tissue engineering and medical sciences were undertaken with 3D printed, sacrificial resin molds to create structures from biological materials and production of medical devices such as stents and splints [64-65]. Only with the development of solvent-free and aqueous-based approaches, 3D printing of biological matrices became relevant. Such scaffolds were typically acellular or had cells seeded manually into the scaffold post-fabrication [66]. As a next step, living cells were directly integrated in the manufacturing process. Today, biofabrication is defined as “the automated generation of biologically functional products with structural organization from living cells, bioactive molecules, biomaterials, cell aggregates such as micro-tissues, or hybrid cell-material constructs, through bioprinting or bioassembly and subsequent tissue maturation processes” [67]. Since the requirements for handling living matter are fundamentally different from the processing of plastic, metal or ceramics, substantial adaptations of the technologies were necessary.

Initially, three central strategies for bioprinting and patterning of biological materials emerged: inkjet, laser-induced forward transfer and microextrusion [64, 68]. Like traditional inkjet printers for paper, inkjet bioprinting deposits droplets of a liquid ink onto a build plate. While inkjet bioprinters are cheap,

print fast and have excellent resolution in 2D, control over the third dimension is difficult. Laser-induced forward transfer propels a small droplet of biological matrix from a sacrificial donor slid that gets collected on the build plate <sup>[64]</sup>. This allows precise control of individual droplets, however, such printers are expensive and relatively slow in their printing process, which complicates the production of macro sized constructs <sup>[69]</sup>. The principle of microextrusion bioprinting is closest to popular filament 3D printers found throughout makerspaces all over the world. An extruder filled with bioink is mounted on a dispensing robot and by computer-controlled x-y-z movement, material is deposited on a build plate in a layer-by-layer fashion. To ensure high resolution and stability in such constructs, bioinks need to fulfill a range of mechanical requirements <sup>[70]</sup>. As this material is simultaneously the cell-carrier and the stabilizing matrix after the printing process, suitable bioinks are critical for successful bioprinting.

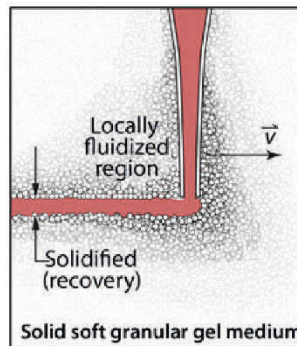


**Figure 1.3** Illustration of suspension bioprinting. Bioink is extruded in a self-healing support hydrogel which has a fluid region around the moving nozzle but solidifies when the nozzle moves away. Adapted from T. Bhattacharjee, S. M. Zehnder, K. G. Rowe, S. Jain, R. M. Nixon, W. G. Sawyer, T. E. Angelini, *Science advances* **2015**, 1, e1500655 under CC BY-NC 4.0.

Further innovation in additive manufacturing lead a new generation of 3D bioprinters. As direct adaption of the simpler forms of additive manufacturing (filament extrusion, spraying) came with many limitations, more sophisticated bioprinting techniques emerged. Fabrication inside a support

bath became one prominent strategy to improve extrusion bioprinting [71-74]. Later termed suspension bioprinting, this method enables the use of low-viscosity bioinks, since extruded material is no longer deposited on a build plate, but inside a suspension media [71]. This suspension media confines the bioink after deposition and prevents flow. A prominent example of such an approach is the freeform reversible embedding of suspended hydrogels (FRESH) [75]. Opposed to conventional microextrusion printing in which the bioink needs to fulfill certain rheological properties to ensure flow during extrusion and stability after deposition, these requirements are overtaken by the support hydrogel (**Figure 1.3**). In the FRESH approach, extruded liquid is confined by micron sized fragments of a gelatin gel. Further development in this approach lead to more controlled support baths based on hydrogel microbeads or fluid gels to increase the resolution [72, 76-78]. As the bioink is confined by a granular support bath, the structure of this support bath is inevitably imprinted into the surface of the printed construct. The increased variability for bioink materials therefore results in reduced control over the surface of bioprinted constructs.

Another idea to remove the high rheological requirements on bioinks is core-shell printing. If the deposited filament is stabilized by an outer shell, the cell-laden hydrogel inside can be maximized for biocompatibility [79]. Such core-shell systems can be split into two categories: in the first, core and shell consist of the same polymer but differ in their crosslinking, while in the second different polymers are used to create core and shell respectively. Co-axial printing of alginate (inner needle) with a crosslinking solution of  $\text{CaCl}_2$  (outer needle) led to stable filaments with a round cross-section [80]. Other applications are already targeted at making this technology accessible to the clinics. A handheld, co-axial extrusion device was developed for *in situ* cartilage repair [79, 81]. The same polymer mix was used for core and shell extrusion, but cells were only embedded in the core, while a photoinitiator was added to the shell to allow crosslinking. Co-axial printing is also highly interesting for channel formation. When the crosslinker is extruded through



the core and the hydrogel precursor solution through the shell, tubular constructs can be created <sup>[82-83]</sup>. In combination with microfluidics, a core-shell bioprinter was developed and demonstrated capable of printing PEG-Fibrinogen fibers, a non-easily processable material for bioprinting <sup>[84]</sup>. Major drawbacks of co-axial bioprinting, however, are the demand for a specific setup, materials and the tight control over these parameters. Since two components need to be extruded in parallel, even slightest changes in material composition, viscosity or extrusion speed can lead to disturbances and problems in the printing process. Deployment of this technology in the field has therefore be rather limited and restricted to specific applications.

Advances in polymer chemistry drew a lot of attention to photo-crosslinked systems. Since UV-exposure is a constant concern for clinical translation, photoinitiators with sensitivity for light in the visible spectrum were developed <sup>[85-87]</sup>. A new generation of photoinitiators with reduced toxicity and sensitivity for biologically less detrimental wavelengths lead to greatly increased cell viabilities <sup>[88-90]</sup>. Together with advanced 3D printing concepts such as stereolithography (SLA) and digital light processing (DLP) this led to a new design of bioprinters <sup>[91]</sup>. In general, this additive manufacturing technique utilizes a photoinitiator and a crosslinkable resin or other fluid, confined in a vat. Selective crosslinking of the bottom layer happens either by a fast-moving focused laser beam (SLA) or by simultaneous illumination of selected pixels of an LCD array (DLP). After a layer is cured, the whole construct is elevated, and a thin layer of fresh resin occupies the space between photonic source and the printed construct to form the next layer. These techniques have improved printing resolution compared to filament extrusion techniques, while still being able to achieve relevant sizes. Adaption to a biological setup is not trivial though, as suitable biological matrices often exhibit viscous behavior in relevant concentrations which complicates manufacture <sup>[92-93]</sup>. Crosslinked polymers need to be rigid enough to keep shape and stability during the printing process. Lastly incorporation of cells is challenging from a logistics point of view, as cells need to be evenly

distributed throughout the fluid reservoir, often requiring a stabilizing agent and huge quantities of cells <sup>[94]</sup>. Only sporadic examples of SLA/DLP bioprinting, thus creation of cell-laden structures, can be found in the literature and more innovations will be needed to master this technique.

## 1.5 Materials in Tissue Engineering

Finding the optimal material for a tissue engineering approach is paramount for the successful maturation of a cell-laden matrix into a functional tissue. Besides the mechanical requirements specific for the different methods of fabrication, an ideal matrix for tissue engineering needs to provide an optimal physiological environment to aid cells in this process. More than half of the weight of a human body comes from water and therefore it comes naturally that hydrated matrices are the preferred choice for many biomedical and tissue engineering applications <sup>[95-98]</sup>. Hydrogels are a polymer-network created by cross-linking individual polymer chains to create a highly water absorbent material <sup>[99-100]</sup>. In a swollen state, they can contain over 90% water without dissolving due to the internal cross-links. Two classes of hydrogels can be distinguished: physical and chemical. Physical hydrogels are held together by reversible bonding through weak interaction such as ionic, H-bonding or molecular entanglement <sup>[96]</sup>. Chemical hydrogels on the other hand, are formed by covalent crosslinks. In recent years a plethora of hydrogel variations have been developed, covering a vast amount of materials as well as crosslinking strategies <sup>[101-103]</sup>. Some of the most impactful classes of hydrogels will be detailed in the following paragraph.

## 1.6 Evolution of Hydrogels

Tight control over crosslinking kinetics of hydrogels is important for biofabrication. Several strategies have been developed and successfully used in tissue engineering to create *in situ* crosslinkable polymers. In temperature sensitive hydrogels, gelation kinetics are governed by weak interactions and allow a sharp transition from fluid precursor liquids to a solid gel structure.

Such hydrogels precursors can be injected into tissues or lesions and ensure good contact with the surrounding tissue before gelation happens <sup>[104-106]</sup>. Promising strategies to create temperature-sensitive hydrogels are based on the use of polyester block copolymers, poly(N-isopropylacrylamide), poly(dimethyl acrylamide) or polyethylene glycol <sup>[105, 107-110]</sup>.

Other means to crosslink hydrogels on demand are based on self-assembly of molecules. In nature, proteins adopt a well-defined, specific 3D structure after their assembly from single amino acids. Facilitation into these structures is encoded in the arrangement of the amino acids and is responsible for the formation of tropocollagen <sup>[111]</sup>. A similar effect has also been exploited to form 3D structures of DNA through what was later named DNA origami <sup>[112]</sup>. This supramolecular assembly has also been employed for building hydrogel networks and has led to a range of novel biomaterials such as bionanotubes <sup>[113-114]</sup>. Other approaches are based on host-guest chemistry, in which highly specific complexes between molecules are formed, often with the beneficial side effect of giving the hydrogel self-healing properties due to <sup>[115-116]</sup>.

With deeper understanding of organic chemistry, even more advanced hydrogels have been developed. Enzyme catalyzed hydrogels became of increasing interest due to their biocompatibility and their tunable gelation kinetics <sup>[117]</sup>. Since enzymatic reaction occur under physiological conditions, biocompatibility is good and toxicity of the crosslinking process is low <sup>[118]</sup>. Stability of enzymes and spatial control over the gelation reaction is limited, however.

Radical polymerization together with means to control radical formation e.g. via a photoinitiator molecule gave rise to a whole subsection of biofabrication methods discussed previously. Nearly any arbitrary polymer can be relatively easy modified to contain methacrylate or acrylate moieties to benefit from radical polymerization <sup>[119]</sup>. This led to a variety of natural polymers being modified with this approach, with prominent examples such as gelatin

methacrylol (GelMA) and hyaluronic acid methacrylate (HA-MA) [120-124]. Formation of hydrogels is fast, with superior temporal and spatial control compared to *in situ* crosslinkable approaches [125]. New possibilities such as patterning and non-uniform crosslinking densities throughout the hydrogel opened up [126]. Two potential drawbacks need to be considered. The dependence on an external source, often UV-light is controversial, as this can increase the mutational load of encapsulated cells. Second, cytotoxicity of photoinitiators has been widely characterized and cyto-compatible levels identified, but the effects on intra-cellular signaling are still poorly understood [127-128].

Composing a hydrogel of more than one component can greatly increase its relevance. One example are double-network hydrogels that have physical as well as chemical crosslinks [129]. Applications are manifold ranging from delivery of biomolecules to interpenetrating networks with extreme mechanical properties [130-131]. It is also possible to combine natural and synthetic polymers to benefit from the ease of use of synthetic as well as the biocompatibility of natural polymers [132]. Composite hydrogels, in which a second component is embedded within the polymer network can yield enhanced mechanical and biological properties. Incorporation of hydroxyapatite has been shown to promote and aid bone mineralization while carbon nanotubes or nanocellulose can increase stability and provide desirable rheological properties to a polymer precursor solution [133-137].

While first progress has been made to create a controlled microarchitecture in the hydrogel, parameters like macroporosity, gradient crosslinking or anisotropic alignment are still scarce in bulk hydrogels [138-139]. Such applications are mostly limited to very specific material choices and crosslinking systems. A recent trend has emerged to no longer see the hydrogel as a single building block for tissue engineering, but to use microgels, micron sized hydrogels as building blocks to make up the complete structure [140-141]. By reducing the size of the manipulated object, consequent application

will allow the scientific community to increase control over the complete construct.

## 1.7 Microgels – a Next Step?

Hydrogels have been predominant as platform for cell culture and tissue repair strategies. They excel at recreating the high water content of human tissues, but fail to reproduce some of the more advanced characteristics of cellular niches<sup>[142]</sup>. Specifically, the omnipresent heterogeneity and anisotropy of native tissue is poorly mimicked by a bulk hydrogel construct. Furthermore, mass-transport and gas exchange in hydrogels is often limited by the dense polymer network that permits diffusion<sup>[143]</sup>. Granular hydrogels made from a multitude of micron sized hydrogel particles (microgels) are an emerging alternative<sup>[142-143]</sup>. Even though the underlying polymer might be identical to bulk hydrogels, microgels offer completely new ways to architect biofabricated constructs<sup>[142, 144]</sup>. Granular hydrogels have interconnected microporous networks that greatly enhance fluid flow, mass-transport, permeability and cell-infiltration compared to bulk hydrogels<sup>[143]</sup>. Heterogeneity is another key property, as different microgels in varying concentrations can be combined to fabricate a granular hydrogel. These new possibilities, provided with microgel based approaches, have attracted the attention of the biofabrication community to better address the challenges in mimicking the complex architecture of native human tissue<sup>[145-146]</sup>.

Traditionally, microgels were prepared with electro-spraying and microfluidics to prepare spherical microgels<sup>[143]</sup>. In the electro-spraying process, a high voltage is applied to a polymeric liquid to disperse it into an aerosol that gets crosslinked subsequently<sup>[147]</sup>. A similar process can be reproduced with a nebulizer, in which compressed gases or ultrasonic power is used to create aerosols<sup>[148]</sup>. Cell-delivery with spraying is possible through a process called bio-electrospraying (BES)<sup>[149]</sup>. Application remains challenging, though, as voltage and appropriate flow-rate needs to be

controlled meticulously to present a stable environment <sup>[150]</sup>. These methods depend on aerosol formation and therefore have strong limitations regarding applicable materials. Even slightly viscous fluids can interfere with the formation of a Taylor cone and prohibit relevant plumes, which are critical for the formation of an aerosol in these techniques.

Preparation of microgels with a microfluidic approach has been widely applied <sup>[148]</sup>. When fluids are precisely controlled in a sub-millimeter scale, capillary forces govern mass transport which allows for new ways of manipulating liquids. To exploit these properties for droplet creation, fluids with immiscible phases and low Reynolds number in a laminar flow regime are required. In a simple setup, an aqueous liquid is projected into an oil phase. This results in droplet formation, which can be modulated by flow rate. Aqueous droplets are stable inside the oil phase and can be further processed, e.g. crosslinked into stable spheres. Such microspheres allow to incorporate cells or other biological relevant cargo by simply adding it to the aqueous phase during preparation. Stress applied to cells is minimal and the method allows to embed single or multiple cells with high viability <sup>[151-152]</sup>. Cell-laden microspheres can be purified to remove any residual oils and jammed into a condensed state <sup>[153-154]</sup>. In this overpacked state, interpenetration and shape deformation occurs and new properties emerge in the colloidal particles <sup>[154]</sup>. Of special interest for extrusion based bioprinting, are the rheological properties of these materials, as they exhibit shear thinning and shear recoveries with a yield point that give printability to jammed microgels <sup>[155]</sup>. Since interaction between spherical microgels is limited, secondary crosslinking is usually required to stabilize microspheres after deposition <sup>[156-157]</sup>. One of the key characteristics of these materials is the high porosity that results from the close-packing of equal spheres. As microspheres deform only when high mechanical force is applied, spheres commonly arrange in a lattice packing. In such a geometrical lattice, spheres can occupy a maximum of 74% of the space and therefore a significant amount of void space is created (**Figure 1.4**) <sup>[158]</sup>. Correspondingly, interconnectivity of the pores has been

reported in literature <sup>[157, 159-160]</sup>. But a spherical building block is not ideal for all scenarios. Even though preparation of anisotropic or aligned structures is theoretically possible by utilizing spherical microgels of varying sizes, this would require a level of positioning and control that has not been demonstrated yet.

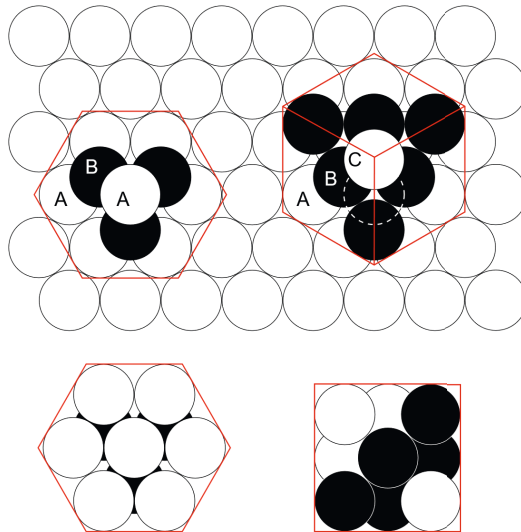


**Figure 1.4** Illustration of the two possible lattices in close-packing of equal spheres

Anisotropic microgels can overcome some of these limitations of spherical microgels. Production of microgels with non-spherical shape required the development of new fabrication techniques. Particle replication in nonwetting templates (PRINT) enables to manufacture microgels with precise shape control <sup>[161]</sup>. PRINT advances the process of traditional imprint lithography methods in which creation of isolated objects is very challenging, since a thin, connecting layer of residual material (scum layer) is often formed (**Figure 1.5**). By introducing a non-wetting, perfluoropolyether (PFPE) substrate for the imprinting, the liquid precursor is confined inside the features of the mold <sup>[162-163]</sup>.

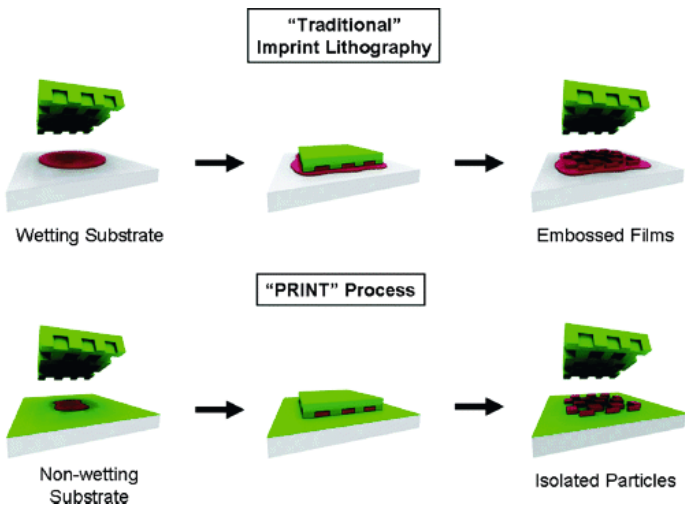


**Figure 1.5** Top: traditional imprint lithography results in particles connected by a scam layer. Bottom: introduction of a non-wetting substrate layer allows for creation of individual particles. Reprinted from J. P. Rolland, B. W. Maynor, L. E. Euliss, A. E. Exner, G. M. Denison, J. M. DeSimone, *Journal of the American Chemical Society* **2005**, 127, 10096, with permission from American Chemical Society, © (2005).

Gel structures prepared with PRINT can be controlled within the nanometer range and advanced 2-dimensional shapes can be created. The process of PRINTing microgels still needs to be improved though, to yield sufficient quantities of microgels for tissue engineering and 3D bioprinting.

Another versatile method to manufacture anisotropic microgels based on a microfluidic chip with segmented illumination is termed “compartmentalized jet polymerization”<sup>[164]</sup>. Hydrogel precursor solution is confined as a thin strand through microfluidic channels and oils and selectively photo-crosslinked in this state. Pulsed, phototriggered gelation results in rod-shaped microgels, while continuous exposure allows to create continuous strands. With this method, it is also possible to tune stiffness and size of microgels through modulation of the light source and flow rate<sup>[164]</sup>. The usual



limitations of microfluidic setups apply, which limits the availability and since the crosslinking is carried out under microfluidic flow, other shapes besides strands and rods are difficult to realize.

When less control over the individual microgels, but a general anisometric scaffold is required, wet spinning can be employed. Importantly, this method was used to create gelatin microribbons ( $\mu$ RBs) which could be secondarily crosslinked to create porous scaffolds. Microribbons are prepared by continuous extrusion of gelatin into a bath of ethanol that results in an immediate precipitation of the gelatin solution [165]. The precipitate was chopped into smaller pieces, crosslinked, methacrylated, purified and lyophilized. Resulting microribbons were stable, could be formed into scaffold by photexposure and showed promising results for cartilage regeneration [165-166]. Extensive use of chemicals in the production, however, prohibits the encapsulation of cells within the microgels. Control over the orientation of microribbons still has to be demonstrated to increase the relevance for tissue types that require aligned structures. Finally, deconstructing bulk gels into gel particles and elongated hydrogel strands have been reported [167-168]. Granular hydrogels are a relatively new class of biomaterials utilized in biofabrication. Their unprecedented opportunities to architect tissue engineered grafts, however allowed them to gain traction and quickly spread in the field.

## 1.8 Tissue Engineering Liquids

A plethora of biofabrication techniques were developed over the last years, but they nearly exclusively focus around the idea of culturing cells in a stable hydrogel material. Tight control over the shape of the fabricated construct is important, but taking a lesson from cellular self-organization and organoid formation, cells need spatial freedom to assemble and condense into functional structures [169-170]. Organoid formation takes place in very soft hydrogels or even liquids, however such materials are rarely applied in biofabrication of tissues [171-172]. The low rigidity of these materials, which can

often barely support its own shape, poses a great challenge if used with techniques like bioprinting <sup>[173-174]</sup>. Even with internal mechanical support, the biological matrix needs to adhere and support its own weight. Therefore, materials which are too soft (e.g. Matrigel) are not suitable for bioprinting <sup>[175-176]</sup>. To resolve this issue, the scientific community resorted to multilateral bioinks in which these soft hydrogels are only one of several components <sup>[176-177]</sup>. As this greatly alters the mechanical and physiochemical environment, cell response varies as well and does not correspond to the initially sought-after properties.

Taking a look at nature, two distinct ways of stabilizing soft matter are common. Internal skeletons found in animals and humans, in which a set of support structures gives a central anchor point to the soft tissue. Soft tissues adhere to the endoskeleton but need to have some inherent stability as well. Another strategy is to confine soft tissue or fluids with an exoskeleton as it can be found in insects or hydroskeletons which are driven by fluid pressure <sup>[178-179]</sup>. Through a combination of external support, confinement and internal pressure, soft tissue is given its required shape <sup>[178]</sup>. Taking inspiration from this, a novel way of culturing cells inside unstable, soft or even liquid materials was developed as part of this thesis.

---

## Scope of the Thesis

Tissue engineering as a discipline of personalized and regenerative medicine started with the promise to deliver, lab-grown, readily available, functional tissue when the natural healing capacity is at its limit. Even though tremendous amounts of resources were invested, the grand goal has not been achieved yet. The aim of this thesis was to develop and use advanced biofabrication to push the boundaries of what is possible today and come closer to the vision of creating cartilage tissue *de novo*.

The first goal, described in Chapter II, was the creation of advanced, clinically relevant bioinks for microextrusion 3D bioprinting through a multipolymer approach. Four different polymers, each with a specific role, were combined to create more complex, but also more versatile bioinks. It was possible to print biologically relevant shapes with high precision and increase retention of growth factors, necessary for chondrogenic maturation. Bioprinted scaffolds deposited an abundant, cartilaginous extracellular matrix *in vitro* and first tests to understand the clinical potential were developed and conducted. Finally, when bioinks were evaluated *in vivo*, the outcome was heterogeneous and partially contractionary to the *in vitro* results. Even though promising results were achieved, the high complexity that resulted from the interplay of four different materials made it a difficult system to master and further studies are needed to develop these bioinks.

A method to deconstruct bulk hydrogels into entangled microstrands that excel as bioinks for extrusion 3D bioprinting was the second scope of this thesis, presented in Chapter III. Entangled microstrands had various highly beneficial properties including porosity, enhanced stability in aqueous solutions and individual strands have been aligned through extrusion. Myoblasts were encapsulated within or around the gel-phase of the material and bioprinted into biologically relevant shapes with excellent cell viability. Alignment of microstrands guided the embedded cells to fuse and form aligned myotubes. In a first proof of principle for cartilage tissue engineering,

chondrocytes deposited vast amounts of extracellular matrix in bioprinted scaffolds, which led to an increase of compression modulus, approaching that of native cartilage. The system is highly tunable and applicable to a wide range of material choices, making it an ideal platform for future tissue engineering approaches.

In the third study, presented in Chapter IV, a novel way of culturing cells inside unstable, soft or even liquid materials was developed. A thin, shape defining, hydrogel shell was created and subsequently filled with cell-laden material. The hydrogel worked as a semi-permeable membrane that allowed diffusion of gases and nutrients inside the biofabricated construct, but confined cells and high molecular weight polymers within. Chondrocytes were combined with a range of materials previously not used in tissue engineering to screen the potential for a tissue engineering approach. Extracellular matrix deposition of cells annealed and stabilized granular and weak hydrogels, while chondrocytes cultured within uncrosslinked hyaluronic acid solution condensed and formed cartilaginous structures. This illustrates the feasibility of culturing cell-laden infill materials inside a semi-permeable hydrogel shell and demonstrates the relevance of innovative, new methods for tissue engineering.

The impact and relevance of these advanced biofabrication techniques is elucidated in Chapter V. Important knowledge gained during the work on this thesis is discussed and recommendations for future development of a translatable cartilage tissue engineering approach is given.

Additional research in this thesis has been conducted on the topic of surface modification, with regards to a potential application for tissue engineered constructs. A cell compatible surface modification method based on reversible deactivation radical polymerizations is the focus of Appendix I. Controlled growth of polymer brushes by surface-initiated atom transfer radical polymerization (SI-ATRP) is usually depended on a cytotoxic catalyst such as copper. The use of zerovalent iron ( $\text{Fe}^0$ ) transformed this system into

a versatile, cytocompatibility method for specific surface modification. Reaction process was optimized for cell culture conditions and could be applied to tune the physiochemical properties of tissue engineered constructs. To conclude, this thesis aimed at developing current and new research approaches into successful biofabrication techniques. The relevance of these techniques was demonstrated at the example of cartilage tissue engineering. These advanced biofabrication methods provide the scientific community with new tools to tackle the challenges in creating *de novo* tissue.



# **Chapter II - Clinically Relevant Bioinks for Cartilage Tissue Engineering**

## **Contributions:**

---

Benjamin Kessel and Marcy Zenobi-Wong designed the study. B. Kessel performed the research and analyzed it together with M. Zenobi-Wong. Pierre Guillon designed the 3D model of the human ear and created the algorithm to compare 3D models. Gonçalo Barretto helped with the experiment to measure LPS levels. Animal implantation and surgery was done by M. Zenobi-Wong and B. Kessel. Follow up experiments to investigate collagen type II maturation was a collaborative work of B. Kessel and Clara Levinson. B. Kessel wrote the manuscript.

## Abstract

Formulation and preparation of advanced bioinks, which excel at the mechanical as well as the biological side is one of the great challenges of 3D bioprinting. Sophisticated polymer modification allows to prepare hydrogels that push the boundary of what is possible, however such materials are extremely difficult to translate into a clinical setting. In this study we use multiple polysaccharides with no or minimal chemical modification to prepare increasingly complex bioinks. Each of the materials adds a highly relevant property to strengthen the mechanical and/or biological profile of the bioink, ranging from excellent printability to cell attachment sites and growth factor retention. A thorough characterization of these bioinks for cartilage tissue engineering revealed promising results *in vitro* with excellent cell viability and strong collagen type II deposition and no staining for collagen type I. First tests to understand and tackle possible problems for a translation into a clinical setup have been developed and give insight into challenges that occur on the way to clinically relevant bioinks.



## 2.1 Introduction

Cartilage is a connective tissue which serves several crucial functions in the human body. While articular cartilage allows for low coefficient of friction on the joint surface, elastic cartilage gives structure and function to the ear and nose. Even though molecular composition and architecture varies between hyaline and elastic cartilage, they are both avascular and aneural<sup>[180]</sup>. These characteristics, together with a low cellularity, severely restrict the self-repair capability of cartilage. Since cartilage does not regenerate *in situ* in sufficient quality and quantity, engineering biological, yet lab-grown cartilage grafts to transplant into patients has been proposed as a possible solution<sup>[181]</sup>. So far, treatment options for cartilage damage are limited, often highly invasive and with variable clinical outcome<sup>[182]</sup>. Huge efforts were undertaken in tissue engineering to create grafts that mimic mechanical properties of cartilage as well as molecular composition<sup>[181, 183]</sup>. A key challenge is to recreate the dense extracellular matrix in cartilage that provide the high mechanical properties to the tissue. Finding a suitable biomaterial that can be used to fabricate tissue constructs in specific shapes but allows the embedded cells to transform this scaffold into viable tissue is crucial.

Alginate is an unmodified polymer, abundant in nature and widely used in tissue engineering<sup>[184-185]</sup>. Addition of divalent cations is a simple and cell-compatible way in which alginate solution undergoes gelation. While alginate gels provide a hydrated matrix to the embedded cells, they have only limited use in recreating the complex physical properties of the native cartilage extracellular matrix (ECM)<sup>[186]</sup>. Mimicking electrical charge, chemical composition and ligand affinity of this ECM however, is crucial to guide embedded cells into recreating cartilage tissue<sup>[187]</sup>. Sulfated glycosaminoglycans (GAGs), more specifically heparan sulfate and chondroitin sulfate, are the key contributors to the negative charge and hydration of cartilage ECM<sup>[188]</sup>. These sulfated GAGs have been shown to have high affinity to various growth factors including the transforming

growth factor (TGF) superfamily<sup>[189-191]</sup>. Heparin, a readily available sulfated GAG, has been traditionally used in tissue engineering applications to profit from these beneficial properties<sup>[192]</sup>. Due to variations in degree of sulfation, fast degradation and impurities, working with heparin is highly challenging. This motivated work to develop more defined sulfated molecules that maintain the favorable properties of native GAGs<sup>[193-194]</sup>. Alginate-sulfate, a chemically sulfated variant of alginate showed great success in cartilage tissue engineering and was also found to interact with TGF- $\beta$ 1, one of the most common growth factors to induce chondrogenic maturation *in vitro*<sup>[195-196]</sup>. Moreover, studies found further beneficial properties of alginate-sulfate like anti-inflammatory activity and free-radical quenching<sup>[197]</sup>.

Another polysaccharide that is gaining more and more attention in the context of tissue engineering is hyaluronic acid (HA)<sup>[198]</sup>. This non-sulfated molecule is an important part of the extracellular matrix and can have a molecular weight of several MDa<sup>[199-200]</sup>. Due to its high molecular weight, HA is used as a viscosity enhancing agent or to add thixotropic properties to a solution<sup>[201]</sup>. As a natural component of human extracellular matrix, many human cells have surface receptors to interact with HA, most importantly via CD44<sup>[202]</sup>. Chondrocytes in particular, express CD44 and endogenous high molecular weight hyaluronan plays a key role in cartilage homeostasis<sup>[203]</sup>.

But cartilage is not defined by its extracellular matrix composition alone. It is a tissue with a distinct shape, which is not only relevant for its function, but has crucial impact on visual features of humans. Cartilage is the shape defining tissue for facial features like the outer ear and nose. Damage or defects in those areas are challenging to treat and prosthetic and reconstruction options both poses risks<sup>[204]</sup>. Creating autologous cellular grafts for transplantation from the costal rib cartilage is considered the gold standard, though challenging. Such a reconstruction is highly invasive since tissue grafts often consist of several autologous costal cartilage pieces, combined together and carved into shape<sup>[205]</sup>. Therefore, visual outcome of those treatments is often dependent on not only the medical expertise of the

surgeon, but also their artistic skills. 3D bioprinting allows to elegantly address the challenges that come with the recreation of such an intricate structure as the outer ear. Analog to 3D printing of plastics, 3D bioprinting allows the controlled deposition of a cell-laden polymer solution called bioink, to make up the final object in a layer-by-layer fashion <sup>[64]</sup>.

For successful extrusion-based 3D bioprinting, bioinks need to fulfill a wide range of rheological and mechanical properties. Unlike a Newtonian liquid, whose flow is linearly correlated to the strain rate, bioprinting works best if the bioink behaves like a non-Newtonian fluid, more specifically a Bingham plastic <sup>[206]</sup>. Such materials have characteristic changes in their fluid behavior according to the stresses exerted on the material. At low stresses a Bingham plastic remains solid and does not flow. This changes as soon as a certain level of stress, the yield stress, is surpassed at which this material starts to flow like a fluid. In the context of bioprinting, this allows a bioink to be readily extruded through at a specific stress level to shape the required structure. As soon as the bioink is deposited on the build plate, the exerted stress drops and the bioink switches back to a solid-like state. This allows to precisely create a 3D structure that keeps its shape even without additional support <sup>[64, 207-208]</sup>.

Gellan gum is a bacterial polysaccharide widely used in food science as a thickener, emulsifier and stabilizer but also approved for cosmetic and pharmaceutical use <sup>[209]</sup>. Gellan forms thermoreversible gels when a hot solution is quiescently cooled down <sup>[210]</sup>. Such a bulk gel, however, is not extrudable and incompatible with bioprinting. A well-known method to modify and tune the properties of gels is continuous shear during the gelation period. This will result in molecular ordering under shear and a material called fluid gel that consist of gelled particles in the micron scale. Unlike quiescently formed bulk gels, fluid gels often have Bingham plastic properties and are therefore an ideal material to give printability to a bioink <sup>[211-212]</sup>. One potential issue related to the use of microbial polysaccharides is endotoxin contamination. Gellan is produced by *pseudomonas elodea*, a gram-negative bacterium, which can be problematic, since endotoxins, also known

as lipopolysaccharides (LPS) are found in the outer membrane of gram-negative bacteria. Endotoxins can cause toxic effects even in smallest amounts and absence of LPS is therefore of paramount importance for any implant. Strict guidelines from regulatory authorities like the US federal drug administration (FDA) enforce safe levels of LPS <sup>[213]</sup>. Proofing compliance with these regulations will therefore be an important first step to demonstrate clinical relevance for bioinks.

Since the start of 3D bioprinting, bioinks were required to combine two seemingly oppositional properties and bioinks had either high mechanical properties (printability, stability) or good biological properties (cell viability, cell instructiveness, bioactivity). Improving one often has a detrimental impact on the other. The great challenge of bioprinting today is to proceed to so called advanced bioinks that unite both, mechanical and biological properties to prepare high quality tissue scaffolds <sup>[214]</sup>.

In this study we want to approach this challenge with a multipolymer approach. By combination of up to 4 different materials, we created 3 different bioinks of increasing complexity. Bioink A consisted of alginate and gellan to allow 3D bioprinting with high precision and versatility through gellan fluid gels as well as a simple hydrated matrix through cross-linking of alginate. Hyaluronic acid was added to create Bioink B and therefore provide attachment sites for cells. In Bioink C, alginate-sulfate was included to closer mimic the physiochemical properties of the cartilage niche. All three bioinks were carefully characterized and their potential for cartilage tissue engineering was evaluated. To investigate the clinical relevance of these bioinks, endotoxin content was measured and shape retaining potential of 3D bioprinted structures was analyzed. Finally, 3D bioprinted tissue grafts were implanted into a subcutaneous pocket of nude rats to evaluate stability and chondrogenic maturation of these bioinks *in vivo*.

## 2.2 Materials and Methods

### *Materials*

All chemicals were purchased from Sigma-Aldrich and used as received unless stated otherwise. Gellan gum was received as a free sample from C.P. Kelco, utrapure alginate was purchased from NovaMatrix and hyaluronic acid from Lifecore Biomedical. Small parts and consumables for the 3D bioprinter were bought from Nordson EFD.

### *Cell isolation*

**Bovine chondrocytes:** Samples of the femoral cartilage of 6 month old calves were obtained from the local slaughterhouse. Cartilage from the medial and lateral condyle was cleaned, minced in approximately 1 mm<sup>3</sup> pieces and digested by 0.1% collagenase solution (from *Clostridium histolyticum*) over night.

**Human chondrocytes:** Human ear cartilage was received (Ethical Approval Number: 2017-02101), cleaned, washed with PBS and isolated following the same protocol as for bovine chondrocytes. Isolated cells were cultured under humidified atmosphere with 5% CO<sub>2</sub> at 37°C. High glucose Dulbecco's modified Eagle's medium (DMEM, Gibco) supplemented with 10% (v/v) FBS (Gibco), 50 µg ml<sup>-1</sup> L-ascorbic acid 2-phosphate sesquimagnesium salt hydrate and 10 µg ml<sup>-1</sup> gentamycin sulfate (Gibco) was used as cell media. Cells were passaged at 90% confluency by detachment with 0.25% trypsin/EDTA (Gibco) and used for experiments at passage 3.

### *Polymer Modification*

Sulfation of alginate was carried out as reported previously [215]. Ultrapure high viscous alginate was dissolved in formamide and 96% chlorosulfonic acid was added subsequently to a final concentration of 2% v/v. The solution was constantly stirred and left to react for 2.5 hours at 60°C. Product was precipitated with ice-cold acetone followed by centrifugation. Alginate was

re-dissolved in ultrapure water and constantly neutralized with 5 M NaOH until the polymer was completely solubilized and no further change in pH was observed. Solution was dialyzed against 100 mM NaCl and deionized water before it was lyophilized.

### *Bioink Preparation*

Polymers were dispersed in given concentrations in isotonic, HEPES-buffered glucose solution. Solution was heated up to 90°C and stirred with a magnetic stirrer for 30 minutes to ensure complete solution of polymers. Polymer solution was then constantly sheared with a metal spatula until mixture was cooled down to room temperature. Polymer mix was pressed through a 100 µm nylon grid to break up any possible lumps and subsequently centrifuged down at 2500 g to remove any trapped air bubbles. Polymer mix was then combined with a dense cell solution ( $100 \times 10^6$  cells  $\text{ml}^{-1}$ ) via repeated pipetting or with a double barrel syringe and a static mixer system (MedMix) at a ratio of 10:1 to create cell-laden bioink.

### *Bioprinting*

Cell-laden bioink was extruded with a commercial 3D bioprinting solution (RegenHU Discovery). 3D models were sliced with Slic3r 1.3 and subsequently processed with an in-house developed post-processing script. Cell-laden bioink was loaded into 10 cc extrusion cartridges and pneumatically extruded through a conical needle with an inner diameter of 0.41 mm and a printing speed of 15 mm  $\text{sec}^{-1}$ . Extrusion pressure used was between 30 and 40 kPa with slight variations between bioinks and batches. 3D bioprinted structures were crosslinked into stable scaffolds by submersion in a buffered crosslinking solution based on 100 mM  $\text{CaCl}_2$  for 1 hour (small scaffolds) or 2 hours (ear shaped, large scaffolds) and subsequently cultured /in cell culture.

*Quantification of TGF- $\beta$ 1 retention*

30  $\mu$ l samples were prepared and incubated in a solution of TGF- $\beta$ 1 (Peprotech) to load the samples with an initial dose of 50 ng per scaffold. To study release, samples were kept in release buffer (150 mM NaCl, 5 mM CaCl<sub>2</sub> and 0.1% bovine serum albumin (BSA) for 1 week. Buffer was replaced at pre-determined timepoints and stored at -20°C until analysis. TGF- $\beta$ 1 release from hydrogels was quantified with a commercially available TGF- $\beta$ 1 ELISA kite (R&D systems) according to the manufacturer's protocol.

*Unconfined Compression*

Prior to compression, scaffolds were cut with parallel blades to a height of 2 mm and a 4/6 mm cylinder (cellular/acellular experiments) was punched out. The cylinder was tested with a texture analyzer up to a compression of 15% strain at a preload of 0.1 g. Bulk modulus was calculated as the slope of the first 3% strain of the stress / strain curve.

*Rheology*

To assess rheological properties of the samples, all measurements were conducted on an Anton Paar MCT 301 rheometer equipped with a 20 mm parallel plate geometry at 25°C in a humid atmosphere with a gap distance of 1 mm. Rheological properties of samples were examined by oscillatory shear sweeps (1% strain, 1 - 100 Hz), ramped shear rate (0.01 - 50 1 s<sup>-1</sup>) and strain sweeps (1 Hz, 0.01 - 1% strain) to evaluate storage and loss modulus, yield point and shear thinning behavior. To investigate shear recovery properties, samples were exposed to repeating cycles of alternating phases of strain (1 Hz, 1% and 500% strain). To assess crosslinking characteristics, samples were kept at constant strain (1 Hz, 1% strain) and crosslinking solution was added around the sample after 5 minutes to trigger gelation.

### *Cell Viability*

Disc shaped scaffolds (d = 4 mm, h = 2 mm) were bioprinted and cultured for up to 21 days and viability was assessed 1, 7 and 21 days after printing. Scaffolds were washed with HEPES buffered DMEM. Encapsulated cells were stained with propidium iodide ( $0.5 \mu\text{g ml}^{-1}$ ), calcein AM (0.008 mM) and Hoechst 33342 ( $5 \mu\text{g ml}^{-1}$ ) for 30 minutes, washed in HEPES buffered DMEM and imaged with fluorescent light microscopy (ZEISS, Axio Observer). Picture analysis was automatically performed with FIJI and a custom macro (Code 1). Experiment was done in triplicates, with the viability of each sample averaged over 3 pictures of randomly chosen positions inside the hydrogel.

### *Histological staining*

Samples were submerged in a solution of 50 mM  $\text{BaCl}_2$  to substitute calcium ions with barium and therefore ensure thorough stability of samples during histological processing. Samples were then fixed in 4% paraformaldehyde for 2 hours, dehydrated, paraffinized (LogS, Milestone) and embedded into paraffin blocks. Blocks were cut with a microtome in 5  $\mu\text{m}$  thick sections and adhered to polylysine slides (Polysine, Thermo Scientific). Tissue sections were stained with Alcian blue according to standard protocols. For colorimetric, immunohistochemical stainings of collagen type I and type II, tissue sections were digested in hyaluronidase solution ( $1200 \text{ U ml}^{-1}$ , *Streptococcus equi*) for 30 minutes at  $37^\circ\text{C}$ . Including this step, samples were kept under humidified atmosphere when incubation times exceeded 15 minutes to avoid drying artifacts. Sections were washed twice with PBS and blocked with 5% normal goat serum (NGS) in PBS for 1 hour at room temperature. Subsequently, slides were blotted and primary antibody in 1% NGS was applied. Anti-collagen type I antibody (mouse, Abcam #ab6308) was used at 1:1500 dilution, while anti-collagen type II antibody (mouse, DSHB #II-II6B3) was used at 1:200 dilution. On the following day, samples were washed thrice with PBS and any remaining endogenous peroxidase or



pseudoperoxidase activity of the tissue was quenched with 0.3% H<sub>2</sub>O<sub>2</sub> to prevent non-specific signals. Samples were washed in PBS before the secondary antibody (goat, anti-mouse IgG (HRP), Abcam #ab6789) was diluted 1:2000 in 1% NGS and added to the samples. After incubation for 1 hour, samples were washed again and DAB substrate (ab64238, Abcam) was added and left to react for 8 minutes. Sections were washed again and counterstained with Mayer's hematoxylin solution. Finally, samples were mounted and coverslipped with resinous mounting media (Eukritt) and imaged with a histology slide scanner (Pannoramic 250, 3D Histech).

#### *Endotoxin content evaluation*

A commercial LPS detection kit based on engineered HEK cells with stable expression of TLR4 and NF- $\kappa$ B inducible reporter genes was used.

#### *Swelling feature loss evaluation*

Ear models were crosslinked and scanned using a commercially available 3D scanner (mono Scan, Smart Optics). Scanned ear model was compared to the original 3D model used to create the g-code for bioprinting. Comparison was done with an in-house developed algorithm.

#### *Subcutaneous implantation*

Animal studies were performed in compliance with ethical license (Application No. ZH185/16). Nude rats (CrI:NIH-*Foxn1*<sup>tmu</sup>) were obtained from Charles River. All animals were female with an age of 2-5 months. Animals were housed in groups of 3 and were not restricted in their movement. Before surgery, animals were anesthetized with 4.5% isoflurane and Meloxicam (Metacam, 2mg kg<sup>-1</sup>). To prevent desiccation of the cornea, eye cream was applied and anesthesia with 1.5 – 3% isoflurane was continued throughout the whole surgery. For small samples, two randomized samples were implanted, with one sample in an independent subcutaneous on each side. For large samples, only one sample was implanted. To prepare subcutaneous pocket, an incision lateral to the dorsal midline was made.

Incisions were closed with surgical staples. Any remaining staples were removed under anesthesia with isoflurane 7 days after surgery. Animals were euthanized after 6 weeks via CO<sub>2</sub> asphyxiation and samples explanted. Explants were fixed for 3 hours in 4% paraformaldehyde, dehydrated and embedded in paraffin.

#### *Statistical Analysis*

Statistical analysis was conducted with GraphPad Prism (v. 8.2.0 (425)) with an alpha of 0.05. Bulk modulus and viability of samples was compared by one-way analysis of variance (ANOVA) with Tukey post hoc tests.




## 2.3 Results

A bioink based on alginate and gellan was previously developed in the laboratory <sup>[216]</sup>. Both polymers have no bioactive site for human cells, but rather serve as a simple but effective hydrated matrix (alginate) as well as a printability enhancer (gellan). This bioink, named Bioink A, was used as a standard to compare other advanced formulations of bioinks. To improve bioactivity of human cells to this bioink, hyaluronic acid was added to the bioink (Bioink B). Addition of hyaluronic acid had a significant influence on the compression modulus of 3D printed scaffolds ( $F_{(3, 43)} = 4.61, P = 0.007$ ). However, there was no significant difference found between addition of 0.1% or 1% HA to Bioink A ( $P = 0.928$ , **Figure 2.1A**). Therefore, the highest concentration of HA (1%) was chosen to be added into the bioink to have the strongest positive impact on cells. This formulation was named Bioink B. Previous studies have shown a strong potential for chondrogenic maturation of alginate-sulfate, gel forming capability and gel strength, however, were impaired due to the functionalization <sup>[195]</sup>. To address this issue, only a fraction of the alginate in Bioink B was substituted with alginate-sulfate. Samples of bioinks with different ratios of alginate and alginate-sulfate were prepared and tested for long term stability in standard cell culture media. Strong swelling to the point of disintegration was observed for all samples with a content of alginate-sulfate higher than 0.5%. Therefore, 0.5% of alginate was substituted with alginate-sulfate to prepare a third bioink formulation - Bioink C. An overview of the concentrations of each of the polymers in the three bioinks can be found in **Table 2.1**.

Besides introducing strong negative charges, one of the main benefits of addition of alginate-sulfate to create Bioink C is the retention of growth factors from the TGF superfamily. Since the concentration of alginate-sulfate in the final bioink had only a concentration of 0.5%, Bioink C was tested for its retention potential of TGF- $\beta$ 1, one of the main growth factors used to induce chondrogenic maturation of de-novo cartilage in tissue engineering.

Release profile of bioinks significantly differed ( $T(5) = 5.22$ ,  $P = 0.003$ ) with  $62 \pm 2.1\%$  of TGF- $\beta$ 1 released after 7 days from Bioink C while  $90.6 \pm 6.7\%$  was released from Bioink A (**Figure 2.1B**).

**Table 2.1:** Concentrations of different polymers used for preparation of different bioinks used in this study

	Color	Alginate	Gellan	Hyaluronan	Alginate-S
<i>Bioink A</i>		2%	3%	-	-
<i>Bioink B</i>		2%	3%	1%	-
<i>Bioink C</i>		1.5%	3%	1%	0.5%

In a next step, printability and crosslinking behavior of the different bioinks were investigated. All three bioinks showed shear thinning behavior with a sharp drop in viscosity when shear rate (and therefore shear stress) was increased (**Figure 2.1C**). To investigate shear recovery properties, bioinks were exposed to repeated cycles of high and low strain rate (**Figure 2.1D**). Storage modulus of all bioinks showed a fast and reversible transition from high values (low strain) to low values (high strain). This transition from elastic, solid-like state to a fluid one is crucial for a high quality print and a key factor to reduce applied shear stress to embedded cells during 3D bioprinting.

All three bioinks could be rapidly gelled with 100 mM calcium chloride solution (**Figure 2.1E**). Final storage modulus after 1 hour of gelation differed between bioinks (Bioink A: 283 kPa, B: 146 kPa, C: 81.2 kPa) but was sufficient to allow mechanical handling of all samples with tweezers and spatulas without damage to printed structures. Crosslinking profile and final storage modulus could also be tuned by changing the concentration of cations in the crosslinking solution. (**Figure 2.1F**).

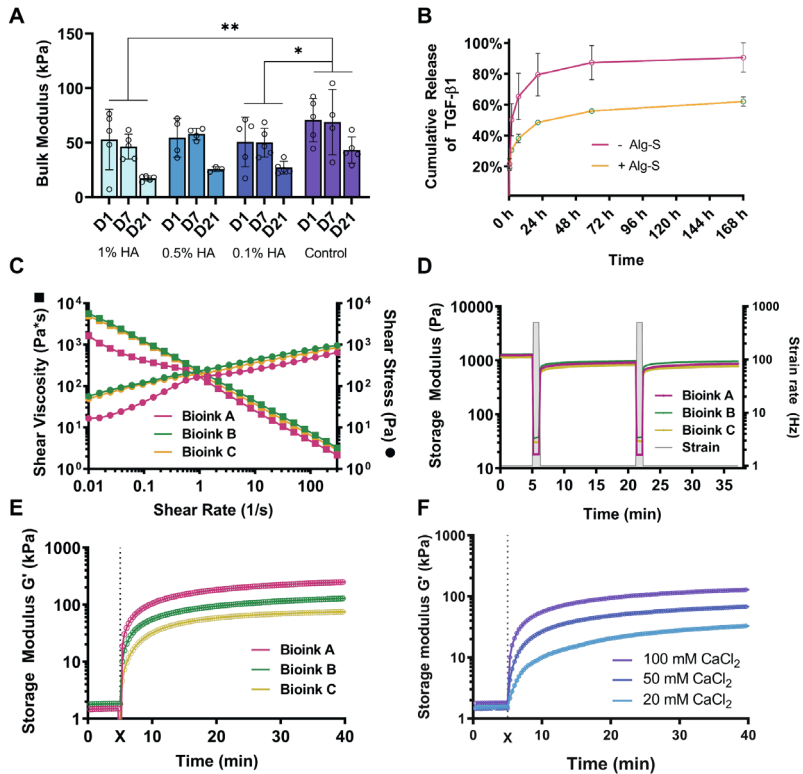


**Figure 2.1** (A) Addition of HA influenced bulk modulus of crosslinked bioinks. (B) Release profile of TGF- $\beta$ 1 from bioinks with and without Alginate-sulfate. (C) Shear thinning behavior of bioinks. (D) Storage modulus of bioinks in response to cycles of low and high strain. Crosslinking profiles of the three different bioinks (E) and of Bioink A crosslinked with CaCl<sub>2</sub> solutions of different concentrations (F). X marks the addition of the crosslinking solution to trigger gelation.

Significant swelling and phase separation inside printed scaffolds were observed for Bioink A (Sup 1). Extend of this phenomenon could be reduced by preparation of Bioink A with high molecular weight alginate. However, it was not possible to completely avoid phase separation in Bioink A. Addition of high molecular weight HA suppressed the occurrence of phase separation

in scaffolds, therefore phase separation was not observed for scaffolds prepared with Bioink B and C.

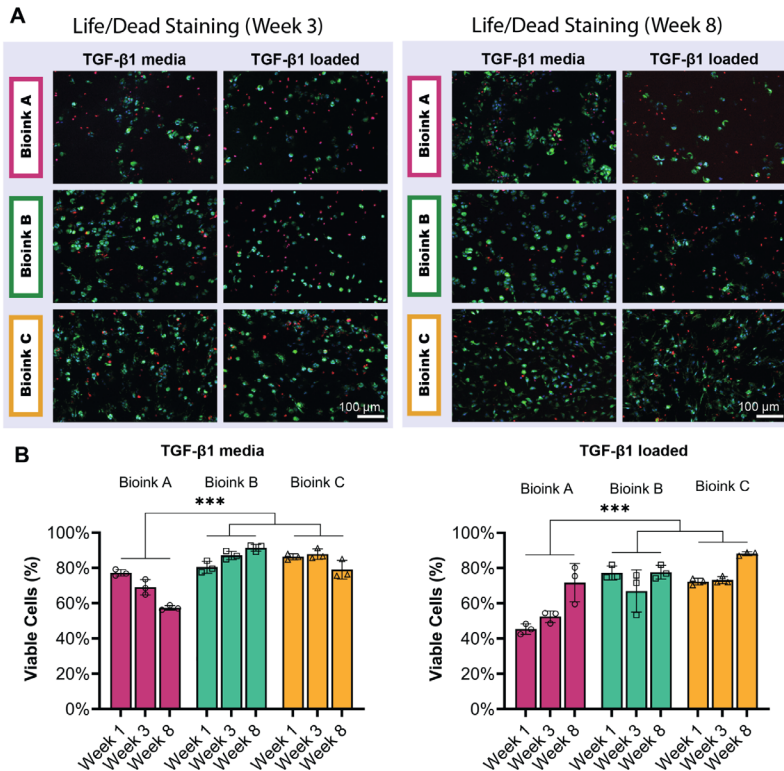


**Figure 2.2** (A) Fluorescent staining for live (green) and dead (red) cells as well as nuclei (blue). Scaffolds were prepared from different bioinks and cultured in TGF-β1 supplemented media or loaded with a one-time dose of TGF-β1 (200 ng/ml) and no additional supplementation. (B) Quantification of cell viability of this experiment.

To investigate the cellular behavior and response in the three bioinks, primary bovine chondrocytes were combined with the polymer solution to create cell-laden bioinks. 3D bioprinted samples were either cultured in TGF-β1 supplemented media or loaded with a one-time dose of TGF-β1 and

subsequently cultured in TGF- $\beta$ 1 free media. Clear differences in cell density and phenotype could be observed in samples supplemented with TGF- $\beta$ 1 media (**Figure 2.2A**). Cells appear smaller and more clumped in Bioink A and more homogeneously dispersed in Bioink B and C. In Bioink C some cells adapted a spread phenotype not typical for chondrocytes in 3D culture, but previously observed with Alginate-sulfate hydrogels and found to be connected to a strong chondrogenic maturation<sup>[195]</sup>.

For TGF- $\beta$ 1 loaded samples, increased cell death and lower cell density was observed for Bioink A and B. However, cell density and viability of Bioink C was comparable to the media supplemented condition. An even more spread phenotype than in TGF- $\beta$ 1 supplemented media was observed in these samples. Viability of cells in Bioink A was significantly lower compared to Bioink B and C for both conditions (Media:  $F(2, 18) = 99.24, P < 0.001$ ; Loaded:  $F(2, 18) = 32.85, P < 0.001$ ; **Figure 2.2B**). It is noticeable that viability of cells in Bioink are steadily declining with media supplementation and steadily increasing in loaded conditions. This effect was not present for Bioink B and C.

Since cartilage tissue is strongly defined by its dense extracellular matrix, histological stainings for collagens were conducted to evaluate chondrogenic maturation.

TGF- $\beta$ 1 supplementation is highly relevant for collagenous matrix deposition. Only faint stainings for collagens were observed in TGF- $\beta$ 1 free controls (**Figure 2.3**). As an exception, samples of Bioink C had a collagen I deposition even in TGF- $\beta$ 1 free controls. In this samples though, only minimal deposition of type II collagen was observed, which is the predominant type in healthy hyaline cartilage. When TGF- $\beta$ 1 was supplemented in the media, all three bioinks had strong, comparable deposition of collagens of both types after 3 weeks of culture. This situation changed at week 8, in which samples from Bioink A and C have a slightly stronger staining for both collagen types compared to week 3. Bioink B,

however, had a strong staining for collagen type II and only minimal staining for collagen type I.

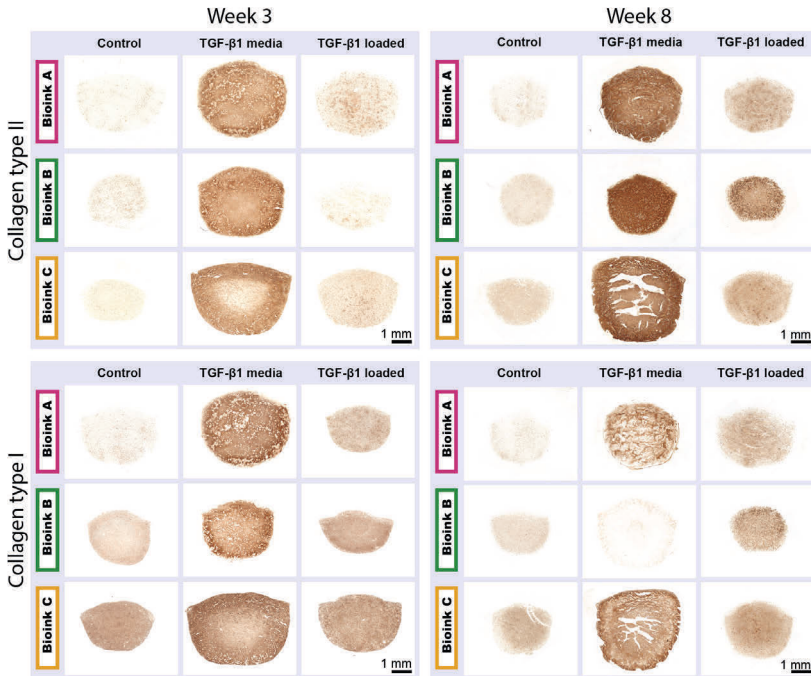


**Figure 2.3** Immunohistochemical analysis of 5µm-thick paraffin cross-sections of bioprinted scaffolds with specific stainings for collagen type I (bottom row) and II (top row).

Similar results were found for TGF-β1 loaded samples: stainings for collagens in Bioink A and C intensified with time. Again, after 8 weeks of culture, Bioink B had significant stronger staining for both collagen types compared to week 3 but also to week 8 of other bioinks. Pattern of deposition also varies between Bioinks but stayed similar throughout TGF-β1 treatments (**Figure 2.3, Figure S2.3**). Bioink A showed patches of strong and faint staining adjacent to each other with sudden



transitions. This effect can probably be linked to the phase separation present in this bioink. Bioink B had a very homogenous pattern with clear distinction of cell-filled lacuna and extracellular matrix covering the remaining area. In Bioink C, the core area of the sample fractured and deposition of extracellular matrix is heterogeneous. This problem might be linked to the weaker affinity of alginate-sulfate to calcium ions compared to unmodified alginate that also resulted in a lower initial bulk modulus of those gels. In a prolonged culture, a critical amount of calcium ions might have leached out of the scaffold resulting in collapse of the hydrogel network.

In a next step, we wanted to tackle several hurdles that prohibit possible translation of bioinks into the clinics. One challenge in creating clinically relevant bioinks is to reproducibly combine cells with the polymer mixture. Since the bioink is shear thinning, stress is required to transform the bioink into a fluid, mixable state. At the same time, applying strong or repeated stress to cells will result in cell death. A widely used method is continuous pipetting until a homogeneous solution is achieved. On a more professional level, double barrel syringes together with static mixers are common. To compare both methods, dense solutions of cells were combined using either methods and subsequently quantified (**Figure 2.4A**). Viability of cells combined with the bioink via a static mixer was high ( $88.2 \pm 4.9\%$ ) and significantly higher compared to samples mixed with the pipetting method ( $70.4 \pm 2.4\%$ ,  $F_{(2,9)} = 30.73$ ,  $P < 0.001$ ). To simulate the printing process, bioink was also extruded through a conical printing nozzle of  $410 \mu\text{m}$  diameter. However, no adverse effects on viability were found ( $P = 0.81$ ), indicating that actually the mixing and not the extruding process is crucial for high cell survival in 3D bioprinted constructs.

To identify if LPS contamination is a problem for bioinks made with gellan, a LPS sensitive HEK-cellline was utilized. While the standard and spiked samples showed a clear response, minimal to no response was measured throughout all samples (**Figure 2.4B**). A minor, stepwise increase was found

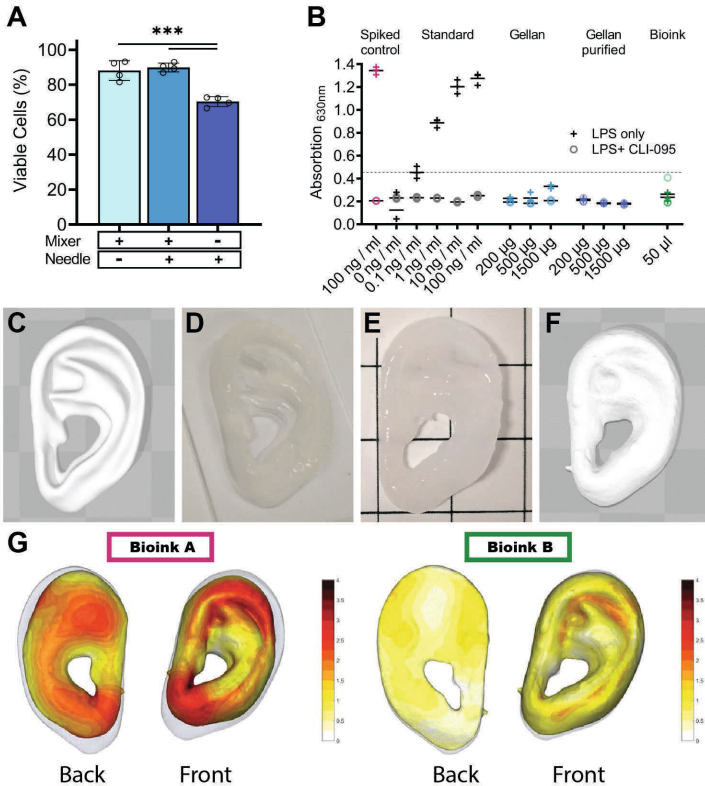


**Figure 2.4** (A) Viability of cells combined with the polymer solution by a static mixer or repeated pipetting and subsequent extrusion through a 410 µm needle. (B) Absorption readout of a commercially available LPS detection kit based on LPS sensitive HEK cell line. Dashed line indicates a concentration of 0.1 ng / ml. (C) 3D model of a hypothetical ear implant. Bioprinted ear implant before (D) and after (E) crosslinking. (F) 3D scan of the crosslinked 3D bioprinted ear scaffold. (G) Overlay of the scanned with the original model. Color indicates deviations in mm.

for increased amounts of unpurified gellan samples. However, measured response was still below the standard sample corresponding to 0.1 ng / ml LPS. Further purified samples of gellan as well as samples of the bioinks, had no measurable response et all.

Resolution of 3D bioprinting is limited by nozzle size and precision of the device on the one hand, but also chemical and biological factors play a role. Deformation of the printed samples, especially during the crosslinking process is a crucial factor often overlooked. We designed and 3D bioprinted a relevant 3D model of a human ear for possible use in surgical procedures (**Figure 2.4C,D**). The 3D bioprinted ear was subsequently crosslinked and scanned to create a 3D model resembling the actual final object (**Figure 2.4E,F**). An in-house developed algorithm was used to compare initial and final model to find deviations (**Figure 2.4G**). A combination of swelling and contraction was found for Bioink A that resulted in a smaller final structure as well as a loss of features with prominent examples in the area of the triangular fossa as well as the antitragus. Less overall deviations and only minimal size discrepancies were found for Bioink B. Even though expansion of thin structures in the area of the antitragus and triangular fossa was observed, difference between initial and final model was limited to a maximum deviation of 1.5 mm in Bioink B compared to 3 mm in Bioink A.

Finally, we wanted to evaluate the bioinks together with human articular chondrocytes in an *in vitro* as well as an *in vivo* environment. First, 3D bioprinted, disc shaped specimen were created and viability of embedded cells was assessed (**Figure 2.5A**). Similar to previous results, viability of cells significantly differed between Bioinks ( $F_{(2,18)} = 19.07$ ,  $P < 0.0001$ ), with Bioink B and C having a significant higher overall viability measured (B:  $74.7 \pm 6.7\%$ ,  $P < 0.0001$ ; C:  $73.0 \pm 2.8\%$ ,  $P = 0.0071$ ) compared to Bioink A ( $64.4 \pm 10.8\%$ ).

Native cartilage has a high compression modulus to withstand mechanical forces exerted during movement. To evaluate chondrogenic maturation besides ECM deposition, bulk modulus was evaluated. Samples were compressed and bulk moduli were calculated from the stress strain curve. All bioinks increased in compression modulus over the course of 9 weeks (**Figure 2.5B**).

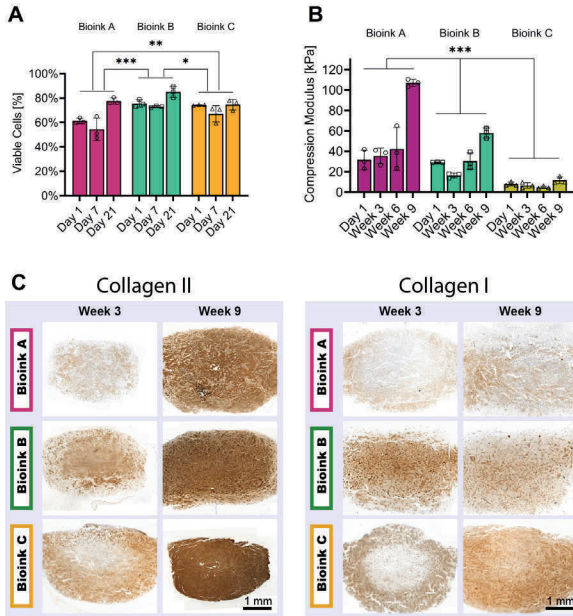


**Figure 2.5** (A) Viability of cells was investigated for the first 3 weeks with a fluorescent live/dead staining. (B) Profile of compression modulus over the measured timeframe. (C) Stainings for collagen type I and II of 3D bioprinted scaffolds containing human auricular chondrocytes. Samples were culture *in vitro* for up to 9 weeks.

It is striking, that only a minor net increase was observed over the first 6 weeks, but a doubling or even more potent increase in storage modulus was observed between week 6 and week 9 for all conditions (Bioink A:  $+199.9 \pm 125.6\%$ , Bioink B:  $+100.7 \pm 52.3\%$ , Bioink C:  $+157.5 \pm 98.3\%$ ). In absolute values however, compression modulus of Bioink C was dramatically lower than Bioink A and B. This came in effect already at day 1 and continued until the end of culture after 9 weeks.

While Bioink A and B started with comparable storage moduli, modulus of Bioink B dropped significantly at week 3 and recovered from this point on with a steady increase. On the other hand, storage modulus of Bioink A never

decreased, but increased slightly over the first 6 weeks with a sharp, significant increase between week 6 and week 9 ( $P < 0.001$ ). As a second parameter, deposition of extracellular matrix was measured. After 3 weeks of culture, faint stainings for collagens of both types were observed (**Figure 2.5C**). After 9 weeks of culture, strong stainings for collagen II and fainter stainings for collagen type I were observed for all conditions. Inhomogeneous stainings with a stronger stained outer ring and a fainter core section were prevalent for Bioink C.

In a last step, samples of all bioinks were implanted into a subcutaneous pocket of nude rats to evaluate stability of samples and chondrogenesis *in vivo*. Two types of samples were used in this experiment: small rectangular specimen with 3 replicates to investigate differences between bioinks as well as single large, ear shaped specimen of Bioink A and B to explore the feasibility to implant large constructs.

Small samples were either pre-cultured *in vitro* for 3 weeks prior to implantation or implanted directly after 3D bioprinting. After 1.5 months, rats were sacrificed to recover samples from the subcutaneous pocket. Upon sample recovery, it became apparent that major damage occurred to several samples with some samples being fractured and some samples not being recoverable. Bioink B had the most samples successfully retrieved after implantation with 5 of 6 total samples retrieved, followed by Bioink A with 4 of 6 samples and Bioink C with only 3 of 6 samples.

Recovered samples were fixed and further analyzed with histological stainings (**Figure 2.6A**). Samples without pre-culture in TGF- $\beta$ 1 supplemented media had suffered from structural damage and the initial square shape was not recognizable anymore. When precultured, samples from Bioink A and B conserved the shape of the originally printed structure. For Bioink C, only fragments of the original samples were recovered. Viable cells and staining for collagens was scarce in recovered samples. In Bioink B and C, only single, isolated cells with pericellular matrix deposition were found.

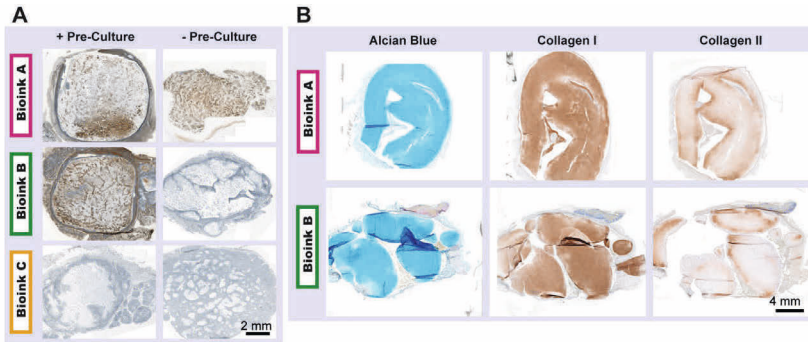


**Figure 2.6** (A) Immunohistochemical Collagen II staining of scaffolds retrieved after 6 weeks of maturation in a subcutaneous pocket of a nude rat with or without 3 weeks of *in vitro* preculture. (B) Histological stainings of 3D bioprinted, ear shaped grafts 3 months after subcutaneous implantation.

For samples from Bioink A, patches of viable cells with deposited collagens were found, but those patches only covered only approximately 10% of the total area.

Results of large, ear shaped scaffolds were in strong contrast. Scaffolds were successfully recovered, however, structural damage happened to samples of Bioink B. Larger fragments of the ear were still intact, allowing for histological staining and approximate identification of original regions (**Figure 2.6B**). Samples from both bioinks had strong staining for collagen type I that covered the full sample as well as a strong staining for collagen type II at the outer 0.5 – 1 mm of the sample with a faint staining in the center region.

## 2.4 Discussion

In this study we wanted to further advance bioinks for 3D bioprinting of cartilage tissue with a multipolymer approach. The bioinks prepared from alginate, gellan gum, hyaluronic acid and alginate-sulfate are versatile materials with mixed, yet promising outcome for 3D bioprinting. While all bioinks had excellent printing properties, strong and significant differences in mechanical and biological properties became apparent in this study. Addition of hyaluronic acid and or alginate-sulfate resulted in beneficial as well as detrimental effects. Phase separation in the center of 3D printed scaffolds was distinctive in 3D printed scaffolds of Bioink A. This effect could be reduced by preparation of this bioink with higher molecular weight alginate (Bioink A) and completely avoided with high molecular weight hyaluronic acid (Bioink B, Bioink C). A possible explanation for the phase separation might be in the extrusion process in which shear stress applied is not uniformly throughout the whole cross-section of the deposited filament but primarily at the edges. The longer chains of the high molecular weight molecules might be able to translate some of the stresses and therefore prevent separation of the polymer phases. Since this phenomenon seemed to be linked to the length of the polymer chains an even higher molecular weight alginate than the ones used in this study might have eliminated this problem. Unfortunately, there were no commercial alginates of the same purity, but with a higher polymer length available.

Bioinks with hyaluronic acid also had reduced feature loss during crosslinking. When samples from Bioink A were submerged in crosslinking solution, a dense shell of crosslinked alginate formed immediately on the outside of the sample. This shell hindered diffusion of ions into the center region that was therefore more slowly crosslinked which resulted in an irregular crosslinking profile that might have caused problems. Addition of HA probably interfered with the molecular assembly of alginate chains during crosslinking and therefore significantly weakened the mechanical properties of the crosslinked

construct. However, this interference might have led to a more loosely crosslinked outer shell and the occurrence of a pore network that might allow stronger diffusion of ions. This might be highly beneficial, since several studies have shown the advantage of macroporosity in tissue engineering as nutrient transport and gas exchange are dependent on diffusion alone.

Addition of hyaluronic acid also significantly increased viability of embedded cells and led to a dense extracellular matrix deposition resembling native, healthy cartilage with strong collagen type II deposition and minimal collagen type I. The pattern of matrix deposition in this bioink was also superior to the two other bioinks. Smooth, homogeneous deposition of matrix through the whole construct for histological stainings was observed for samples with bovine as well as human cells in Bioink 2, similar to healthy native cartilage.

Alginate sulfate in Bioink C allowed to load and retain TGF- $\beta$ 1 within in construct to supply this growth factor for chondrogenic maturation rather than constant supplementation in the culture media. However, this property could not be exploited to its full potential, as this bioink was significantly weaker in terms of compression modulus as well as long term stability.

Bioink B and C were both inferior in mechanical properties when compared to a Bioink A. This is especially critical when samples are transplanted into a mechanically challenging environment as it is the case for *in vivo*. Most *in vivo* samples of Bioink B and all samples from Bioink C showed structural damage, while samples from Bioink A kept their shape or had only minor damage. Small transplanted samples showed complete or nearly complete absence of initially embedded chondrocytes and extracellular matrix. Large, ear shaped samples on the other hand showed presence of cells and extracellular matrix deposition over the full thickness of the scaffold. This discrepancy between samples sizes cannot be linked to a clear factor but is rather ambiguous. Since samples were prepared in parallel with the same material batches and processes, batch to batch variations or contamination of



a reagent can be excluded. Amongst other possible reasons, the size of samples might have resulted in a different effective mechanical stress on the samples under the skin. A specific size might also be needed to trigger a vascularized fibrous capsule around the scaffold to ensure sufficient nutrient and gas exchange.

In summary, we presented and thoroughly characterized new multipolymer bioinks for extrusion 3D bioprinting. In this study we went from the initial design of a worthwhile polymer combination to the usual characterization done in the field all up to possible problems that might hinder a future translation to the clinics. With a static mixer system, we were able to reproducibly combine polymer and cells while even increasing viability of encapsulated cells. Endotoxin content of possible problematic microbial polysaccharides were tested and found to be below 0.1 ng/ml. This is in accordance with US Food and Drug Administration (FDA) requirements for medical products of less than 0.5 endotoxin units/ml, which equals approximately 0.1 ng/ml <sup>[213]</sup>.

In general, addition of HA and Alginate-sulfate greatly improved *in vitro* performance in these bioinks at the cost of *in vivo* performance. This emphasizes the importance of choosing the right model and the challenge of finding advanced bioink with great mechanical as well as biological properties. Since the best conditions *in vitro* are not necessarily the best *in vivo*, a delicate balance between sufficient testing *in vitro* and early *in vivo* tests has to be found.

Pre-culture time is another parameter that should be tuned according to mechanical properties. A relevant increase of mechanical properties was only observed after 9 weeks of pre-culture for all scaffolds while e.g. Bioink B had the lowest compression modulus at the time of transplantation (week 3). While this parameter is certainly dependent on the hydrogel system used, it would be valuable for the scientific community to find a minimum set of mechanical properties required to sustain the forces within a subcutaneous

pocket. It is also highly interesting to note that no clear correlation between compression moduli of samples and extracellular matrix deposition was found. While all samples had dense extracellular matrix deposition, mechanical properties greatly varied between the different bioinks even after 9 weeks. This indicates, that extracellular matrix alone is not sufficient for a relevant increase in mechanical properties. In native cartilage, collagens are bundled and arranged according to the mechanical stresses. Since no mechanical stimuli was presented to samples cultured *in vitro*, collagen fibrils in scaffolds might not be aligned and therefore lack mechanical properties. Reconstruction of collagen architecture might be one key aspect to tissue engineer cartilage tissue <sup>[217]</sup>. Future work should therefore not only consider the density of the deposited extracellular matrix, but also visualize the alignment of collagen fibers by either second harmonic generation or polarized light microscopy. A first experiment following up on this idea can be found in supplementary **Figure S2.4**.

## 2.5 Acknowledgments

I want to acknowledge the support of Clara Levinson and Emma Cavalli for their help and training in many scientific methods. Specifically, for teaching me the isolation of chondrocytes from native tissues and the basics of histology. Further, I want to thank the whole Tissue Engineering + Biofabrication lab for constructive feedback and criticism.

This work was supported by the Swiss National Science Foundation (Grant number: CR3213\_166052).

## 2.6 Supporting Information

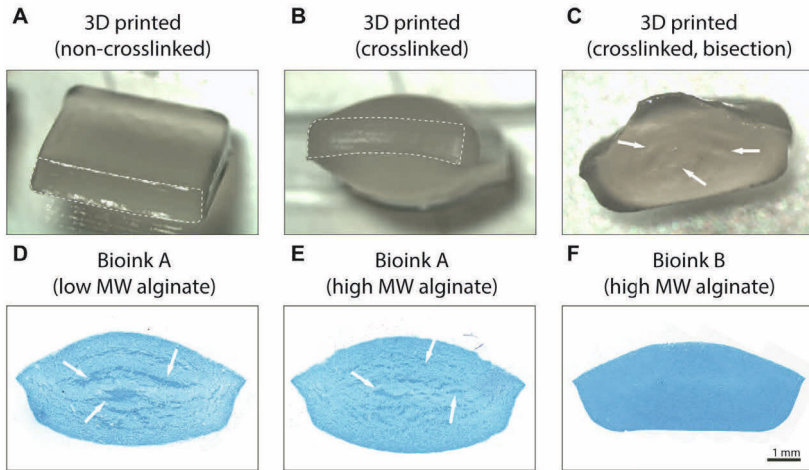


**Figure S2.1** Pictures of a sample after bioprinting (A), after crosslinking (B) and cut in half to reveal cross-section (C). Arrows indicate areas of phase separation. Alcian blue stainings of sections with phase separation of Bioink A prepared with low (D) and high (E) molecular weight alginate. (F) Section of Bioink B have no visible phase separation.

## Life/Dead Staining (Day 1)

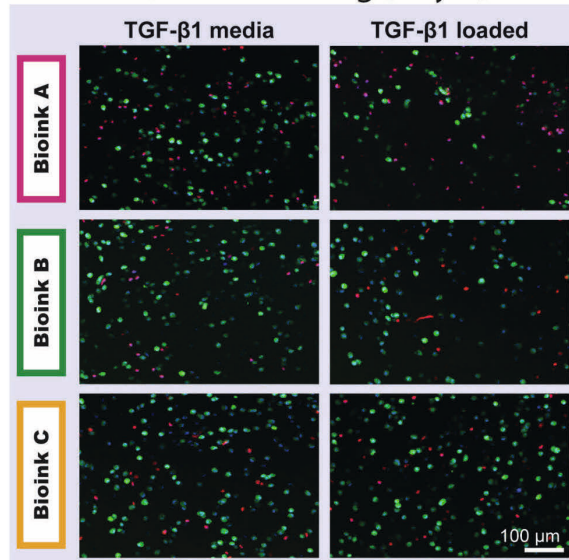


**Figure S2.2** Fluorescent viability stainings of samples 1 day after 3D bioprinting. Alive cells are stained green, dead cells are stained red and the nucleus of all cells is stained in blue.

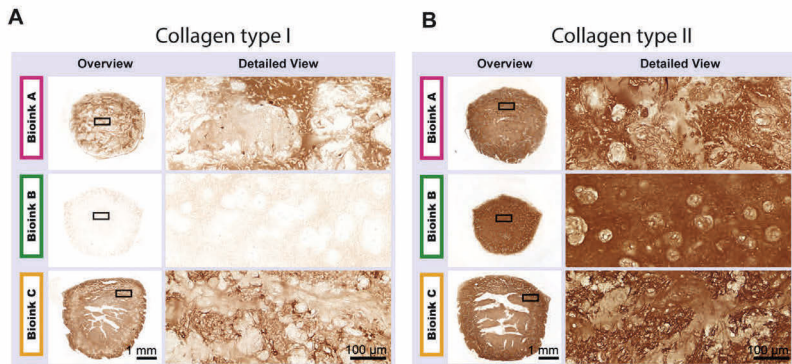


**Figure S2.3** Immunohistochemical stainings for collagen type I and II of representative samples depicting the complete sample as well as a close up area thereof

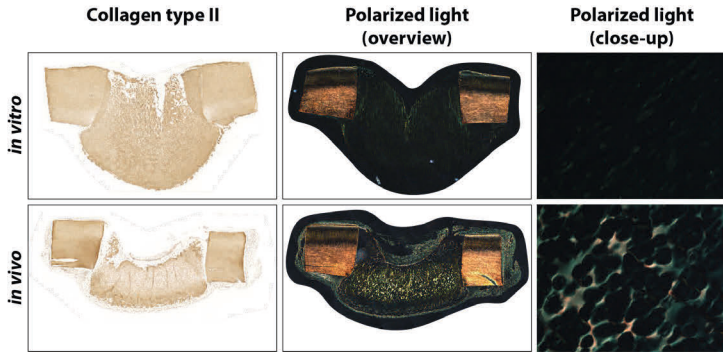


**Figure S2.4:** Polarized light can be employed to get information on the maturation status of a tissue engineered construct. HA-TG hydrogels were cultured in a cartilage plug and stained for collagen type II as well as picrosirius red. Polarized light microscopy was employed to visualize fiber formation in samples stained with picrosirius red. Even though *in vitro* cultured scaffolds have a strong staining for collagen type II, comparable to that of the cartilage plug, collagen did not mature into fibers. For *in vivo* samples, both, a strong antibody staining for collagen as well as fiber formation was observed.

**Code 1:** Macro to analyze fluorescent micrographs for stained cells with subsequent, automatic quantification

```
macro "Life / Dead "{
    input = getDirectory("Choose Source Directory ");
    output = getDirectory("Choose Destination Directory ");

    list = getFileList(input);
    setBatchMode(true);
    for (i = 0; i < list.length; i++)
        action(input, output, list[i]);
    function action(input, output, filename){
        run("Bio-Formats Windowless Importer", "open="+ input + filename);
        title=getTitle;
        getDimensions(w, h, channels, slices, frames);
        run("Z Project...", "stop=5 projection=[Max Intensity]");
        selectWindow(title);
        close();
        rename(title);
        run("8-bit");
        run("Split Channels");

//      PI Channel
        selectWindow("C1-"+title);
        run("Auto Local Threshold", "method=Phansalkar radius=10
parameter_1=0 parameter_2=0 white");
        run("Despeckle");
        run("Invert");
        run("Fill Holes");
        run("Watershed");
        run("Analyze Particles...", "size=15.00-250.00 circularity=0.40-1.00
show=Outlines clear summarize");
        save As("Tiff", output+"PI-"+title);
        close();

//      Calcein Channel
        selectWindow("C2-"+title);
        run("Auto Local Threshold", "method=Phansalkar radius=10
parameter_1=0 parameter_2=0 white");
        run("Despeckle");
        run("Invert");
        run("Fill Holes");
```

```
        run("Watershed");
        run("Analyze Particles...", "size=25.00-500.00 circularity=0.20-1.00
show=Outlines clear summarize");
        saveAs("Tiff", output+"Calcein-"+title);
        close();

//      Hoechst33342 Channel
        selectWindow("C3-"+title);
        run("Auto Local Threshold", "method=Phansalkar radius=10
parameter_1=0 parameter_2=0 white");
        run("Despeckle");
        run("Invert");
        run("Fill Holes");
        run("Watershed");
        run("Analyze Particles...", "size=15.00-250.00 circularity=0.40-1.00
show=Outlines clear summarize");
        saveAs("Tiff", output+"Hoechst33342-"+title);
        close();

    }
selectWindow("Summary");
saveAs("Results", output+"Summary.csv");
}
```



# Chapter III - 3D Bioprinting of Macroporous Materials Based on Entangled Hydrogel Microstrands

This study has been published in *Advanced Sciences* as: *3D Bioprinting of Macroporous Materials Based on Entangled Hydrogel Microstrands*, B. Kessel, M. Lee, A. Bonato, Y. Tinguely, E. Tosoratti, M. Zenobi-Wong. A previous version of this manuscript named “3D Bioprinting of Architected Hydrogels from Entangled Microstrands” is archived at [bioRxiv.org](https://doi.org/10.1002/advs.202001419)

<https://doi.org/10.1002/advs.202001419>

## Contributions

---

Benjamin Kessel, Mihyun Lee, Angela Bonatao and Marcy Zenobi-Wong designed the study. B. Kessel performed the research with help from M. Lee, A. Bonato, Yann Tinguely and Enrico Tosoratti. M. Lee acquired electron microscope pictures of entangled microstrands, A. Bonatao helped in design of schematics and experiments revolving around C2C12 cells, Y. Tinguely helped with general preparation of materials and conducted most mechanical measurements, E. Tosoratti assisted in set-up and execution of experiments. B. Kessel and M. Zenobi-Wong analyzed the data and wrote the manuscript.

## Abstract

Hydrogels are excellent mimetics of mammalian extracellular matrices and have found widespread use in tissue engineering. Nanoporosity of monolithic bulk hydrogels, however, limits mass transport of key biomolecules. Microgels used in 3D bioprinting achieve both custom shape and vastly improved permissivity to an array of cell functions, however spherical microbead based bioinks are challenging to upscale, are inherently isotropic and require secondary crosslinking. Here bioinks based on high aspect ratio, hydrogel microstrands are introduced to overcome these limitations. Pre-crosslinked, bulk hydrogels are deconstructed into microstrands by sizing through a grid with an aperture of 40-100  $\mu\text{m}$ . The microstrands are moldable and form a porous, entangled structure which is stable in aqueous medium without further crosslinking. Entangled microstrands have rheological properties characteristic of excellent bioinks for extrusion 3D bioprinting. Furthermore, individual microstrands align during extrusion and facilitate the alignment of myotubes. Cells could be placed either inside or outside of the hydrogel phase with >90% viability. Chondrocytes co-printed with the microstrands deposited abundant extracellular matrix, resulting in a modulus increase from 2.7 kPa to 780.2 kPa after 6 weeks of culture. This powerful approach to deconstruct bulk hydrogels into advanced bioinks is both scalable and versatile and represents an important toolbox for 3D bioprinting of architected hydrogels.

## 3.1 Introduction

Microextrusion 3D bioprinting has recently been used to create functional analogues of many tissues including myocardium, skeletal muscle, liver, skin, bone, and cartilage.<sup>[218]</sup> Importantly, *in vivo* evaluation of bioprinted constructs have shown key advantages compared to non-printed, control samples made from bulk materials.<sup>[143]</sup> The field has profited from a flurry of recent hardware and material advances, however existing bioinks still have critical limitations. A major challenge is to control their flow properties to enable reproducible and accurate bioprinting with full biocompatibility. Commonly, bioinks are prepared from a solution of hydrogel precursors whose rheological properties have been tuned so the bioink flows out of the nozzle as a continuous strand. The strands are then collected on a buildplate and stacked in a layer-by-layer fashion to create a 3D object. The challenge of extrusion bioprinting, referred to as a “race against instabilities”, is to prevent flow and preserve the fidelity of the print until it can be stabilized by crosslinking.<sup>[219]</sup>

To address the flow challenges of common bioinks, the field has resorted to a number of approaches. Increasing the polymer content of bioinks enhances printability, but the resulting densely crosslinked networked can affect cell viability and spreading.<sup>[220]</sup> Methods to print low content bioinks include 1) the addition of flow modifying fillers or additives 2) printing within a sacrificial support material 3) partially crosslinking the bioink before or during extrusion to increase yield stress, 4) templating using a rapidly crosslinkable material, often alginate and 5) sequential crosslinking of individual layers directly after deposition.<sup>[221-225]</sup> In general, stability of structures during printing is challenging given the high water content of most bioinks and the tendency of heavy and tall structures to sag under their weight.<sup>[226]</sup> To make matters more challenging, many approaches, which improve printability, have a detrimental effect on the biological properties of the material.<sup>[68]</sup> There is a pressing need for advanced bioinks which combine both excellent printing and bioactive properties.<sup>[214]</sup>

Microgel bioinks have been proposed as a promising strategy, which could fulfill both requirements.<sup>[145-146]</sup> To address the flow problem, microgel bioinks have the advantage that they are not liquids and have little intrinsic flow behavior. Such bioinks have inherent shear thinning and shear recovery properties based on weak particle-particle interactions which are disrupted during extrusion in the nozzle and reformed during the post-print phase.<sup>[223]</sup> When the microgels are ‘jammed’ into a close-pack state, they have moderate printing properties.<sup>[155]</sup> Simultaneously, due to the inherent void space between the microgels in a close-packed state, cells within these materials have enhanced viability, spreading and migration compared to bulk monolithic materials.<sup>[142, 144]</sup>

Current approaches to prepare spherical microgels for extrusion bioprinting and other biomedical applications include spraying, microfluidic, emulsion and stereolithography.<sup>[143]</sup> Despite many advantages, such approaches are still associated with important limitations, including poor scalability, the need for oils and additives and/or restriction to the use of low viscous polymer solutions. Another strong limitation of these approaches is related to the sphericity of the microgels themselves, as the close-packed lattice limits interaction between individual spheres and precludes any anisotropy of the printed material. Consequently, current microgel bioinks need to be secondarily crosslinked to be stable in aqueous media and do not provide important guidance cues to align cells of anisotropic tissues like muscle and tendon.

The use of high aspect ratio microgels has long been explored in tissue engineering. In fact, cell-laden hydrogel microfibers have been used as a potent building block.<sup>[227-228]</sup> In addition, the ability of elongated microgels has been shown to be useful in guidance of neurons.<sup>[229-230]</sup> Recently, scaffolds prepared from wet-spun micro-ribbons showed the possible advantages of anisotropic gels in cartilage engineering.<sup>[165]</sup> However, a facile and cell friendly method to produce large volumes of high-aspect ratio microgels is

needed. This paper presents a new class of microgels, termed entangled microstrands, which overcomes many of the disadvantages of spherical microgel materials and demonstrates the first use of elongated microgels in 3D bioprinting.

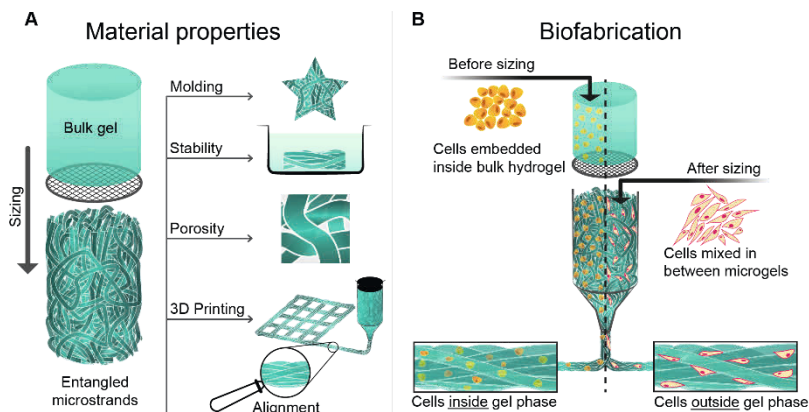


**Figure 3.1** Graphical abstract (A) Bulk hydrogel is mechanically extruded through a grid to deconstruct it into microstrands. In this process, microstrands randomly entangle with each other and form *entangled microstrands* a stable material with properties relevant for tissue engineering: mouldability, stability in aqueous solutions, porosity, printability and alignment of microstrands by extrusion. (B) A bioink can be prepared by embedding cells in bulk hydrogel before the sizing that results in a spatial deposition of cells inside the gel phase. Alternatively, cells can be mixed in between already prepared entangled microstrands, so cells occupy the space outside the gel phase.

Entangled microstrands were prepared by pressing a bulk hydrogel through a grid with micron-sized apertures to deconstruct the hydrogel into individual microstrands (**Figure 3.1A**). The production is fast, requires no specialized equipment and can be used with a wide range of hydrogels of arbitrary polymer content, composition, crosslinking chemistry and crosslinking density. Due to the simplicity of the production method, it can be upscaled to liter volumes. The void space between strands forms an interconnected porous network and entangled microstrands exhibit long term stability in aqueous solutions, even without secondary crosslinking. The material is moldable and

exhibits all relevant rheological properties for 3D bioprinting. Furthermore, cells can be included in the bulk gel or added to the individual microstrands during printing (**Figure 3.1B**). High fidelity 3D printing could be achieved with a wide range of materials, even with polymer concentrations that typically require the use of support baths or additives to be printable. Finally, we demonstrate the power of this approach for tissue engineering by 3D bioprinting chondrocytes and hyaluronan hydrogel microstrand and showing the *in vitro* maturation of these constructs into a tissue with mechanical properties approaching that of native cartilage.

## 3.2 Materials and Methods

All chemicals were purchased from Sigma-Aldrich unless stated otherwise.

### *Hyaluronic Acid Methacrylate (HA-MA)*

Hyaluronic acid (1 gram, HTL Biotechnology) was dissolved in ultrapure water (400 ml) and kept at 4°C overnight to ensure complete dissolution. Ice-cold DMF (267 ml) was added under continuous stirring. To start the reaction methacrylic anhydride (2370  $\mu$ l) was added and the pH kept between 8 - 9 through the addition of 10 M NaOH for 4 hours. Solid sodium chloride was dissolved in the solution to achieve a concentration of 0.5 M and the polymer was subsequently precipitated with ethanol (Merck). The precipitate was washed with ethanol, dried and dissolved in ultrapure water. Solution was purified by diafiltration (Äkta 3, 10 NMWC hollow fiber). The purified product, hyaluronic acid methacrylate (HA-MA) was lyophilized dissolved in deuterium (Cambridge Isotope Laboratories) and characterized by  $^1\text{H}$  NMR spectroscopy and stored at -20°C in the dark until used.

NMR spectra were recorded at room temperature on a Bruker AV-NEO 600 MHz spectrometer equipped with a TCI cryo probe. Spectra were obtained with 1024 scans using a 5 s recycle delay. To determine the degree of substitution, we compared the ratio of the sum of the integrated peaks of the methacrylate protons (peaks at ~6.1 and ~5.6) and the integrated peak of the methyl protons of HA (~1.9 ppm). For gel preparation, HA-MA was dispersed in PBS and kept at 4°C until complete dissolution. HA-MA solution was mixed with a 1% lithium phenyl-2,4,6-trimethylbenzoylphosphinate (LAP) stock solution to create a 2% HA-MA and 0.05% LAP solution and crosslinked by controlled photoexposure in the UV-A range (Omniscure Series 100, 400 nm wavelength, 9.55 mW  $\text{cm}^{-1}$ ).

### *Gelatin Methacryloyl (GelMA)*

Gelatin type A was dissolved in PBS at pH 7.4 and warmed up to 50°C under vigorous stirring. Total used MA volume was split into five and after every addition, pH was adjusted with NaOH and the solution left to react for 30 minutes. After the last addition, reaction was diluted 2 fold and left to react for another 30 minutes. Product was cleaned by subsequent dialysis (10-12 kDa Cutoff) against ultrapure water for 4 days. Solution was filtered, lyophilized and stored at -20°C until use. For gel preparation, GelMA and gelatin was dissolved in 70°C hot PBS. GelMA solution was mixed with LAP stock solution (1%) to achieve a final concentration of 2% GelMA, 2% gelatin and 0.05% LAP. Bulk gel was formed through thermoreversible gelation and sized into microstrands. To ensure stability in cell culture at 37°C, microstrands were photocrosslinked by controlled photoexposure in the UV-A range.

### *Hyaluronic acid transglutaminase (HA-TG)*

For HA-TG hydrogel precursors, two different batches of HA were substituted with reactive glutamine (HA-TG/Gln) and lysine (HA-TG/Lys) residues respectively following published protocols <sup>[19c]</sup>. For gel preparation, HA-TG/Lys and HA-TG/Gln were dissolved in TBS buffer (150 mM NaCl, 40 mM CaCl<sub>2</sub>, 50 mM TRIS, pH 7.6) and combined at equal volume to form HA-TG solution. To initiate gelation, a solution of thrombin (Baxter, 500 U ml<sup>-1</sup>) and factor XIII (Fibrogammin, CSL Behring, 200 U ml<sup>-1</sup>) was added to form a gel with final concentrations of 3% HA-TG.

### *t-carrageenan (t-CRG)*

300 mg of *t*-carrageenan particles (Genuvisco CG-131, GP Kelco) were added to 4°C cold buffer solution (10 ml, 150 mM KCl, 20 mM HEPES, pH 7.4) to allow hydration of particles. Dispersion was then heated to 80°C, stirred until complete dissolution, and transferred into a 10 ml syringe. Solution was cooled down and stored at 4°C to form a 3% (w/v) gel.



### *Gelatin*

Gelatin particles from porcine skin (type A, 300 mg) were added to 4°C cold PBS (10 ml) and left to hydrate for 15 minutes with subsequent heating to 70°C until complete dissolution. The solution was transferred into a 10 ml syringe and cooled down to 4°C to form a 3% (w/v) bulk gel. To ensure reproducible results, gelatin solution was stored at 4°C for 24 h to minimize variances due to the hardening of gelatin gels.

### *Hyaluronic acid divinyl sulfone (HA-DVS)*

A solution of 3% (w/v) hyaluronic acid, 3% (w/v) NaCl and 0.2 M NaOH was prepared and stirred vigorously until complete dissolution of hyaluronic acid. Double the amount of divinylsulfone was added to the hyaluronic acid (w/w). Solution was mixed to ensure a homogeneous distribution and left to gel for 3 hours at room temperature. Gel was then washed for 2 days in deionized water and used for experiments.

### *Carbodiimide crosslinked collagen (Collagen-EDC)*

Two different concentrations of Type I collagen solution (5 mg ml<sup>-1</sup>, Symatase; 80 mg ml<sup>-1</sup>, 3dbio) were mixed on ice to achieve a final concentration of 20 mg ml<sup>-1</sup>. An equal amount (w/w) of 3,3'-Dithiobis(propionohydrazide) (DTPHY) was directly dissolved in this solution and 6 times excess of 1-Ethyl-3-(3-dimethylaminopropyl)carbodiimide (EDC) was first dissolved in MES buffer and subsequently added to the solution. Solution was mixed and left to react at 4°C over night to form a stable gel.

### *Deconstruction of Bulk Gels into Microstrands (sizing)*

To prepare entangled microstrands, bulk hydrogels were prepared inside a 10 ml syringe and manually pressed through a nylon sieve (Millipore, Filter code: NY41 for 40 µm, NY1H for 100 µm) and directly used for experiments.

### *Rheology*

To assess rheological properties of the samples, all measurements were conducted on an Anton Paar MCT 301 rheometer equipped with a 20 mm parallel plate geometry at 25°C in a humid atmosphere with a gap distance of 1 mm. Rheological properties of samples were examined by oscillatory shear sweeps (1% strain, 1-100 Hz), ramped shear rate (0.01 – 50 s<sup>-1</sup>) and strain sweeps (1 Hz, 0.01-1% strain) to evaluate storage and loss modulus, yield point and shear thinning behavior. To investigate shear recovery properties, samples were exposed to repeating cycles of alternating phases of strain (1 Hz, 1% and 500% strain).

### *Compression modulus measurements*

Disc shaped test specimen with 8 mm diameter and 2 mm height were stamped out of the bulk gel for acellular samples. For cellular samples, bioprinted constructs were used and exact dimension measured before testing. Samples were tested by unconfined compression using a texture analyzer (TA.XTplus, Stable Microsystems). A 500 g load cell and a flat plate probe with a diameter of 15 mm were used. Samples were compressed to a final strain of 15% at a rate of 0.01 mm s<sup>-1</sup>. The compression modulus was calculated from the slope of the linear first 3% of the stress-strain curve.

### *Elastic Modulus*

Bulk gels with defined crosslinking were prepared and dumbbell shaped specimens according to ISO 527-2-5B were stamped out. Specimen were attached in a custom clamp system, and elongated until failure at a rate of 0.01 mm s<sup>-1</sup>.

### *Swelling*

Bulk hydrogel discs were prepared and weighted before immersion in PBS to induce swelling. For each time point, samples were removed from the PBS,

blotted with a tissue to remove excess PBS and weighted. The degree of swelling was calculated using following equation.

$$\text{degree of swelling [\%]} = \frac{(\text{mass of swollen gel}) - (\text{mass of dried gel})}{(\text{mass of dried gel})} * 100$$

### *3D Printing*

Entangled microstrands were loaded into printing cartridges (Nordson EFD) and printed through a 410  $\mu\text{m}$  conical needle (Nordson EFD) with a pneumatic driven extrusion 3D bioprinter (3D Discovery, RegenHU). 3D models for grid and disc structures were created with OpenSCAD version 2015.03-2. 3D models were processed with Slic3r version 1.3.0 dev to create machine code (G-Code).

### *Scanning electron microscopy (SEM)*

Entangled microstrands were extruded as straight lines through a 410  $\mu\text{m}$  conical needle and collected on a glass plate. Bulk HA-MA hydrogel and freshly prepared entangled microstrands were also prepared as control. All samples were frozen in liquid nitrogen and lyophilized. For SEM analyses, the lyophilized samples were coated using Pt/Pd (80/20) at a thickness of 10 nm by a sputter coater (CCU-010 HV, Safematic). The imaging was performed using a SEM instrument (JSM-7100, JEOL).

### *Macroporosity*

Entangled inks were prepared as described and submerged in PBS containing a high molecular weight, fluorescent FITC-dextran (average molecular weight of 500 kDa). Entangled microstrands were then imaged by two-photon microscopy (SP8, Leica).

### *Stability*

Entangled microstrands were prepared as described, cut into cylinders and transferred into well plates. Samples were submerged into PBS for up to 7

days and PBS was removed and exchanged after 5 min, 1 hour, 24 hours and 7 days.

*Cell laden microstrands (inside)*

C2C12 mouse immortalized myoblasts were obtained from ATCC. Cells were cultured in a humidified atmosphere (5% CO<sub>2</sub>, 37°C) in Dulbecco's modified Eagle's medium (DMEM GlutaMAX, Gibco) with fetal bovine serum (FBS, 10%, Gibco) and gentamycin sulfate (10 µg ml<sup>-1</sup>, Gibco). Cells were passaged at 90% confluence and detached by Trypsin/EDTA (0.25%, Gibco). Encapsulation solution (2% gelatin, 2% GelMA and 0.05% LAP) was prepared and kept at 37°C to avoid solidification. Freshly detached C2C12 were added to the solution and gently mixed by continuous pipetting to achieve a final concentration of 10 x 10<sup>6</sup> cells ml<sup>-1</sup>. After homogeneous distribution was achieved, solution was transferred into a syringe and cooled in an ice bath for 1 hour, while the syringe was constantly rotated for the first 5 minutes to avoid sedimentation. After gelation period, cell containing bulk gel was pressed through a nylon grid (sized), secondarily crosslinked by photoexposure in the UV-A range and kept in culture media. Cells were then cultured in differentiation medium composed of high glucose DMEM, insulin (1%), transferrin and selenium mix (ITS+, Corning) and horse serum (2%, Gibco) and gentamycin sulfate (10 µg ml<sup>-1</sup>). Medium was changed thrice a week.

*Bioprinting of entangled microstrands (outside)*

Primary articular chondrocytes were isolated from the femoral cartilage of 6 month old calves obtained from the local slaughterhouse. Cartilage from the medial and lateral condyle was harvested, minced and digested by collagenase solution (0.1%, from *Clostridium histolyticum*) over night. Cells were cultured in a humidified atmosphere (5% CO<sub>2</sub> at 37°C) and high glucose Dulbecco's modified Eagle's medium (DMEM, Gibco) supplemented with FBS (10%), L-ascorbic acid 2-phosphate sesquimagnesium salt hydrate (50 µg ml<sup>-1</sup>) and

gentamycin sulfate ( $10 \mu\text{g ml}^{-1}$ ). Cells were passaged at 90% confluence by detachment with trypsin/EDTA (0.25%) and used for experiments at passage 3.

To prepare bioink, entangled microstrands and dense solution of bovine chondrocytes ( $100 \times 10^6 \text{ cells ml}^{-1}$ ) were loaded in separate chambers of a double barrel syringe with a chamber ratio of 10:1 (Medmix). The two components were mixed by extrusion through a static mixing element (Medmix) to prepare cell-laden entangled microstrands. Bioink was transferred into a printing cartridge (Nordson EFD) and printed into discs ( $d = 5 \text{ mm}$ ,  $h = 2 \text{ mm}$ ). To ensure long-term shape fidelity, microstrands were annealed by UV-A exposure (15 s). Constructs were cultured in high glucose DMEM supplemented with ITS liquid media supplement (1%, Fisher Scientific), proline ( $40 \mu\text{g ml}^{-1}$ ), ascorbic acid ( $50 \mu\text{g ml}^{-1}$ ), gentamycin sulfate ( $10 \mu\text{g ml}^{-1}$ ) and TGF- $\beta$ 3 ( $10 \text{ ng ml}^{-1}$ , Preprotech) for up to 6 weeks with full media change three times a week.

#### *Live/Dead Staining*

Bioprinted constructs were cut in half, washed with phenol-free DMEM (Gibco) and stained with propidium iodide ( $0.5 \mu\text{g ml}^{-1}$ ), calcein AM (0.008 mM) and Hoechst 33342 ( $5 \mu\text{g ml}^{-1}$ ) for 20 minutes and imaged with fluorescent light microscopy (ZEISS, Axio Observer Z1). Z-stack images spanning  $100 \mu\text{m}$  were acquired from the center of the scaffold and analyzed with FIJI. Experiment was done in triplicates, with the viability of each sample averaged over three pictures of randomly chosen positions inside the center of the hydrogel.

#### *Histological evaluation*

Samples for histology were fixed in paraformaldehyde for 2 hours, dehydrated and paraffinized (LogosJ, Milestone). Paraffin blocks were cut with a microtome in  $5 \mu\text{m}$  thick sections, dried deparaffinized and hydrated. Tissue

sections were stained with SafraninO, hematoxylin and eosin (H&E), Picosirius red and Alizarin Red according to standard protocols.

For colorimetric, immunohistochemical stainings of collagen type I and II, sections were first digested in a hyaluronidase solution (1200 U ml<sup>-1</sup>, from *Streptococcus equi*) for 30 minutes at 37°C. Sections were then washed and blocked with normal goat serum (NGS, 5%) in PBS for 1 hour at room temperature. Subsequently, slides were blotted and primary antibody in NGS (1%) was added and left overnight in humidified atmosphere to avoid drying. Anti-collagen type I antibody (mouse, Abcam #ab6308) was used at 1:1500 dilution, while anti-collagen type II antibody (mouse, DSHB #II-II6B3) was used at 1:200 dilution. On the following day, sections were washed with PBS and treated with 0.3% H<sub>2</sub>O<sub>2</sub> to quench any endogenous peroxidase or pseudoperoxidase activity to prevent non-specific signals. After an additional washing step, secondary antibody (goat, anti-mouse IgG (HRP), Abcam #ab6789) in NGS (1%) solution was added and left under humidified atmosphere for 1 hour. Secondary antibody was removed by three washes in PBS and DAB substrate (ab64238, Abcam) was added and left to react for precisely 3 minutes. Sections were washed again and counterstained by Mayer's hematoxylin solution. All samples were mounted and coverslipped with resinous mounting media (Eukitt) before imaging with a Panoramic 250 histology slide scanner from 3D Histech.

### *Statistical analysis*

Statistical analysis was conducted with GraphPad Prism (v. 8.2.0 (425)) and statistical significance was assumed for  $P < 0.05$ . For acellular samples, storage modulus, elongation, compression and shear thinning between samples were compared with one-way analysis of variance (ANOVA) with a Tukey post hoc test. For swelling of samples, a mixed-effects model with Geisser Greenhouse correction was used.

The influence of mesh size and crosslinking degree on the formation of macroporosity was investigated with a two-way ANOVA. To analyze the

viability of encapsulated and bioprinted cells, one-way ANOVA was used. To compare viability of freshly trypsinized cells with encapsulated ones, an unpaired, two-tailed T-Test was conducted.

Mechanical properties of cellular, tissue engineered constructs were compared with a Brown-Forsythe and Welch ANOVA test due to unequal standard deviations. Additionally, Day 42 samples were compared to native cartilage with an unpaired, two tailed T-Test.

Mechanical properties of cellular, tissue engineered constructs were compared with a Brown-Forsythe and Welch ANOVA test due to unequal standard deviations. Additionally, Day 42 samples were compared to native cartilage with an unpaired, two tailed T-Test.

### 3.3 Results

#### Entangled Microstrands are Moldable, Stable in Water and Macroporous

Here we report a robust and versatile method for preparing ‘entangled’ microstrands using hyaluronan-methacrylate (HA-MA) as model system. Bulk HAMA hydrogels were mechanically pressed through a sieve with pores ranging from 40 to 100 microns. This process deconstructed the gel into microstrands, which randomly entangled within each other and made up a structured material consisting exclusively of high aspect ratio hydrogels. When a 2% bulk HA-MA (degree of substitution 0.28, UV-A exposure; **Figure S3.1**) was passed through a 40 micron sieve, this resulted in a macroporous material, which was visibly opaque and permeable to dyes (**Figure 3.2A,B; Movie S3.1**). When entangled microstrands were probed with forceps, single microstrands could be visualized (**Figure 3.2C**). Entangled microstrands were also deformable and moldable (**Figure 3.2D**). Secondary crosslinking of entangled microstrands (UV-A exposure) created a rigid, macroporous structure which could be handled with forceps (**Figure 3.2E,F**).

To investigate the tunability of entangled microstrands for 3D printing, a range of different HA-MA bulk gels were prepared. Crosslinking of HA-MA gels was terminated at three different time points, to create bulk hydrogels with a low (*Low*), medium (*Med*) and high (*High*) degrees of crosslinking (**Figure S3.2A**). These hydrogels had significantly different mechanical properties: storage moduli ( $F_{(2,24)} = 12164$ ,  $P < 0.001$ ), compression moduli ( $F_{(2,12)} = 34$ ,  $P < 0.001$ ), maximum elongation until rupture ( $F_{(2,6)} = 44.2$ ,  $P < 0.001$ ), and swelling behavior ( $F_{(2,14)} = 463.2$ ,  $P < 0.001$ ; **Table S3.1** and **Figure S3.2B-E**). These three distinctively different bulk hydrogels were then further processed by sizing them through nylon meshes of two different apertures (40 and 100 microns) to create a total of 6 different variants of entangled microstrands.



Entanglement of microstrands allowed for long-term cohesion in aqueous medium, when compared to repeatedly sized, granular microgels.

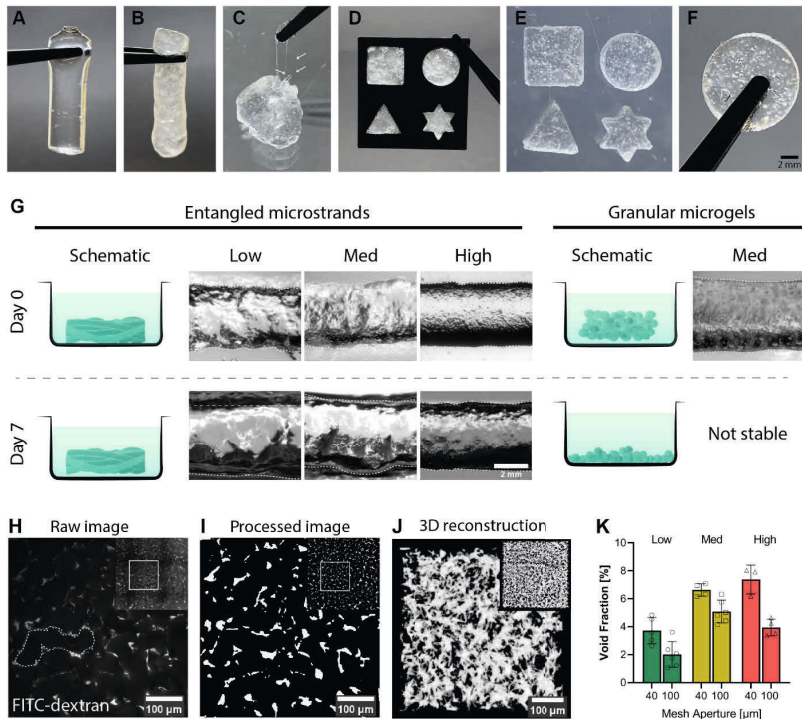


**Figure 3.2** Stability and macroporosity of entangled microstrands (A) crosslinked bulk HA-MA hydrogel (B) entangled microstrands prepared from such bulk hydrogel (C) when entangled microstrands are extended, single microstrands become visible (arrows) (D) entangled microstrands are mouldable (E) secondarily crosslinked custom shapes prepared by casting (F) secondary crosslinking tightly anneals microstrands (G) entangled microstrands show long-term stability in aqueous solution even without secondary crosslinking, while granular microgels loose cohesion and disintegrate (H) multiphoton image of entangled microstrands submerged in FITC-dextran (I) the same image after processing with a thresholding algorithm (J) 3D reconstruction of the porous network (K) Void fraction significantly varies with crosslinking density ( $F(2, 22) = 41.05$ ;  $P < 0.001$ ) as well as mesh size ( $F(1, 22) = 48.40$ ;  $P < 0.001$ )

To compare stability, entangled microstrands and granular microgels were extruded through the grid, submerged in PBS for up to 7 days at 37°C with constant agitation (**Figure 3.2G**). All six entangled microstrand materials (40 and 100 microns, *Low*, *Med*, *High* crosslinking) were stable for the entire period without secondary crosslinking, while all granular microgel materials based on the same hydrogels dissociated within 1 hour of incubation ( $n = 3$ ). Porosity is a critical property of materials employed in tissue engineering as this parameter strongly influences transport of nutrients, gas exchange and cell activity.<sup>[231-232]</sup> Pore size is also relevant for blood vessel infiltration as well as cell migration.<sup>[233-234]</sup> To assess the porosity of HA-MA entangled microstrands, freshly prepared entangled microstrands were submerged in a fluorescent high molecular weight dextran dye. **Figure 3.2H** shows a multiphoton image of the dye distribution taken within the central region of the structure. The void space and hydrogel strand could be clearly distinguished. The labeled dextran could enter the space between individual microstrands, but due to the high molecular weight, dextran was unable to penetrate the gel phase of the hydrogel. Since the dye was detectable within the central region and diffusion through the hydrogel microstrands was not possible, the pore space in between microstrands deemed to be interconnected. To calculate the void fraction of entangled microstrands, images were thresholded to achieve distinct transitions between microstrands and pores. An acquired image before and after processing can be seen in **Figure 3.2H,I**. A 3D reconstruction of the interconnected network can be seen in **Figure 3.2J** while a quantification of the void fraction is displayed in **Figure 3.2K**. Calculated void fractions ranged from  $2.0 \pm 0.8\%$  for the *Low* (100  $\mu\text{m}$ ) condition to  $7.4 \pm 0.9\%$  for *High* (40  $\mu\text{m}$ ). Void fraction significantly varied with crosslinking density ( $F_{(2,22)} = 41.05$ ,  $P < 0.001$ ) as well as mesh size ( $F_{(1,22)} = 48.40$ ,  $P < 0.001$ ).

## Entangled Microstrand have Shear Thinning/Recovery Properties and Clear Yield Points

Entangled microstrands exhibited all relevant rheological properties necessary for extrusion 3D (bio)printing. All prepared variants of entangled microstrands showed shear thinning behavior (**Figure 3.3A,B**). To identify the yield stress necessary to induce flow, different methods can be employed.<sup>[235-236]</sup> In this study we used the crossover of  $G'$  and  $G''$  to identify the flow point.<sup>[237]</sup> The required stress to reach crossover was lowest in *High* samples and highest in *Low* samples for both mesh apertures (40  $\mu\text{m}$ : *Low* = 450 Pa, *Med* = 409 Pa, *High* = 141 Pa; 100  $\mu\text{m}$ : *Low* = 659 Pa, *Med* = 559 Pa, *High* = 225 Pa, **Figure 3.3C,D**).

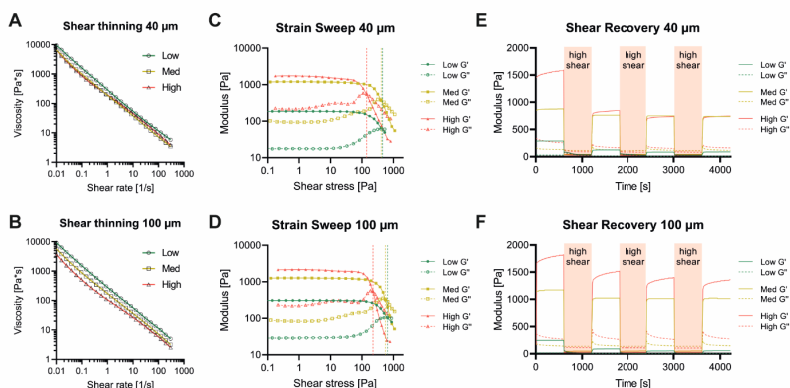


**Figure 3.3** Rheological characterization of HA-MA entangled microstrands (A - B) entangled microstrands created by sizing with a grid with aperture size of 40 and 100  $\mu\text{m}$  exhibit shear thinning behavior (C - D) clear flow points can be determined (Crossover points for 40  $\mu\text{m}$  samples: *Low* = 450 Pa, *Med* = 409 Pa, *High* = 141 Pa; 100  $\mu\text{m}$  samples *Low* = 659 Pa, *Med* = 559 Pa, *High* = 225 Pa) (E - F) when subjected to repeated cycles of low and high shear, shear thinning and shear recovery behavior can be observed for all conditions

To simulate the printing process, shear recovery tests based on oscillatory strain sweeps with cycles of high and low strain were conducted. At low strains, microstrands exhibited a solid-like elastic behavior ( $G' > G''$ ) that rapidly changed into a viscous liquid-like behavior ( $G' < G''$ ) when high

strains were applied (**Figure 3.3E,F**). These transitions are crucial for high quality 3D printing as it ensures even material flow during extrusion and shape retention upon deposition on the collector plate.

### **Entangled Microstrands have Excellent Printability and form Anisotropic Structures when Printed**

Two-layered grid structures were printed with entangled microstrands prepared from HA-MA (**Figure 3.4A**). All six variants were printed with good shape retention and printing resolution. Anomalies arose for lower crosslinked samples when sharp edges were printed. This phenomenon was especially pronounced in *Low* (40  $\mu\text{m}$ ) samples where sharp edges of the model printed with a very rounded appearance and the filament was dragged away during printing. This problem could be explained by the higher mechanical strength of the microstrands compared to that of a typical polymer solution. In typical bioinks, deposited filaments and the reservoir within the printing nozzle are separated as soon as the printing head retracts. In *Low* microstrand samples, however, microstrands spanned the distance between the printed construct and the printing nozzle. This connection did not rupture right away, but instead the deposited filaments were slightly dragged to the new printing position. Since the more crosslinked samples *Med* and *High* were more brittle and ruptured at lower elongation distances, the printing accuracy was higher in these samples.

Since all variants of microstrands prepared from HA-MA were successfully printed, we investigated the versatility of the approach by using other hydrogel systems commonly used in tissue engineering and 3D culture. The tested systems included gelatin, a thermoresponsive denatured form of collagen together with its photoresponsive derivative, gelatin-methacrylol (gelMA), iota-carrageenan, a highly sulfated polysaccharide that forms ionic crosslinks upon addition of monovalent as well as divalent cations, and enzymatically or chemically crosslinked hyaluronan hydrogels.<sup>[106, 238-240]</sup> Finally, collagen, a material prevalent in tissue engineering because of its

abundance in the extracellular matrix of many tissues, was crosslinked with carbodiimide chemistry and tested.<sup>[241]</sup> Although derived from a wide range of materials and crosslinking methods, all bulk hydrogels were successfully sized and the entangled microstrands could be 3D printed according to the grid model used for the HA-MA microstrands (**Figure 3.4B-E**).

In a next step, we explored the potential of microstrands by bioprinting large, complex constructs. A biologically relevant structure was printed with entangled microstrands prepared from bulk carrageenan (ear, **Figure 3.4F-H**). This 3D model represents a human ear printed at 50% size and demonstrates the power of this approach to create macro-sized scaffolds (28 x 14 x 7 mm). Printed structures were stable and no flow of the bioink was observed, even after 15 layers were stacked in z-direction. Moreover, individual layers and deposited filaments remained visible and clearly mirrored the printing path created by the slicing software (**Figure 3.4H**).

Anisotropy in tissues like muscle, tendon or nerves is difficult to replicate with conventional tissue engineering approaches. Several studies have shown the possibility to align (nano-)fibers and anisotropic particles with the direction of flow.<sup>[242-244]</sup> Extruded microstrands showed alignment with 3D printing, as observed after HA-MA microstrands were extruded through a 410 micron conical printing nozzle and imaged with scanning electron microscopy (**Figure 3.4I**). Clear differences between bulk gel and microstrands (pre- and post-printed) were apparent. Bulk hydrogels had an even surface, whereas microstrands before printing were randomly entangled within each other and had no clear orientation. Extrusion through a nozzle oriented the microstrands and post-printing, microstrands were aligned in the direction of printing.

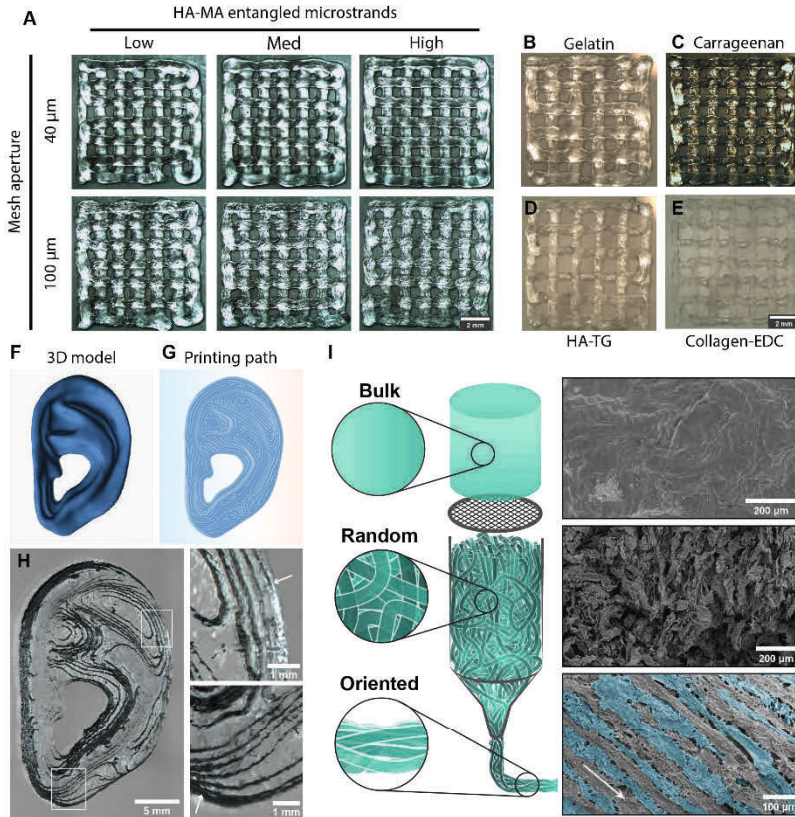


**Figure 3.4** Entangled microstrands are printable and align during extrusion (A) Different HA-MA entangled microstrands printed in a grid structure (B) Entangled microstrands prepared and printed from i-carrageenan (ionic crosslinking), (C) gelatin (thermal crosslinking), (D) HA-TG (enzymatic crosslinking), (E) Collagen-EDC (carbodiimide crosslinking) (F) 3D model and (G) printing path of a human shaped ear (H) 3D-printed with entangled microstrands prepared from carrageenan (arrows point toward sharp transitions between layers) (I) SEM images of bulk gel, freshly prepared entangled microstrands in random orientation and aligned microstrands after extrusion through a printing nozzle (arrow indicates the direction of extrusion).

### Cellular Entangled Microstrands Lead to Rapid Tissue Maturation

To explore the potential for 3D bioprinting with entangled microstrands, two possible cell delivery approaches were investigated (Fig 1B). Firstly, cells were embedded inside the bulk hydrogel before the hydrogel was sized into microstrands to create cell-laden microstrands (*Inside*). Alternatively, entangled microstrands were mixed with a cell suspension, leaving cells to occupy the void space between microstrands (*Outside*).

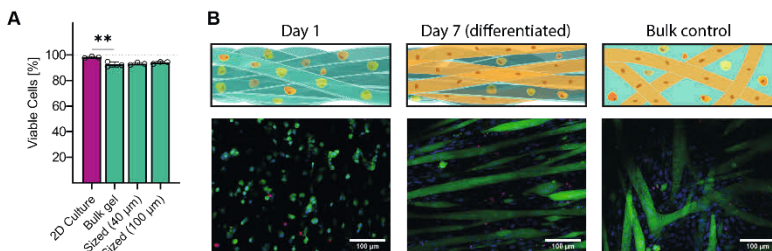


**Figure 3.5** Microstrands can trigger aligned myotube formation (A) C2C12 could be embedded in bulk hydrogel and subsequently sized into cell-laden microstrands without negative impact on viability. Fluorescent images of cell-laden entangled microstrands bioink (green = alive, red = dead) show a healthy population of cells and quantification reveal a significant, but minor drop on viability when cells are encapsulated but not when sized through the grid. (B) After differentiation, cell fusion and aligned myotube formation could be observed.

For anisotropic tissues like muscles, the *Inside* approach enables to confine cells within the gel microstrand and give orientation during tissue maturation. As a first proof of principle, C2C12 cells were embedded within a bulk gel of 2% gelatin and 2% GelMA, and subsequently sized (Cells inside gel phase). A significant, but minor drop of viability was observed for cells embedded in bulk hydrogel compared to freshly trypsinized cells (**Figure 3.5A**, 2D  $98.2 \pm 0.6\%$ ; Bulk =  $92.6 \pm 1.6\%$ ; T (4) = 4.6,  $P < 0.01$ ). The viability of cells in hydrogels that have been sized into entangled microstrands was high ( $40 \mu\text{m} = 93.2 \pm 0.8\%$ ,  $100 \mu\text{m} = 94.1 \pm 0.7\%$ ) and no significant difference in viability was found between either of the sized samples and the bulk gel controls ( $F_{(2,6)} = 0.96$ ,  $P = 0.443$ ). Differentiation media was added to trigger myotube formation of cultured C2C12 cells and subsequent cytoplasmic Calcein AM



staining revealed cell fusion and formation of myotubes aligned with the orientation of entangled microstrands (**Figure 3.5B**).

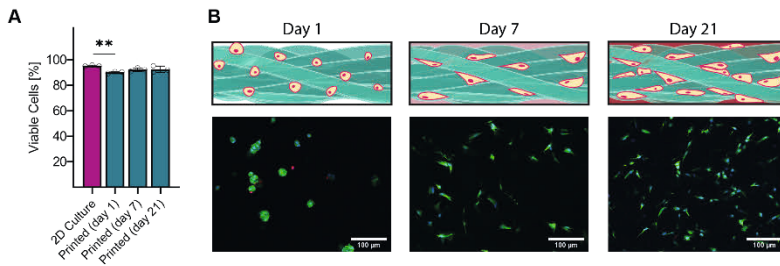


**Figure 3.6** Entangled microstrands allow 3D bioprinting with high cell viability (**A**) Chondrocytes could be mixed with already prepared entangled microstrands (outside) and 3D bioprinted with minimal impact on cell viability. (**B**) Fluorescent images showed high viability of cells after the printing process and cells adhering to the outer surface of entangled microstrands. Chondrocytes occupied and proliferated in the void space between microstrands at Day 7 and Day 21.

In the *outside* approach, cells were present within the void fraction of the entangled microstrands and not embedded within the polymer network of the hydrogel itself. In this case, cells were less confined, since they were able to utilize the porous network to migrate, proliferate and deposit extracellular matrix. The *outside* approach was used to engineer de novo cartilage tissue. Bovine chondrocytes were combined with HA-MA microstrands and 3D bioprinted into cylindrical discs. Cell viability was above 90% for the entire duration of the experiment (**Figure 3.6A**, Pre-printing =  $95.3 \pm 0.5\%$ ; Day 1 =  $90.1 \pm 0.6\%$ ; Day 7 =  $92.3 \pm 1.1\%$ , Day 21 =  $92.6 \pm 2\%$ ). Even though there was a significant drop in cell viability when bioprinted cells were compared to the original cell population ( $T(4) = 9.6$ ,  $P < 0.001$ ), cell viability decreased by only  $5.2 \pm 1.2\%$  (Pre-Printing to Day 0). Cell viability remained high and no statistical difference in viability was found between printed cells at day 1, 7 and 21 ( $F(2,6) = 1.873$ ,  $P = 0.233$ ). In the fluorescent Live/Dead staining, chondrocytes showed a rounded phenotype after 3D bioprinting, but proliferated and displayed a more elongated phenotype after 7 and 21 days in culture (**Figure 3.6B**).



Immediately after fabrication, bioprinted scaffolds were transparent and slightly opaque. After 6 weeks of culture, the discs appeared cartilage-like and white, indicating deposition of a dense extracellular matrix (**Figure 3.7B**). To confirm this, cultured tissue constructs were fixed and histologically stained for cartilage specific markers. A representative sample ( $n = 6$ ) is depicted in **Figure 3.7D**. Staining with Safranin O showed an increased intensity with time, indicating strong proteoglycan content in the samples. Staining with Hematoxylin & Eosin (H&E) resulted in a contrast between stained cells and unstained entangled microstrands. While high levels of collagen type I were detected 3 weeks after fabrication, collagen type I staining was reduced after 6 weeks of maturation. Collagen type II was present after 3 weeks but restricted to the void space in between microstrands. After 6 weeks of culture, collagen II staining intensified and showed deposition inside the void space, as well as the hydrogel network of the entangled microstrands. The difference in staining between time-points was particularly striking in the outer  $\sim 400$   $\mu\text{m}$  of the sample. After 3 weeks, staining for cartilage-ECM markers as well as abundance of cells in the outer area of the sample was lower compared to the central part of the scaffold. This distribution was reversed after 6 weeks of culture as there was a very dense deposition of ECM as well as cells in the outermost part of the scaffold. At the week 6 time-point, cells in the outermost part did not show the initial pattern of thin lines and small clusters also found in Live/Dead staining anymore but had a more homogeneous distribution. This suggests that cells were able to migrate into the space previously occupied by the hydrogel microstrands.

The mechanical properties of cartilage tissue are highly important for its functions, especially the crucial ability to sustain load. Compression modulus of freshly bioprinted samples was very low ( $2.7 \pm 0.3$  kPa) but showed a significant increase over time ( $F^*_{(2,15)} = 44.38$ ,  $P < 0.001$ ), reaching  $212 \pm 83.7$  kPa after 3 weeks and  $780.2 \pm 218.4$  kPa after 6 weeks (**Figure 3.7C**). While this was still significantly lower when compared to native articular bovine cartilage which has a compression modulus of  $1829.8 \pm 72$  kPa ( $T(10) = 10.2$ ,

$P < 0.001$ ), this is a remarkable increase. Since the material used in this study had very little resistance to compression on its own, change in compression modulus could exclusively attributed to the abundant deposition and maturation of extracellular matrix

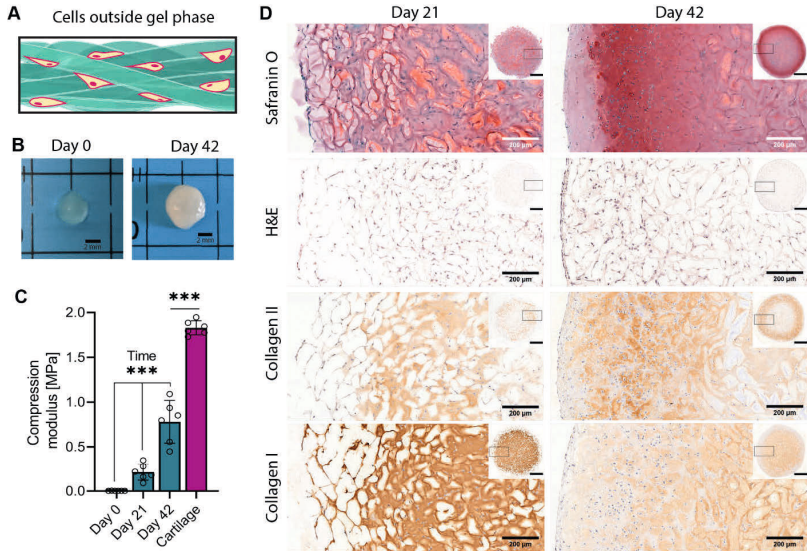


**Figure 3.7** Entangled microstrands mature into cartilage-like tissue (A) In this experiment, bovine chondrocytes were mixed with already prepared HA-MA microstrands (B) appearance of 3D bioprinted discs changed from transparent (day 0) to shiny-white (day 42) (C) comparison of compression modulus of freshly bioprinted entangled microstrands, after *in vitro* culture and healthy articular cartilage (D) histological staining to highlight the strong deposition of cartilaginous matrix entangled microstrand scaffold directly after printing and after 6 weeks of culture

### 3.4 Discussion

Advanced bioinks that excel at both biofabrication and cell compatibility are needed to address the challenges in the field of 3D bioprinting.<sup>[214]</sup> Prior studies and recent reviews have documented the strength and potential of microgels for tissue engineering.<sup>[142-143, 163-164, 167]</sup> However, production of microgels with conventional methods is challenging and limited by the materials which can be used. In this study, we demonstrated a simple and effective approach to deconstruct bulk gels into entangled microstrands which allows preparation of microgels in large quantities from many types of hydrogels. The facile preparation method allows the translation to most hydrogels used in tissue engineering.

Entangled microstrands can be 3D printed into constructs, closely mirroring the desired printing path. Since microstrands are solid elements, flow of microstrands after deposition on the buildplate is minimal. This can greatly increase resolution of printed constructs, especially with regards to multilayer constructs or sharp edges, in which cohesive forces cause layers of liquid bioinks flow into each other. Additionally, first demonstration of extrusion-driven alignment of entangled microstrands was shown. These aligned hydrogel strands were effective cues which allowed embedded C2C12 cells to form oriented myotubes. Creation of relevant alignment in tissue engineering is critical for the creation of anisotropic structures like muscles, tendons and nerves. Realization with spherical microgels, however, is extremely challenging, as this requires manipulation of the arrangements of microgels at a level, which has not been demonstrated yet.

First results of entangled microstrands as a platform for tissue engineering have been promising. Two distinct ways to prepare cell-laden bioinks were demonstrated: inside the gel phase and within the porous network outside the gel phase. Both methods yielded a remarkable percentage of viable cells for a microextrusion-based approach, especially when compared to other extrusion

based biofabrication methods.<sup>[64]</sup> This is also true when directly compared to alternative microgel techniques, in which cells are encapsulated within hydrogel microbeads. Although cells are protected from shear stress in such a setup and no drop in viability is observed after 3D bioprinting, microfluidic preparation impairs viability at similar or greater levels and usually results in reported viabilities of 70-90%.<sup>[145-146]</sup> Cell-laden microstrands were also able to mature towards functional tissue. In an approach to create cartilage tissue, chondrocytes were incorporated in the void space between entangled microstrands, which they utilized to proliferate and deposit extracellular matrix. The abundant cartilaginous extracellular matrix deposited translated into a significant increase in stiffness, approaching that of native articular cartilage.

Even though successful maturation of tissues was shown, some aspects of this approach still offer room for improvements. The void fraction of the entangled microstrands was significantly lower compared to scaffolds based on spherical microgels.<sup>[159-160]</sup> Even though our data shows that an interconnected network was formed that cells could utilize, some tissues might benefit from an increased void fraction. For such tissues, tuning of the pores would be possible. Indeed, grids used in this study could be substituted by photo-etched metal plates with apertures of custom cross section e.g. star shaped, to further increase distance between microgels or modulate the 3D environment. Further limitations of the method are that tough and/or fibrillar hydrogels like externally crosslinked alginate were difficult to size. Hydrogels whose breaking strength is higher than their water retention capability, are squeezed rather than cut into microgels.

Entangled microstrands, like microbeads, are compatible with a multimaterial approach. Two paths forward to introduce heterogeneity into the method are envisioned, either using a starting bulk gel based on multiple polymers (either homogeneously mixed or compartmentalized within the bulk) or by mixing microstrands prepared from different bulk gels. The first would allow double

network microstrands and double polymer systems in which only one sacrificial polymer (e.g. gelatin) is crosslinked and sized, while the other could be crosslinked at a later stage. In the second option, microstrands with differing mechanical properties or biological cargo could be combined to create precisely tuned bioinks for specific applications. This would also allow the creation of sacrificial microstrands to counter the limited void fraction compared to spherical microgel systems. Even though a homogeneous mixture of different microstrands without any damage to the material might be challenging to prepare, multi-barrel syringes with intricate outlets could solve this problem. Such system would greatly benefit from an in-line preparation, in which a bulk gel is automatically cut into microstrands and directly fed into an extrusion device. This would open the possibilities for an interchangeable printhead, compatible with current 3D bioprinters to further increase the ease of usability.

It should be acknowledged that this work is a first exploration of the potential of entangled microstrands. Further research and analysis is required to develop this approach and resolve the problems and challenges faced in the development of advanced bioinks. The simplicity and universality of this method though, provides an invaluable tool to the scientific community to create microstrand bioinks with unlimited material versatility upon which novel architected hydrogels are possible.

## 3.5 Acknowledgments

We want to thank Dr. Alvar Diego Gossert and Philipp Rössler for their help with the NMR-spectra acquisition. We also want to thank David Fercher, Dominic Rütische and Riccardo Rizzo for their help in the preparation and synthesis of HA-TG, Collagen-EDC and GelMA.

This work was supported by the Swiss National Science Foundation (Grant number: CR3213\_166052).

## 3.6 Supporting Information

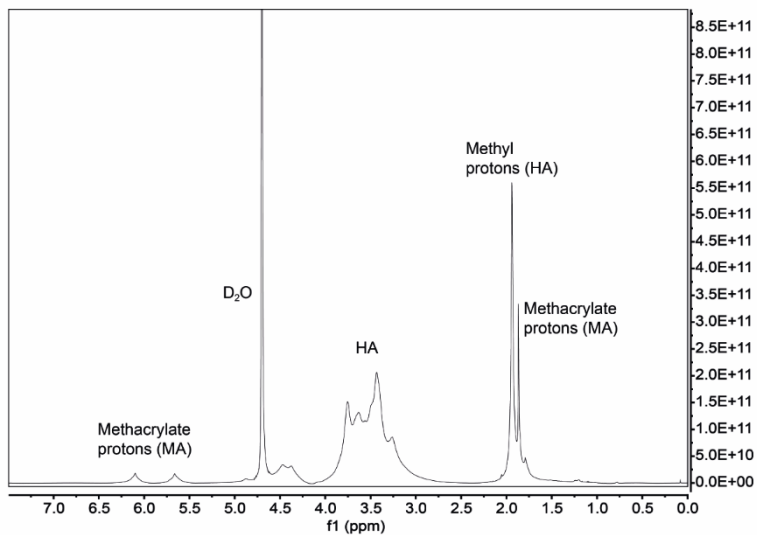


**Figure S3.1** NMR spectra of synthesized HA-MA

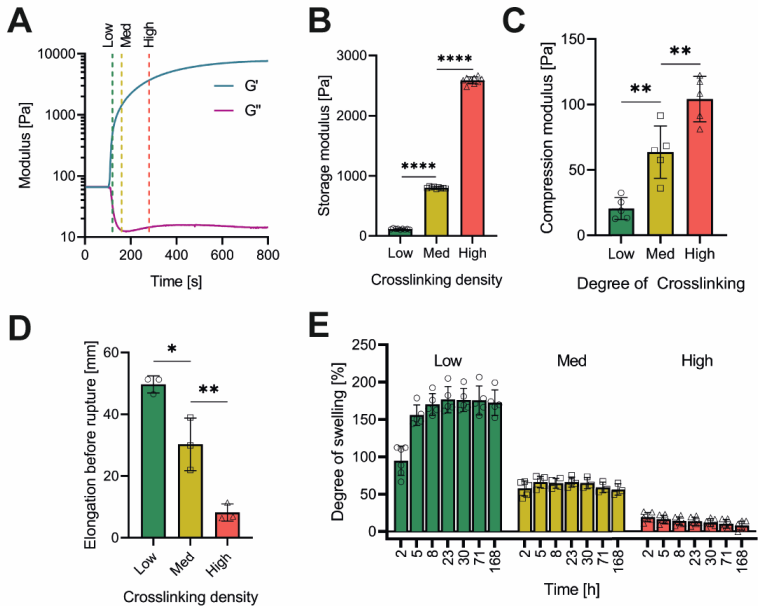


**Figure S3.2** Mechanical properties of HA-MA gels (A) Photocrosslinking behavior of HA-MA with three different time points representing different degrees of crosslinking (Low, Med, High) (B) Storage modulus significantly differs between samples ( $F(2,24) = 12164, P < 0.001$ ) (C) Compression modulus between these samples is significantly different ( $F(2,12) = 34, P < 0.001$ ) (D) Rupture of a dumbbell shaped samples happens after significant different elongation ( $F(2,6) = 44.24, P < 0.001$ ) (E) Swelling ratio is different between samples prepared with different crosslinking degrees



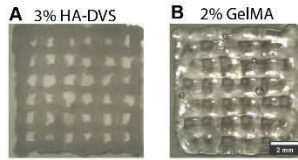


**Figure S3.3** 3D printed GelMA and HA-DVS entangled microstrands prepared and printed from HA-DVS (A) and GelMA (B)

**Table S3.1.** Mechanical Properties of Different HA-MA Bulk Gels

	Crosslinking time [s]	Storage modulus [Pa]	Compression modulus [kPa]	Maximum elongation
Low	20	114.1±8.1	2.0±0.8	49.7±2.3
Med	60	803.6±14.1	6.4±1.8	30.3±6.9
High	180	2587.8±54.3	10.4±1.6	8.2±2.3



# **Chapter IV - Shape Defining, semi-permeable Hydrogel Shells as Culture Chambers for Tissue Engineering**

## Contributions:

---

Benjamin Kessel, Enrico Tosoratti and Marcy Zenobi-Wong designed the study. B. Kessel and E. Tosoratti performed the research together. B. Kessel, E. Tosoratti and M. Zenobi-Wong analyzed the data. B. Kessel and E. Tosoratti designed the figures and wrote the manuscript.

## Abstract

Structural stability is a key component for *in vitro* culture of tissue engineered scaffolds. If this role has to be adopted by the cell-laden material, this requirement effectively excludes weakly crosslinked hydrogels, unstable materials and viscous fluids. A novel approach for the 3D culture of such materials is hereby presented utilizing a shape-defining, semi-permeable hydrogel shell. The presented technique allows to fabricate thin hydrogel sleeves at micrometer resolution, capable of enclosing and stabilizing their content while still allowing gas exchange and nutrient transport. Custom shaped alginate shells were prepared using a sacrificial, ion eluting hydrogel mold. In a second step, the hydrogel shells were filled with cell-laden infill materials. As an example of the versatility of this technique, materials previously not available for tissue engineering such as non-annealed microgels or viscous fluids are used for tissue culture. Primary human chondrocytes were cultured using this platform to evaluate its potential for cartilage tissue engineering. After 3 weeks of culture, deposited extracellular matrix stabilized granular materials (e.g. commercial dermal fillers), while cells in non-crosslinked hyaluronic acid self-assembled into high-density, stiff cartilage structures. This novel approach has the potential to completely revolutionize material property requirements in the field of tissue engineering. Thanks to the shape definition and stability provided by the hydrogel shell, a vast range of materials previously inaccessible for the manufacture of 3D tissue grafts may be re-evaluated.

## 4.1 Introduction

Fabrication of tissue and organs on relevant scales is a highly challenging endeavor. 3D bioprinting employs bioinks, cell-laden extrudable materials, to create custom shaped structures <sup>[64]</sup>. However, the field has struggled for a long time to combine excellent mechanical properties (printability, stability) with biocompatibility and bio-instructive properties <sup>[68]</sup>. Recent advances in material sciences have led to the development and characterization of ‘advanced bioinks’ targeted at providing excellent printability and biocompatibility properties alike <sup>[214]</sup>. Nevertheless, soft or even fluid materials have mostly been neglected in biofabrication, as those materials require additional support to be stabilized in a defined 3D shape. Many strategies have been proposed to increase stability and mechanical properties of biofabricated scaffolds, including scaffolding, core-shell printing and compound hydrogels <sup>[111, 207, 245]</sup>. However, these approaches all focus around the idea of stiffening the hydrogel construct and enable it to keep its shape. Inherently, this change in mechanical properties of the construct may have a significant impact on the physiochemical environment of the embedded cells <sup>[246]</sup>.

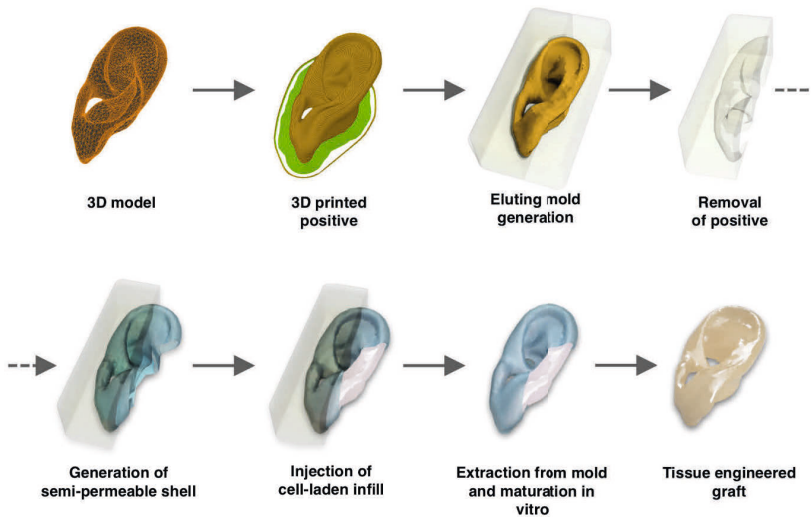
An approach to increase the stability and mechanical properties of unstable materials may be provided by culturing cellular constructs inside a confining insert or chamber. Porosity of such a chamber, however, should not hinder nutrients and molecule transfers as well as gas exchange <sup>[247]</sup>. At the same time, the pore size should be limited to not allow cells and parts of the cultured construct to escape the confinement. Commercially available transwell plates already fulfill the described requirements by using membranes with typical pore sizes in the range of 0.4 – 100  $\mu\text{m}$ . Such inserts are typically used for 2D or 2.5D culture and though transwell systems have been used for 3D tissue engineering constructs with relevant propagation in the z-axis, created tissues are still sheet or disc shaped <sup>[248-249]</sup>. Additionally, transwell inserts are not meant to provide a separate, enclosed environment. Instead, they are designed

for cells to sediment and adhere at the bottom of the well and for cell media and suspended materials to flow around the membrane. Due to these limitations, transwell plates have not been yet used for the manufacture of custom 3D structures.

At the same time, a variety of tissue chamber models have been developed to confine implanted tissue *in vivo*. Implementation, however, has shown to be rather crude with cylindrical chambers made of inert materials like metal, glass or teflon [250-253]. These constructs often have open sides and rather large pores to allow tissue infiltration. Closed porous chambers used to implant tissues into hosts have been described in literature, but are only applicable for flat tissue sections [254]. While these tissue chambers allowed to deepen our knowledge with regards to inflammation, angiogenesis and vascularization, they are unsuitable for the proposed endeavor to create *de novo* tissue *in vitro* [255-256].

In this study, a novel fabrication technique to culture cells and cell-laden constructs is demonstrated. A semi-permeable, custom-shaped hydrogel shell is generated capable of holding viscous liquids without leakage. This semi-permeable shell allows to securely hold material in a defined shape. It confines cells and high molecular weight polymers to the inside of the construct without hindering gas exchange as well as transport of nutrients and bioactive cue molecules. By utilizing a sacrificial hydrogel mold to create the tissue chamber, advanced and biological relevant shapes can be realized without additional components or support materials. Manufacture of alginate tissue chambers is facile and fast, does not need any specialized equipment and requires only cheap, natural polymers. In a first step, a sacrificial hydrogel mold made from carrageenan, locust bean gum and calcium chloride solution is prepared with a positive of the desired shape. This mold is then used to prepare a micrometer-thick alginate shell. This shell can then be filled with uncrosslinked and even fluid cell-laden material. In a second step the alginate shell is sealed to create a tissue chamber that can be cultured *in vitro*.

Thickness of the alginate layer is tunable through time-controlled exposure to the ion eluting hydrogel mold. In culture, the alginate shell remained stable and confined cell-laden infill material inside the chamber. As a first proof of relevance, materials unstable in aqueous solutions, including commercially available dermal fillers, have been used to biofabricate cartilage tissue.



Graphical abstract depicting the manufacture of hydrogel shells for the use as culture chambers in tissue engineering

## 4.2 Materials and Methods

### *Materials*

All chemicals were purchased from Sigma-Aldrich and used as received unless stated otherwise. K-carrageenan was received as a free sample from C.P.Kelco, ultrapure alginate (UP LVG, average molecular weight: 192 KDa) was purchased from NovaMatrix and hyaluronic acid with an average molecular weight of 1.7 MDa from htl biotechnology. Injectable hyaluronic acid dermal fillers of the trade name Gloderm were purchased from easinject GmbH.

### *Preparation of sacrificial hydrogel mold*

Protective hydrogel shells were prepared by a casting technique utilizing a cation eluting hydrogel mold. To create this eluting hydrogel mold, k-carrageenan and locust bean gum was added in different concentrations (1% to 3%) into 100 mM CaCl<sub>2</sub> solution and fully hydrated at 4°C. Polymer slurry was then heated to 95°C until full dissolution. 3D objects resembling the desired outer shape of the hydrogel sleeves were designed in Fusion 360 (v 2.0.8176) and 3D printed using an Anycubic Photon, LCD-based SLA Printer using PrimaCreator Value White DLP Resin. 3D printed samples were washed with ethanol and solidified by 45 minutes UV exposure at 405 nm. Polymer solution heated to 95°C was poured on the 3D object and left to cool down to room temperature form an ion-eluting, tough and flexible hydrogel used as negative mold.

### *Preparation of shape confining hydrogels*

To create cell culture sleeves, a two-step molding procedure was used. In a first step, the main body of the cell culture sleeve was generated with an opening on one side to allow the removal of residual material and injection of cell laden culture material. In a second step, the opening was closed to form a sealed cell culture sleeve. In brief, a solution of low-viscous alginate (0.5 – 2%)



was poured into the cavity of the negative eluting mold. Diffusion of calcium ions from the negative mold into the alginate solution immediately triggered gelation and formation of a thin layer of gelled alginate on the inside of the negative mold. After a defined timeframe, uncrosslinked alginate was removed to stop further thickening of the shell. The crosslinked alginate layer remained in the mold as the uncrosslinked polymer was extracted. Culture material was then injected into the body of the sleeve and the top opening was covered with alginate solution. A top plate of the calcium eluting hydrogel was added to crosslink and bind newly added alginate to the main body. After 30 minutes, casted objects were extracted from the negative mold. A step-by-step guide of the complete process can be found in **Figure 4.1**.

#### *Measurement of thickness*

Alginate solutions of varying concentrations (0.5% (w/v), 1% (w/v), 2% (w/v)) were prepared and poured into eluting molds prepared with 100 mM CaCl<sub>2</sub> to initiate gelling of cell culture sleeves. Un-gelled alginate solution was removed after defined crosslinking times (20s, 60s, 180s) and cell culture sleeves were washed with deionized H<sub>2</sub>O twice to remove any uncrosslinked residual alginate solution from the inside of the cell culture sleeves. Thickness of the formed shells was imaged with a zoom microscope (Leica M205 FA). Area of the cross-section was measured with Photoshop (Adobe, version 10.0.18362.329) to calculate average thickness of the samples.

#### *Alginate sulfate*

Synthesis of alginate sulfate was carried out as previously reported<sup>[195]</sup>. Briefly, ultrapure high viscous alginate was dissolved in formamide under continuous stirring. 96% chlorosulfonic acid was added dropwise to receive a final concentration of 2% (v/v). Solution was left to react for 2.5 hours at 60°C under continuous stirring. Alginate was precipitated by addition of ice-cold acetone and precipitate was isolated by centrifugation. Precipitate was redissolved in ultrapure water and constantly neutralized with 5 M NaOH.

After the polymer was completely solubilized and pH stabilized, solution was dialyzed against 100 mM NaCl and deionized water before samples were snap frozen and lyophilized. Dried samples were stored at  $-20^{\circ}\text{C}$  until use.

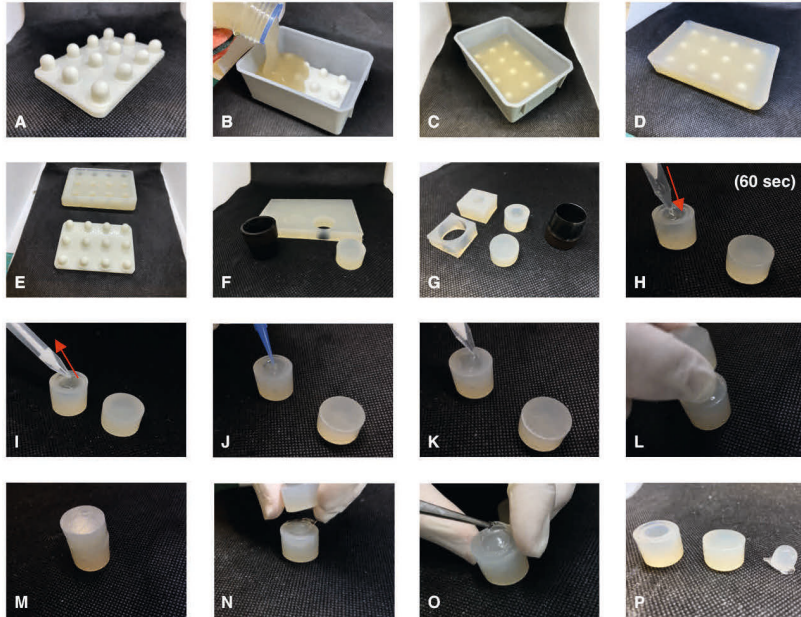


**Figure 4.1** Step by step pictures of the biofabrication process **A**) 3D printed object resembling the final structure (for parallel manufacture of 12 molds) **B**) Object is covered with hydrogel precursor solution of the sacrificial mold **C**) solution is quiescently cooled down to allow homogeneous gelation **D-E**) 3D printed object can be removed from the sacrificial hydrogel mold **F**) plugs of the same material are prepared to close the top of the mold **G**) single pieces of the sacrificial hydrogel mold are cut out **H**) low viscous alginate solution is injected into the mold and left for 60 seconds to form a thin shell **I**) non-crosslinked alginate solution is removed **J**) alginate shell is filled with cell-laden culture material **K**) top opening is covered with non-crosslinked alginate solution **L**) top plug is added to initiate crosslinking process **M**) the two alginate components (body and top) are left for 30 minutes to ensure bonding **N**) top plug of the sacrificial hydrogel mold is removed **O**) alginate shell is extracted **P**) alginate forms a stable, shape-defining shell around the to be cultured material

*Hyaluronic acid methacrylate (HA-MA)*

High molecular weight hyaluronic acid was added to ultrapure water and kept at 4°C until polymer was completely solubilized. Pre-cooled dimethylformamide (DMF) was added under continuous stirring to reach a final ratio of water to DMF of 3:2. Reaction was started by addition of methacrylic anhydride. 10M NaOH was added on demand to keep pH between 8 and 9. After 4 hours, solid sodium chloride was added (finale concentration 0.5 M) and polymer precipitated with pure ethanol. Precipitate was washed, dried and re-dissolved in ultrapure water. Further purification was done with a diafiltration unit (Äkta 3, 10 NMWC hollow fiber), before the product was lyophilized and stored at -20°C until use. To analyze degree of substitution, polymer was dissolved in deuterium (Cambridge Isotope Laboratories) and characterized with <sup>1</sup>H NMR spectroscopy. A Bruker AV-NEO 600 MHz spectrometer equipped with a TCI cryo probe was used. Spectra were obtained with 1024 scans using a 5s recycle delay. To determine the degree of substitution, the ratio of the sum of the integrated peaks of the methacrylate protons (peaks at ~6.1 and ~5.6) and the integrated peak of the methyl protons of HA (~1.9 ppm) were compared. Degree of substitution was found to be 0.28.

*Cell isolation*

Human Infant chondrocytes were extracted from the epiphyseal cartilage of supernumerary digits removed during corrective surgery for polydactyly (ethics approval number KEK-ZH 2014-0390 and informed parental consent). To isolate cells from cartilage, tissue was minced into 1 mm<sup>3</sup> pieces, washed in PBS and digested in collagenase solution.

For 2D expansion culture, cells were kept under humidified atmosphere with 5% CO<sub>2</sub> at 37°C in high glucose Dulbecco's modified Eagle's medium (DMEM, Gibco) supplemented with 10% (v/v) FBS (Gibco), 5 ng per ml of basic fibroblast growth factor and 10 µg per ml of gentamycin sulfate (Gibco). Cells were passaged at 90% confluency by detachment with 0.25%

trypsin/EDTA (Gibco) and used for experiments at passage 3. To create cell-laden filling materials, cells were mixed with microgels and polymer solutions by utilizing a double barrel syringe and a static mixer system (DN2.0x16, Medmix) to achieve a final concentration of 10 mio cells /ml.

#### *Mechanical evaluation*

Mechanical evaluation was performed using a Bioindenter (UNHT<sup>3</sup> Bio, Antoon Paar) equipped with a 500  $\mu\text{m}$  spherical ruby indentation probe. Replicates were cut halfway in either a coronal or transverse way (for more details refer to **Figure S4.1**). One half of the sample was used for indentation while the other for histological analysis. Samples were kept in PBS at 4°C until use before being immobilized on a 35 mm diameter petri dish and submerged in 0.9% NaCl for indentation. For each sample, indentation was performed at three different locations: center, middle and edge region of the sample. Measurement for each region was repeated three times. The indentation protocol was set up as follows. First, a 15  $\mu\text{N}$  force was applied to detect the surface of the sample. Subsequently, samples were indented 75  $\mu\text{m}$  within 5 s to acquire data about mechanical properties. Data was analyzed in the Anton Paar's software to evaluate the Herz modulus of each tested location. Data was plotted in Graphpad Prism (v 7.04) by averaging the three replicates at each location.

#### *Histology*

Samples were washed repeatedly with 0.9% NaCl and fixed in 4% paraformaldehyde for 2 hours at room temperature. Dehydration was done by transfer to 20, 40, 60 and 70% of ethanol for 1 hour each. Samples were infiltrated and embedded in paraffin (LogosJ, Milestone), cut with a microtome into 5  $\mu\text{m}$  thick sections and adhered to polylysine slides (Polysine, Thermo Scientific). Tissue sections were stained with Safranin O according to standard protocols.

For collagen type I and II, colorimetric, immunohistochemical stainings were

performed. First, sections were deparaffinized, hydrated and epitope retrieval was done by digestion with hyaluronidase for 30 minutes at 37°C (1200 U/ml, *Streptococcus equi*). Samples were kept under humidified atmosphere when incubation times exceeded 15 minutes to avoid artifacts through drying. Sections were washed in PBS repeatedly and blocked with 5% normal goat serum (NGS) in PBS for 1 hour at room temperature. Slides were blotted and primary antibodies in 1% NGS were added and slides kept overnight at 4°C. The two antibody types used were: mouse anti-collagen type I and goat anti-collagen type II. On the next day, samples were washed in PBS and remaining endogenous peroxidase or pseudoperoxidase activity of the tissue was quenched with 0.3% H<sub>2</sub>O<sub>2</sub> to prevent non-specific signals. After an additional washing step, secondary antibodies were added: goat, anti-mouse IgG (HRP, Abcam #6789) and goat, anti-rabbit IgG for collagen type I and type II respectively. Samples were incubated for 1 hour and washed in PBS, before DAB substrate (ab64238, Abcam) was added and left to react for precisely 3 minutes. Sections were washed and counterstained with Mayer's hematoxylin solution. To preserve samples, slides were cover slipped with resinous mounting media (Eukritt) and imaged with a with a histology slide scanner (Pannoramic 250, 3D Histech).

## 4.3 Results

### **Sacrificial hydrogel molds enable custom shaped hydrogel shell creation**

To create custom-shaped alginate shells, 3D printed positive of the final structure was placed into a container that was filled with a calcium-loaded carrageenan solution and cooled down to form a sacrificial hydrogel mold. In a next step, the sacrificial hydrogel was cut close to the object to allow extraction of the positive. Due to the toughness and flexibility of the carrageenan hydrogel, even intricate models such as the cartilage part of a human ear, were removed from the mold without damage. For the study of this process, a simpler design, resembling a small Eppendorf tube, was used. Manufacture of the alginate shell was conducted in a second process after the mold was created. Alginate was poured into the mold (**Figure 4.2A**) and a thin shell was formed at the interface to the calcium loaded mold (**Figure 4.2B**). Subsequently, non-crosslinked alginate was removed (**Figure 4.2C**) and an alginate shell in the shape of the initial 3D printed positive was received. Since one side of the alginate solution was not covered with the ion-eluting mold, an opening in the shell persisted which could be utilized to fill the shell with an infill material (**Figure 4.2D,E**). To fully enclose the infill material with a hydrogel shell, additional alginate solution was poured on top the infill (**Figure 4.2F**) and covered with more of the ion-eluting hydrogel mold (**Figure 4.2G**). Alginate solution crosslinked and bonded with the already gelled alginate shell (**Figure 4.2H**). This structure created by enclosing an infill material with an alginate hydrogel shell will be further referred to as culture chamber.

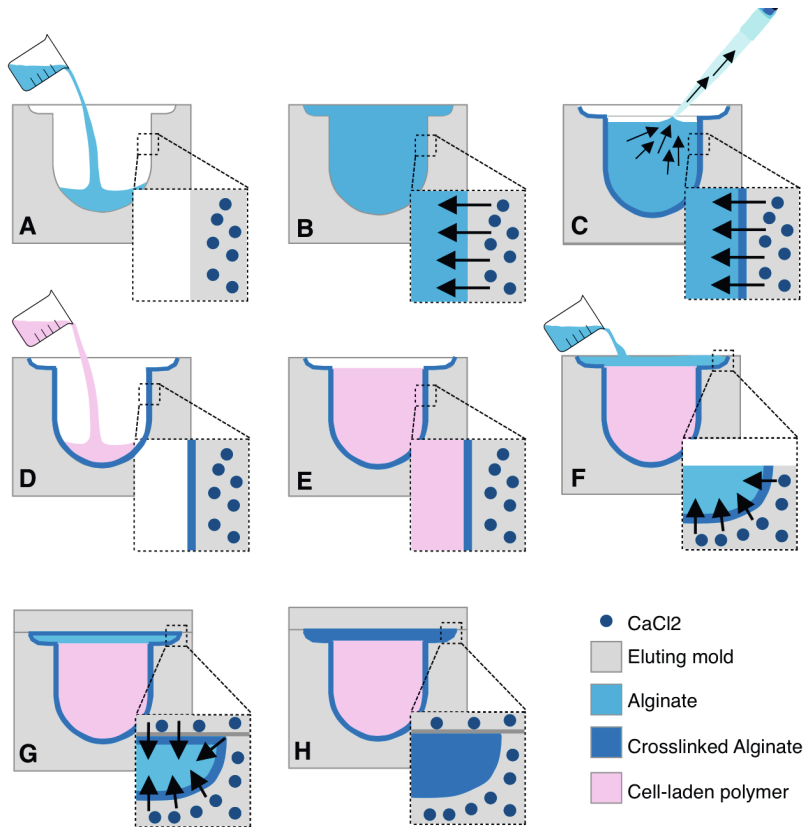


**Figure 4.2** Schematic depicting the fabrication and infill of alginate shells: A) alginate solution is poured inside a ion-eluting mold B) ions diffuse into the alginate solution C) a thin shell of crosslinked alginate is formed and non-crosslinked alginate is removed D-E) alginate shell can be filled with any material F-G) the top opening is covered with more, un-crosslinked alginate and covered with ion-eluting hydrogel H) alginate shell completely encloses the infilled material

### **Alginate shell thickness can be tuned with concentration and gelation time**

Hydrogel shells for tissue chambers are required to find a balance between mechanical properties and thickness. Sufficient mechanical properties are required to allow handling of the shell during fabrication and to ensure infill materials are sealed during culture. At the same time, thin shells are desirable to minimize the diffusion barrier between the culture media and the infill material. Using diffusion coefficients of calcium chloride in aqueous solution previously reported <sup>[257]</sup>, an FEA simulation was performed to predict the diffusion of calcium chloride over time in an aqueous solution. **Figure 4.3A** displays a scatter point predicting the diffusion distance at different times. The simulations were validated by producing a range of alginate shells (**Figure 4.3B**) at different crosslinking times (20 s, 60 s, 180 s). Additionally, the polymer concentration (0.5%, 1%, 2%) was varied to test the mechanical stability of the generated shells. All the alginate shells formed with 0.5% alginate as well as all samples crosslinked for 20 seconds were difficult to handle without damaging the hydrogel. Thickness variations between alginate concentration was found to be significant but can only explain 3.5% of the variation ( $F_{(2, 18)} = 4.5$ ,  $P = 0.027$ ). Time, however, was a highly significant factor ( $F_{(2, 18)} = 105.7$ ,  $P < 0.001$ ). Samples crosslinked for 180 seconds had significantly increased thicknesses compared to those crosslinked for 60 seconds ( $P < 0.001$ ; 60 s:  $308 \pm 47 \mu\text{m}$ ; 180 s:  $609 \pm 64 \mu\text{m}$ ). No significant difference in thickness was found for samples crosslinked for 20 or 60 seconds ( $P = 0.45$ ). The FEA simulations correctly predicted the diffusion distance and consequent crosslinking thickness due to 100 mM  $\text{CaCl}_2$  solution diffusing in the alginate gel from the surrounding eluting mold. The lowest concentration and crosslinking time that still resulted in stable and easily processable hydrogel shells was found to be 1% at 60 seconds with an average thickness of  $242.2 \pm 26 \mu\text{m}$ . This condition was used for further experiments.



### Culture chambers are stable and sealed environments *in vitro*

Culture chambers enables the use of viscous liquids and granular materials which are otherwise unstable in cell culture medium. Three categories of infill materials were prepared and investigated to demonstrate the power of this system: fluid materials, non-annealed granular microgels and very weak, crosslinked hydrogels. An overview over all conditions used as infill can be found in **Table 4.1**.

**Table 4.1:** Infill materials used in combination with culture chambers

<b>ID</b>	<b>Type</b>	<b>Polymer</b>	<b>Conc.</b>	<b>Description</b>
<i>1% HA</i>	Fluid	Hyaluronan	1%	Uncrosslinked hyaluronan
<i>2% HA</i>	Fluid	Hyaluronan	2%	solubilized in PBS
<i>Pure Cells</i>	Fluid	-	-	Dense chondrocyte solution
<i>HA-MA</i>	Granular	Hyaluronan	2%	HA-MA microgels
<i>Glo20</i>	Granular	Hyaluronan	2%	Commercial facial filler based on
<i>Glo30</i>	Granular	Hyaluronan	3%	hydrogel particles
<i>Alg-S</i>	Hydrogel	Alginate-Sulfate	0.5%	Crosslinked for 30 min by CaCl <sub>2</sub> diffusion from the mold
<i>Alg</i>	Hydrogel	Alginate	1%	

Polymers were combined with primary, human articular chondrocytes to investigate cartilaginous tissue development. Chondrocytes were isolated from the joint of supernumerary digits, removed from infant polydactyly patients removed during corrective surgery. All materials could be successfully incorporated inside the alginate shell and enclosed by a top layer of alginate to form a culture chamber. In fluid materials, difficulties arose with the closing process. When alginate was applied to close the top opening, alginate did not form a homogeneous layer on top but sedimented inside the hyaluronan solution. While the chamber was still sealed, the shape was not preserved for all replicates due to some fluid infill escaping the chamber before closure. Following this, insufficient internal pressure lead to the collapse of the

structure and the alginate shell ‘bending in’. Culture chambers were cultured *in vitro* for 3 weeks after which tissue formation was characterized.

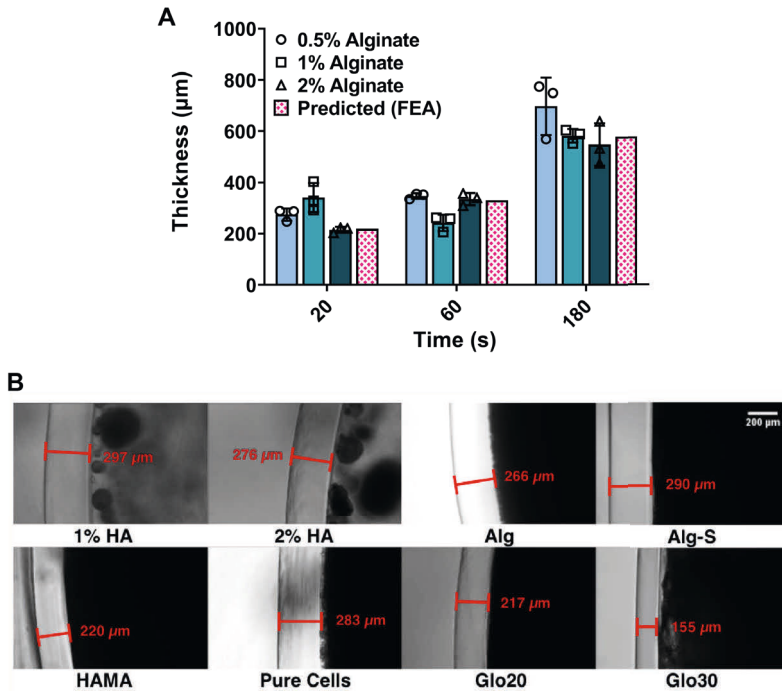


**Figure 4.3:** Preliminary characterization (A) Thickness evaluation of alginate shells generated using different polymer concentrations (0.5% w/v, 1% w/v and 2% w/v) and left to crosslink for different time lengths (20s, 60s and 180s). FEA simulation to predict the diffusion distance of 100 mM CaCl<sub>2</sub> solution in water was used to predict the crosslinking distance in alginate (orange curve). (B) Thickness evaluation of samples after 1 week of culture; the alginate shell is stable for all conditions and supports internal material swelling without rupturing.

The alginate shells remained stable over the whole culture time and neither did cells infiltrate the alginate shell, nor did infill material escape the culture chamber. Visible differences between the materials became apparent already after 1 week of culture. Chondrocytes in uncrosslinked hyaluronic acid condensed into spherical cellular constructs (Figure 4.3B). Glo20 and Glo30

exhibited a strong swelling, slightly deforming the culture chamber into an inflated version. As a consequence, thickness of alginate shell in those two conditions was reduced. After 3 weeks, samples were harvested and visually inspected (**Figure S4.1**). In both concentrations of uncrosslinked HA, white structures of undefined shape could be observed inside the shell. All other conditions had an opaque, yellowish appearance. Initial shape was retained for all conditions except the dermal tissue fillers that had a slightly bloated appearance due to the strong swelling. Subsequently, samples were cut open to investigate the cross-section. The *pure cells* condition did not form a stable material inside the culture chamber and consequently the material did lose the shape and started flowing after the protective environment was removed. Therefore, this condition was excluded from further analysis. Granular and weak hydrogels were stable and could be further processed, while cells in uncrosslinked hyaluronan formed highly flexible cell condensates.

### **Cell chambers enable the use of novel materials for cartilage tissue engineering**

Tissue maturation of infill materials in cell chambers was evaluated by mechanical and histological analysis. Two different categories of materials could be identified in the visual inspection: condensed cell structures from fluid infill materials and stabilized scaffolds from granular and weakly crosslinked hydrogels. Cell condensates had an average Hertz modulus of  $212.9 \pm 76.6$  kPa, indicating a strong deposition and maturation of extracellular matrix (**Figure 4.4**). For the other materials, Hertz modulus was probed at 3 different regions (center, middle, outside) to investigate possible inhomogeneities within the scaffold. Indeed, alginate and HA-MA samples showed an increased modulus at the outside region compared to the core. Hertz moduli of all conditions, however remained relatively low with none of the samples with more than 100 kPa.

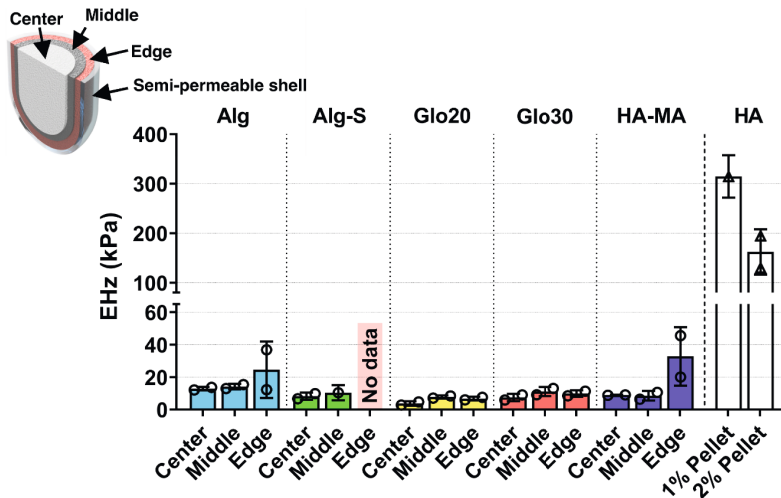


**Figure 4.4:** Mechanical characterization of tissue engineered constructs made with alginate shells. Samples were cultured for 3 weeks in chondrogenic media, cut in the transverse plane and probed at 3 different sections.

Histological evaluation revealed glycosaminoglycan and cartilaginous extracellular matrix deposition in all conditions (**Figure 4.5**). In fluid conditions, cells formed aggregates of approximately 2 mm diameter with strong safranin O staining in the central region and more pronounced collagen staining on the edge region. This general spatial organization is close to native cartilage, however, staining for fibrocartilaginous collagen I was strong in these cell condensates. In granular material, hydrogel particles and the extracellular matrix deposited in the void space in-between was clearly distinguishable. Microgels prepared from HA-MA were smaller and more regular in shape and appearance compared to gel particles in Glo20 and Glo30. First infiltration of ECM inside the gel phase was visible in both conditions with dermal fillers but not in HA-MA microgels. Spatial organization of ECM was again similar to that of native cartilage, with glycosaminoglycans especially pronounced in the center and collagenous matrix at the edge region.

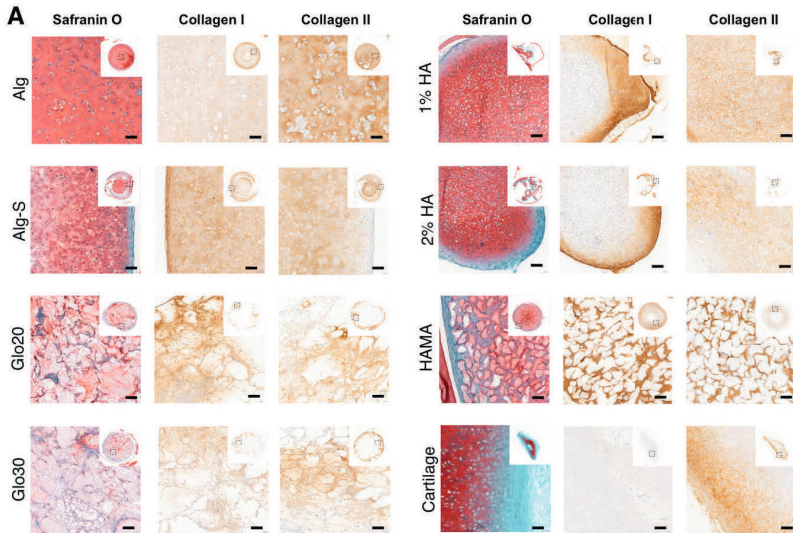


**Figure 4.5** Immunohistochemical staining of 5  $\mu\text{m}$  thick paraffin cross-sections of materials cultured inside alginate shells for 3 weeks. Scale bar corresponds to 100  $\mu\text{m}$ .

Even though staining for collagen I as a fibrocartilaginous marker was present, collagen II, the predominant type in healthy cartilage was stained at similar intensity. In alginate and alginate-sulfate samples, an artifact from the production process was visible in the middle of the cross-section. Since the polymer was filled inside the alginate shell as a liquid pre-cursor and immediately sealed with more alginate on top, some of the alginate added to form the shell penetrated inside the cell-laden infill. This led to a central plug of pure alginate in the central region originating from the top part of the alginate shell. Since the top section was used for histology, these artifacts are visible in the staining. In slightly crosslinked alginate-sulfate gels, major structural damage became visible. Even though the outside shell kept the hydrogel in shape, several cracks were visible through the cross-section of the hydrogel. This degradation happened even though ECM was deposited throughout the whole construct. In slightly crosslinked alginate gels, strong and homogeneous staining for glycosaminoglycans could be observed

through the whole cross-section. In these samples, staining for collagens was also homogeneous through the whole scaffold with type II being the more intensely stained type of collagen in the samples.

## 4.4 Discussion

In this study, a new biofabrication technique for the facile generation of large and high detailed constructs is introduced. With respect to commonly used tissue culture methods, this technique is based on culturing and confining cell-laden materials inside a custom shaped alginate shell. This shell is prepared using a sacrificial molding technique capable of achieving complex structures, overhangs and high resolution with no additional steps. The hydrogel shell function is twofold as it allows uncrosslinked and liquid materials to be stabilized in a desired shape, while at the same time acting as a semi-permeable membrane. This second property allows to confine cells and high molecular weight polymers to the inside of the construct, while still permitting gas and nutrient exchange with the outside. Therefore, culture chambers can be submerged in culture media and processed like any other biofabricated construct.

Tissue engineering in viscous fluids is a topic barely pursued in the scientific community. Even though, addition of viscous components to cell culture media is a simple task, long term culture brings logistic challenges. If cells are distributed and suspended inside the media, media change without disturbing the cell population becomes difficult. Utilizing commercially available semi-permeable membranes e.g. diafiltration membranes, would be one possibility to confine the viscous, cell-laden and separate it from the remaining cell culture reservoir, however, such technique would pose important limitations in terms of possible manufacturable 3D shapes and sizes. In this study, alginate shells were used to culture chondrocytes within a highly viscous environment of hyaluronic acid. Cells cultured in viscous media condensed into cartilaginous structures, while a packed cell solution in without viscosity enhancer did not show such behavior. Even though these experiments are merely a first proof of principle, results are of high interest, especially since viscous suspension culture of mammalian cells seems completely neglected in tissue engineering.

A second crucial role played by the alginate shells regards the structural support and shape definition they provide. Even though several biofabrication methods to prepare custom shape scaffolds have been developed over the last years, each comes with their own drawbacks such as severe material restrictions and/or the requirement of a highly specialized setup. These two issues pose major hurdles for the adoption of such techniques by the scientific community and towards clinical application. The presented methods of using a sacrificial hydrogel molds are facile and comparable to the use of PDMS casting, a simple and established technique. Custom shaped hydrogel shells of a given desired shape can be created and filled with a material of choice with no need for specialized equipment. Even more, as long as the infilled material is dense enough to prevent cell sedimentation, additional stability provided by external components or crosslinking is not required as the support to the shape of the construct in the long term is provided by the alginate shells. Due to the semi-permeable nature of the shell, the infilled material can be cultured in a defined shape while providing cells with, nutrients and biological cues from the culture media to remodel the infilled material into a tissue of choice. Following this approach, a first test using several materials designed for cartilage tissue engineering was conducted. The focus was placed on materials rarely used for 3D cultures. These materials are in fact not stable on their own as they would either dissolve due to their granular composition or exhibit instability in culture due to their low polymer content. Interestingly, after only three weeks of culture all granular materials (HA-MA microstrands, Gloderm20, Gloderm30), were stabilized into one coherent structure through extracellular matrix deposition of embedded cells. This also marks the first use of a commercially available, injectable tissue filler as a tissue engineering matrix. Even though granules of hyaluronic acid gel swelled greatly, resulting in rather large microgel particles and a bloated tissue structure, such adaption of already applied solutions used in the clinics has the potential to accelerate innovation of tissue-culture polymers.



To conclude, alginate shells are a novel technique that gives unprecedented possibilities for tissue engineering and 3D cell culture. Alginate shells can function as semi-permeable, custom shaped tissue chambers that enable to culture of any material, including non-stabilized materials such as degrading hydrogels, granular materials and even viscous fluids.

## 4.5 Supporting Information

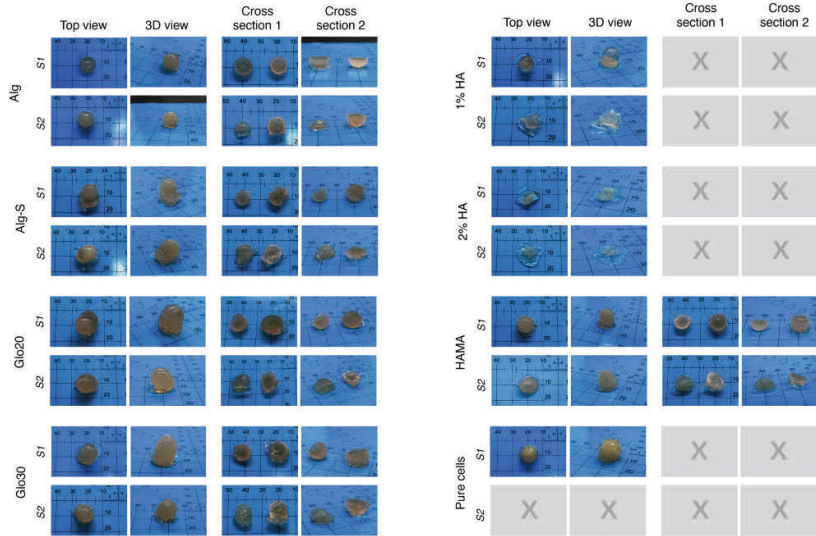


**Figure S4.1** Individual samples of cell-laden materials cultured in alginate shells for 3 weeks.

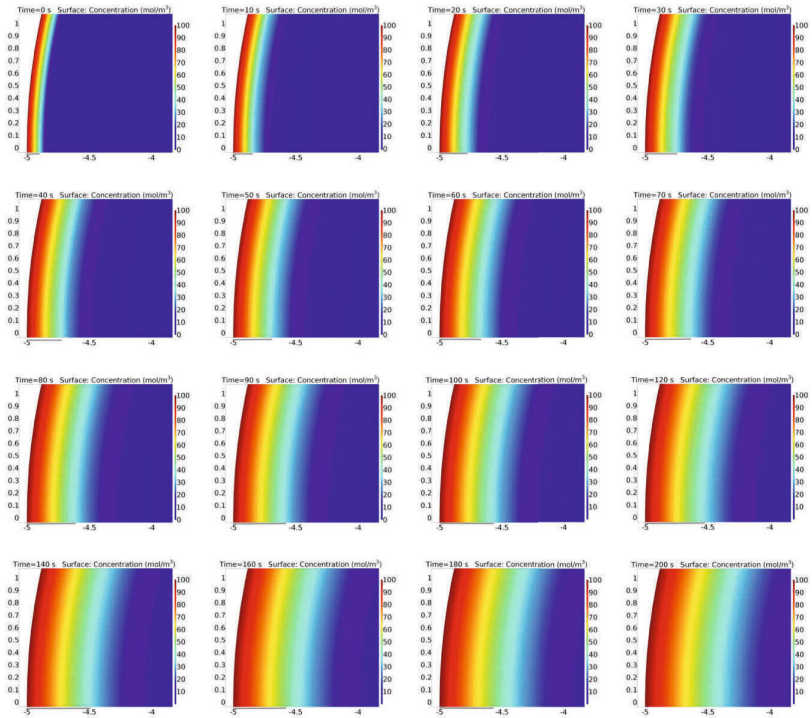


**Figure S4.2** Finite element modelling to calculate penetration depths of eluted calcium ions from the hydrogel mold inside the alginate solution. The figures show the upper left portion of a 5mm disc. Both x and y axis show the distance in mm from the origin. The 5mm 2D disc was simulated as an aqueous solution with all edges in direct contact with a 100 mM  $\text{CaCl}_2$  source. The simulation was run for 200s in 10 s time steps. At 0s, calcium ions diffuse in the disc very fast forming a first layer. As time goes by, the calcium ions diffuse towards the center of the disc. Although this simulation is useful to predict the diffusion of ions in an aqueous solution, errors might increase compared to a crosslinking polymer as the diffusion coefficient change over time.

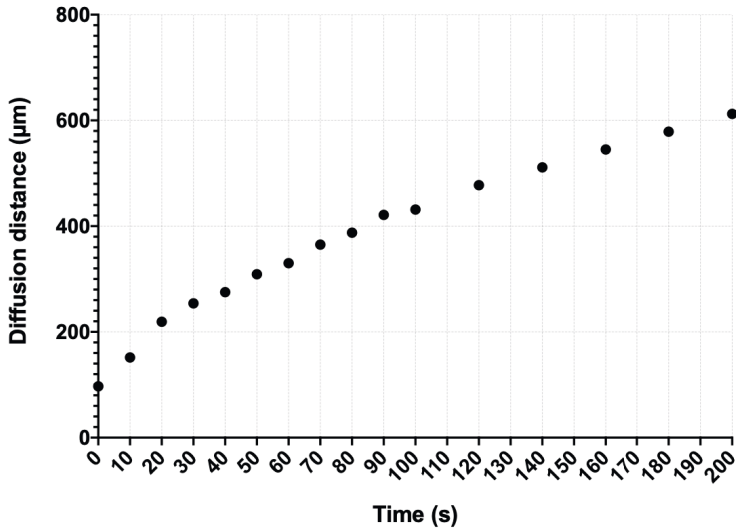


**Figure S4.3** Finite element modelling analyzed penetration depths of eluted calcium ions from the hydrogel mold inside the alginate solution. The penetration depth was extracted from the FEA simulation of **Figure S4.2** and reported as a scatter plot. A characteristic logarithmic skewed penetration depth curve can be observed as 100 mM  $\text{CaCl}_2$  ions diffuse in a 5mm disc composed of an aqueous solution.

## **Chapter V - Conclusions and Outlook**

Though often considered a simple tissue, creation of cartilage tissue is still an open challenge in the field of biofabrication. In this thesis, approaches for advanced biofabrication have been developed and presented. The path to success is rarely straight and learning from the results and failures of the past is crucial to find successful strategies in the future. In this final Chapter, important lessons to take will be deduced from the individual studies as well as the thesis in its entirety.

In Chapter II, a multipolymer approach to find a potent and clinically relevant bioink was pursued. Different polymers, each with their defined role were combined to add mutual benefits to the final formulation. Initial *in vitro* results looked highly promising, with plenty of cartilaginous matrix deposition and increasing mechanical properties with prolonged culture. However, structural integrity *in vivo* was insufficient and secreted extracellular matrix was lost from the scaffolds. Having contradicting results put an emphasis on finding relevant and accepted assays for the definition of a functional cartilage tissue. For years, characterization of tissue engineered cartilage is lacking clear, objective quality assessment: genetic markers or staining for ECM deposition as well as scoring systems suffer from difficult, often subjective quantification. Also, mechanical properties derived from the stress strain curve cannot fully reflect the complexity of the real tissue. Maturation status of collagen fibers is often completely omitted, even though they form highly organized structures in healthy cartilage. In this study, characterization of cartilage constructs was limited to analysis of ECM deposition and a mechanical characterization, as well. As a direct consequence, follow up experiments were started to use polarized light and second harmonic generation as a method to investigate the fiber architecture in future studies.

Defining and proving clinical relevance is a second, difficult task, which was attempted in this study. The importance of finding better treatment solutions and translating bioprinting approaches into the clinics has a broad consensus in the biofabrication community. But finding accepted and relevant tests to

provide data, proving the clinical relevance of a strategy to fabricate tissues is more difficult as it might seem. Highly inflammatory lipopolysaccharides, also called endotoxins, are residuals of gram-negative bacteria and are of high concern for translation of bioinks derived from natural, microbotic polymers. With a standardized LPS sensitive TLR4 cell line we were able to sample the raw materials and the combined bioink and prove the absence of problematic levels of endotoxins. Quality control of biofabricated constructs is another topic, often neglected. By 3D scanning of the bioprinted and crosslinked scaffold, it was possible to identify regions of deformation and deduct problems that inevitably need to be addressed in clinical translation in any biofabricated construct.

A simple and powerful microgel platform for tissue engineering was the topic of Chapter III. Mechanical deconstruction of bulk hydrogels yielded a new material: entangled microstrands. The method is applicable to a wide range of materials and entangled microstrands are an ideal material for biofabrication. First demonstration of elongated microgels for bioprinting revealed rheological properties relevant for extrusion bioprinting and excellent biocompatibility. Two distinct methods of cell encapsulation were pursued: cells inside the gel phase of the microstrands or outside the gel-phase, inside the void space between microgels. In both methods, more than 90% of embedded cells remained viable after extrusion. Strands aligned with the flow during the extrusion process, facilitating microarchitecture inside the hydrogel construct. Further, it was demonstrated that alignment of microstrands can guide myoblasts to form oriented myotubes. Another aspect of this study is the low concentrations of polymers necessary to form stable bulk gels and size them into microstrands. This low polymer content (usually 2-3%) together with the porous network within the construct give cells opportunity to migrate, proliferate and establish their physiological niche. One of the crucial tasks of biofabrication is to spatially pattern cells. But it is also important to not lock them in place, which can happen in bioinks with higher polymer concentrations. The polymer content required for

entangled microstrand preparation is still substantial, though and attempts to reduce concentrations even more ( $< 1\%$ ) have previously failed. Such bulk gels are very weak and were crushed, rather than sized into microstrands. In this process they lost a significant part of their swelling potential, leaving behind indistinct gel particles and unbound water, rather than entangled microstrands.

Chapter IV was driven by the idea of finding a biofabrication method that could work with gels prepared from a minimal polymer concentration or even non-crosslinked polymers. In such an approach, the hydrated matrix should merely suspend cells and give them the maximum possible freedom to self-organize and transform their surroundings into functional tissue. To achieve this goal, a 3D printed positive, resembling the shape of the final structure embedded within a polymer solution to create a sacrificial hydrogel mold. In a second step, the positive was removed and alginate was filled into the cavity of the mold. Cations, embedded inside the hydrogel mold diffused into the alginate solution, forming a few hundreds of microns thin shell at the interface. Subsequently, residual alginate was removed, and any cell-laden material could be filled inside the alginate shell. Infilled material could be completely sealed inside the alginate shell and cultured *in vitro*. Non-annealed hydrogel fragments such as commercial tissue fillers and viscous polymer solutions were screened for their potential in cartilage tissue engineering. Individual gel particles of tissue fillers were stabilized into one coherent structure by ECM deposition. Importantly, alginate shells remained inert and could be removed after culture, resulting in a cartilage tissue graft made alone from cells and a material approved for injection into humans. The use of already clinically approved materials for tissue engineering is a chance to greatly accelerate future clinical translation. In a similar experiment, chondrocytes were cultured inside non-crosslinked hyaluronan. Culturing cells in viscous solutions is logistically challenging, as removal of viscous media without disturbance of embedded cells is difficult. While this problem can be theoretically solved with semi-permeable membranes, no



demonstration of cell culture inside a custom-shaped, semi-permeable membrane has been shown in the field, so far. Alginate shells confined chondrocytes within a chamber of viscous media, free floating inside a reservoir of cell media that could be replenished easily. In this system, chondrocytes condensed and formed highly flexible cartilaginous structures. Consequent use of this method will establish a powerful platform that will significantly advance the materials available for biofabrication.

Concluding the results from the work provided in these studies, some highly relevant points need to be highlighted and should be considered for future projects in the field:

## 5.1 Keep it simple

Small, logical and relevant steps will pave the way to tissue engineered functional tissues. Scientists admire sophisticated solutions to complex problems but finding a simple answer to a problem can be even more challenging. To keep a solution for cartilage tissue engineering as simple as possible is important on many levels. First, it allows for easy protocols, reproducible experiments and large samples sizes. The scientific method works best if an uninvolved party can easily grasp the idea of a study, reproduce and verify results. However, this can only happen if the technology is easily accessible to 3<sup>rd</sup> parties. This marks the cornerstone for a broad acceptance towards a biofabrication strategy in the science and medical community as well as the public. Clinical translation of any tissue engineering product is a daunting task and most likely not to shoulder for a single party alone. Finding support from 3<sup>rd</sup> parties, not only financially but also scientifically and to create a public interest will be key. To achieve this, one should aim towards a logic and understandable strategy not meant to impress but tailored towards addressing the concrete problem.

For a translatable process, simplicity becomes important again as every step

from the isolation of the polymer to any chemical modification and preparation of the material will need to be certified and standardized for the clinics. This thesis aimed at the development of advanced biofabrication methods for cartilage tissue engineering. But advanced does not necessarily mean complicated. A seemingly simple approach in Chapter II that focused on using non- and minimal modified polymers turned out to be extremely complex. The interactions of the different polymers were difficult to predict and therefore hard to master. Learning from this, Chapter III used a single material, bulk hydrogel extruded through a grid to make a microgel material for biofabrication. With a minimal sequence of steps, a powerful platform for tissue engineering has been created. The idea of providing simple but powerful solutions has been continued in Chapter IV, in which established means of manufacturing and unmodified materials were combined in a clever way to create semi-permeable culture chambers.

The scientific community revolves around novelty and highly rewards innovations. This drives scientific exploration but can also result in over-sophisticated systems that might not be relevant to solve the problem at hand. While the advances in the field must be acknowledged, a tissue engineered solution for cartilage repair is a concrete goal that has not been achieved, yet. Pursuing a simple approach, refined but reduced to the essential might be what unites the scientific, medical and public community alike and ultimately leads to the long sought after breakthrough.

## 5.2 Polymer Concentrations

In science, finding the right concentration is crucial, as concentrations can make the difference between a poison and a medicine. In tissue engineering, polymer concentration is one key property of a bioink and directly linked to the biofabricated construct, as well. Polymer content has a huge impact on mechanical properties, which ultimately govern a wide range of scaffold

characteristics. Tuning these properties is critical for the successful maturation of a biofabricated scaffold into a functional tissue. High concentrations of polymer in precursor solution often give viscosity and thixotropic properties, which can allow for 3D bioprinting in reasonable quality and therefore simplify the fabrication process. Once crosslinked, high polymer content can give the construct stability to keep its shape and withstand load. From the biological perspective however, high polymer concentration often results in dense networks, tightly surrounding encapsulated cells. Chondrocytes embedded in a dense bulk hydrogel often remain rounded up, show limited proliferation and form cell aggregates in small cavities. This phenotype is often prevalent in tissue engineered constructs and considered a replication of the structure found in adult articular cartilage, in which cells reside inside a lacuna surrounded by extracellular matrix - but it remains unclear if this is desirable. As cartilage is a tissue with minimal capabilities for regeneration and self-repair, replicating the structure of a 'dormant' tissue, with the goal of *de novo* creation of cartilage tissue seems contradictory. Consequently, the dense matrix of polymer might instruct chondrocytes into a passive rather than an active state. In microgel scaffolds created in Chapter III, cells deposited plenty of cartilaginous, extracellular matrix inside the void space between microgels. At the same time, mechanical properties increased exponentially. We hypothesized that the high local cell density (comparable to pellet culture), together with high freedom for cell movement are the key factors for successful maturation. Following up on this, hydrogel shells as an approach to utilize hydrogels with low polymer content or non-crosslinked materials is shown in Chapter IV. First results proved the feasibility of this approach and extracellular matrix deposition in all scaffolds. Even though mechanical properties did not reach levels of native cartilage yet, deposited ECM stabilized the constructs. Hydrogel shells also enable the investigation of another highly interesting setup for tissue engineering: non-crosslinked suspension systems. Unlike cells embedded in granular and low polymer

hydrogel systems, chondrocytes condensed and formed flexible cartilaginous structures. Even though histochemical analysis hints towards a more fibrocartilaginous type, mechanical properties greatly increased within only three weeks of *in vitro* culture. Hydrogel shells as a biofabrication platform are still in their infancy and more research is required to fully develop this approach. The new possibilities this brings, however, might lead to a paradigm shift of what is considered an excellent material for tissue engineering.

### 5.3 Architected Hydrogels

Recent developments towards smart hydrogels have led to a variety of bulk materials. Self-healing hydrogels and double networks that increase the toughness of tissue grafts have shown the important role, material science play in biofabrication. But it is also time to rethink what we consider the smallest building unit. Biofabricated constructs can be shaped to specific appearance, but typically the result is still a uniform bulk hydrogel. Microgels give us new possibilities in the design and assembly of hydrogel constructs. Even though the chemical composition of a bulk hydrogel and a microgel construct might be identical, the different architecture gives rise to fascinating new opportunities. A variety of shapes (spherical, rods, ribbons) have already been used successfully for tissue engineering. In Chapter III, a new method to create elongated hydrogel microstrands has been introduced, adding another possible shape to the available palette. The inherent porosity and void space between the individual microgels allow for unhindered diffusion and proved an ideal environment for cells to proliferate and deposit extracellular matrix. Manipulation of individual microgels and control over their spatial orientation will be one of the great challenges in the field. In this study, flow-alignment of microgels through extrusion was demonstrated. By introducing this controlled architecture, embedded cells aligned and formed oriented structures within the biofabricated construct. Real modular constructs will be

another milestone to achieve for the biofabrication community. Combination of different shapes and materials will enable tunable complexity in resulting constructs. In Chapter II, a multipolymer approach to create an advanced bioink was presented. The power of this approach, however, was limited as interference between polymers reduced the efficacy. As an example, the weak gel forming strength of alginate-sulfate did not only result in a loose network of alginate-sulfate, but compromised the network strength of unmodified alginate, as well. Transfer of this approach to a microgel system, where each microgel has their own individual environment, seems much more promising. Interaction with other microgels only happens at the surface and therefore negative interactions can be contained or eliminated (e.g. separate microgels for alginate-sulfate and alginate). This would greatly simplify such an approach, as individual microgels can be prepared and characterized separately, allowing for better control and leaving less parameters to consider. Following this path, assembly of such modular constructs into real functional systems will give unprecedented opportunities. Incorporating and combining smart microgels will allow to change physiochemical properties with an external stimulus such as pH, charge or temperature. Even after fabrication and during culture, parameters like stiffness, degradation behavior or drug release could be adapted and tuned. Still dreams of the future, combinations of these approaches will allow scientists to exercise a new level of control over biofabricated constructs.

In the recent years, biofabrication provided more and more possibilities to find a successful approach to create cartilage tissue. In the presented work, additional strategies were developed, further expanding the selection. With ever increasing options in materials to choose from as well as biofabrication strategies to pursue, chances are higher than ever to find a potent and effective method to create *de novo* cartilage tissue. Partaking in this endeavor, and maybe, delivering one of the final clues was the motivation and ambition of this thesis.



# Appendix

Mentionable scientific endeavors outside of the scope of this thesis.

## Cell-compatible Surface Modification

The surface of acellular, orthopedic and other implanted devices commonly undergoes surface functionalization or modification before implantation to improve body response. Any foreign material inside the human body triggers a first form of immune response, in which proteins adsorb onto the surface. This attempt to neutralize and contain non-native material is known as foreign body reaction and often leads to encapsulation by fibrotic tissue [258-259].

For implanted orthopedic devices like bone implants, tuning the adsorption behavior of proteins is paramount for a successful integration [260]. Bacterial colonization and biofilm formation results in infections that often require surgical removal, while encapsulation in fibrous tissue leads to sub-par integration of the implant, hindering its function and also necessitate surgical revision [259-261]. Cardiovascular implants like stents are also challenged by the adsorption of proteins, as it can trigger blood clotting and thrombus formation [262]. Even in non or semi-permanent implants such as sensors or access points to administer medication (e.g. central venous catheter) protein adsorption is problematic as it decreases the potential to interact with the internals of the human body. Tight control over protein adsorption is therefore crucial for successful employment of any kinds of implants inside the human body.

A wide range of surface functionalization processes has been developed to tune protein adsorption and maximize the chances for successful implant integration [260]. Protein immobilization on orthopedic implants to enhance osseointegration has been thoroughly investigated and the initially used, simple systems such as physisorption has since been evolved into advanced and intricate systems [263]. The main contributing factors affecting surface energy and therefore protein-surface interactions are chemistry and topology. Key parameters for surface chemistry are molecular composition, charge and dipole moments which all influence the surface free energy. The surface free



energy determines the way water interacts with a specific surface and if it is classified as hydrophilic or hydrophobic. Surface topology is mainly governed by roughness, which can lead to mechanical interlocking, modification of cellular activity or protein interaction, depending on the scale of roughness [264-267]. First attempts to coat biological material have been conducted for degraded cartilage. Assembly of cyclic polymer brushes on surfaces was shown to give lubricating properties and low coefficients of frictions when opposing surfaces modified with cyclic brushes sheared against each other [268]. Such an coating could possible restore lubrication in joints which are damaged by degenerative diseases such as osteoarthritis, but also possibly applied to tissue engineered constructs [269].

Cellular, engineered tissue implants commonly lack any post-processing steps including surface modification. To state this more precisely, the surface of polymers and hydrogel networks have been post-processed with various methods in bulk to make them more hydrophilic and facilitate cell-attachment [270-272]. However, the outside surface of a matured tissue graft which will form the interface with the body commonly lacks any modification different from the bulk of the construct. The hydrated matrix of scaffolds and the autologous or non-immunogenic cells is often considered to not trigger any adverse immune response, making modifications for better integration superfluous. Since the implantation process is still highly invasive, inflammation, poor integration or encapsulation still regularly occurs [259, 273-274]. It is also still under debate if expanded autologous cells are completely devoid of any potential pathogens, as culture medias are often supplemented with xenogeneic products, such as fetal bovine serum [35]. Since immune system components can also have a positive impact for tissue regeneration, being able to modulate instead of eliminating immune response might be the most promising strategy [275]. So far, use of tissue engineered transplants in clinics is still limited [33, 276-278]. But, considering the importance of surface modification for acellular grafts, it is critical to investigate this parameter for cellular grafts as well [279]. Surface modification processes, however, are

optimized for inert materials like metal and ceramics. Applied conditions are typically harsh and usually not compatible with hydrated environments or living cells <sup>[260, 280]</sup>. First endeavors to surface treat hydrated matrices can be found, but cytocompatibility is not necessarily obtained <sup>[269, 281-282]</sup>. Adaptation of surface treatment processes to be cell compatible and suitable for hydrated environments is critical to fine-tune surface properties of tissue engineered grafts in the future.

# Oxygen Tolerant and Cytocompatible Iron(0)-Mediated ATRP Enables the Controlled Growth of Polymer Brushes from Mammalian Cell Cultures

This study has been published in the Journal of the American Chemical Society as *Oxygen Tolerant and Cytocompatible Iron(0)-Mediated ATRP Enables the Controlled Growth of Polymer Brushes from Mammalian Cell Cultures*, Amine Layadi, Benjamin Kessel, Wenqing Yan, Matteo Romio, Nicholas D. Spencer, Marcy Zenobi-Wong, Krzysztof Matyjaszewski and Edmondo M. Benetti, **2020**, 142, 3158 and was reprinted with permission. Copyright 2020, American Chemical Society.

<https://doi.org/10.1021/jacs.9b12974>

## Contributions:

---

This study was a collaborative study with the Polymer Surface Group of Prof. Edmondo M. Benetti. Benjamin Kessel was responsible for conception, design and statistical analysis of the biological evaluation experiments. B. Kessel was also involved in formulating cytocompatible reaction media. Experimental work and data analysis was conducted together with Amine Layadi. The manuscript was written through contributions of all authors.

## Abstract

The use of zerovalent iron ( $\text{Fe}^0$ )-coated plates, which act both as a source of catalyst and as a reducing agent during surface-initiated atom transfer radical polymerization (SI-ATRP), enables the controlled growth of a wide range of polymer brushes under ambient conditions, and utilizing either organic or aqueous reaction media. Thanks to its cytocompatibility,  $\text{Fe}^0$  SI-ATRP can be applied within cell cultures, providing a tool that can broadly and dynamically modify the substrate's affinity towards cells, without influencing their viability. Upon systematically assessing the application of Fe-based catalytic systems in the controlled grafting of polymers,  $\text{Fe}^0$  SI-ATRP emerges as an extremely versatile technique that could be applied to tune the physicochemical properties of cell's microenvironments on biomaterials or within tissue engineering constructs.

## 6.1 Introduction

Surface-modification strategies involving the controlled growth of polymer brushes by exploiting reversible deactivation radical polymerizations (RDRP) that are tolerant to ambient conditions have been a subject of increasing interest in the materials-science community <sup>[283]</sup>. The most prominent examples of such processes have involved the application of oxygen scavengers, in the form of photosensitizers <sup>[284]</sup>, reducing agents <sup>[285]</sup>, enzymes <sup>[286]</sup>, or zerovalent metal surfaces <sup>[287]</sup>.

While the evolution of oxygen-tolerant, surface-initiated RDRP (SI-RDRP) is paving the way for the translation of “grafted-from” polymers from fundamental studies into technology, the development of controlled polymerizations that are additionally compatible with physiological environments would substantially broaden the applicability of SI-RDRP in materials design. In particular, an RDRP process capable of modifying the physicochemical properties of cellular microenvironments through polymer grafting, without altering cell viability, would allow one to adjust the biological affinity of scaffolds towards a particular cell type during culturing, or alternatively to tune the presentation of biochemical cues triggering a defined cell behavior. More generally, the controlled growth of polymer brushes from cell-loaded supports would enable the fabrication of active biomaterials, capable of re-shaping themselves in a dynamic fashion following biocompatible processes.

Focusing on surface-initiated atom transfer radical polymerization (SI-ATRP), the most widely applied SI-RDRP method, we demonstrate here that the application of Fe<sup>0</sup> plates, acting as a source of both biocompatible catalyst and reducing agent, can enable the controlled, rapid growth of polymer brushes within organic as well as in aqueous and cell-culture media.

While introducing and systematically assessing the use of Fe-based catalytic systems in the fabrication of polymer brushes <sup>[288]</sup>, we show that Fe<sup>0</sup>-mediated

SI-ATRP ( $\text{Fe}^0$  SI-ATRP) can be performed in the presence of primary articular chondrocytes (ACs) that had been previously cultured on initiator-bearing substrates, generating *in situ* polymer brushes that substantially alter the settlement of cells without affecting their viability.



mM of weakly coordinating halide ligands (in the form of tetra-*n*-butylammonium bromide, TBABr) <sup>[290-292]</sup> proceeded slowly, reaching just a few nm of dry thickness in several hours of reaction (**Figure 6.2a**), as measured *ex situ* by variable-angle spectroscopic ellipsometry (VASE). In contrast, when 10 mM Fe<sup>III</sup>Br<sub>3</sub> was added to the mixture, the polymerization proceeded rapidly, leading to a progressive growth of PMMA brushes, which reached ~ 20 nm after 5 hours of reaction. It is important to emphasize that an excess of TBABr with respect to Fe<sup>III</sup>Br<sub>3</sub> was necessary to guarantee the complete dissolution of Fe species, especially in 50:50 anisole:MMA mixtures (*v/v*), where their solubility in the absence of ligand would be limited <sup>[290]</sup>.

In both these cases, an induction time necessary to oxygen consumption was never observed, suggesting that oxidation of Fe<sup>0</sup> surface quickly takes place just at the very early stages of the reaction.

An analogous result was obtained in the case of Fe<sup>0</sup> SI-ATRP of oligo(ethylene glycol) methacrylate (OEGMA) performed in *N,N*-dimethylformamide (DMF), where a comparable amount of Fe<sup>III</sup>Br<sub>3</sub> was required to attain a significant growth of POEGMA brushes, reaching nearly 30 nm of thickness in 5 hours (**Figure 6.2b**).

The role played by added Fe<sup>III</sup>Br<sub>3</sub> was elucidated while monitoring the variation of POEGMA-brush thickness as a function of Fe<sup>III</sup>Br<sub>3</sub> concentration for fixed polymerization times (**Figure 6.2c**). The thickness of POEGMA brushes increased with [Fe<sup>III</sup>Br<sub>3</sub>], reaching a maximum between 5 and 10 mM. Under these conditions, Fe<sup>III</sup> species acted both as a deactivator, suppressing irreversible termination by radical recombination between growing chains, and contributed to generating Fe<sup>II</sup>-based activators through comproportionation with Fe<sup>0</sup> (**Figure 6.1**), in this way accelerating the grafting process <sup>[290]</sup>.



A further addition of  $\text{Fe}^{\text{III}}\text{Br}_3$  beyond 10 mM led to a decrease in brush thickness, suggesting a significant deactivation and a simultaneous slowing down of the polymerization.

It is important to emphasize that the balance between the above-mentioned effects determined the position of the maximum of polymer-brush thickness as a function of  $[\text{Fe}^{\text{III}}\text{Br}_3]$ , which might shift during the progression of the grafting process. An increment in the content of activators through comproportionation led to an increase in brush-growth rate, especially during the early stages of polymerization. Simultaneously, an increase in deactivation by added  $\text{Fe}^{\text{III}}$  species slowed down the grafting process, although it additionally suppressed irreversible termination by radical recombination between propagating grafts, which is especially relevant after relatively long reaction times (for more flexible, high-molecular-weight grafted chains) [293].

$\text{Fe}^0$  SI-ATRP was subsequently investigated in aqueous environments, and using ethylenediaminetetraacetic acid (EDTA) as a ligand. EDTA strongly binds Fe species to form cytocompatible complexes [294] to efficiently catalyze Fe-based ATRP in solution and heterogeneous systems, as previously demonstrated [295-296].

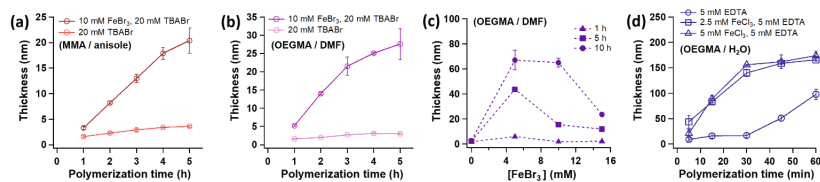


**Figure 6.2** (a) Dry thickness of PMMA brushes measured ex situ by VASE during  $\text{Fe}^0$  SI-ATRP of MMA performed in 50% (v/v) anisole solutions with 20 mM TBABr and with or without 10 mM  $\text{Fe}^{\text{III}}\text{Br}_3$ . (b)  $\text{Fe}^0$  SI-ATRP of OEGMA performed in 50% (v/v) DMF solutions with 20 mM TBABr and with or without 10 mM  $\text{Fe}^{\text{III}}\text{Br}_3$ . (c) Variation of POEGMA-brush thickness measured by VASE, as a function of  $\text{Fe}^{\text{III}}\text{Br}_3$  concentration, while keeping the concentration of TBABr fixed at 20 mM. (d) Dry thickness of POEGMA brushes measured by VASE during  $\text{Fe}^0$  SI-ATRP of OEGMA performed in 50% (v/v) water solutions containing 5 mM EDTA, 10 mM NaCl and variable concentrations of  $\text{Fe}^{\text{III}}\text{Cl}_3$ .

In the exemplary case of  $\text{Fe}^0$  SI-ATRP of OEGMA performed in 50% water mixtures (v/v), the growth of brushes followed much faster kinetics compared to those recorded in organic media, as expected from the significantly larger ATRP equilibrium constant ( $K_{\text{ATRP}}$ ) that is characteristic for aqueous systems [297-299].

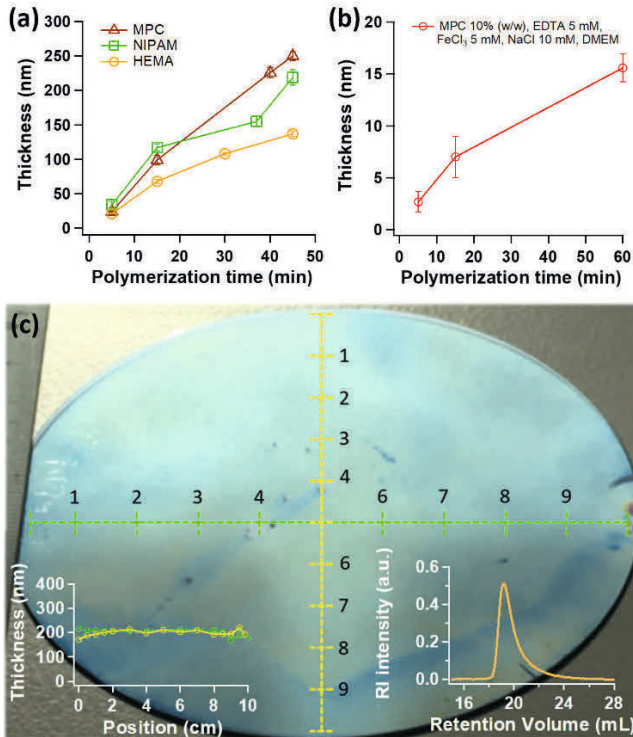


**Figure 6.3** (a) Evolution of brush thickness measured by VASE during  $\text{Fe}^0$  SI-ATRP of MPC, NIPAM and HEMA. (b) PMPC-brush thickness measured by VASE during  $\text{Fe}^0$  SI-ATRP performed in 0.3 M MPC DMEM solutions. (c) PMPC brushes grafted from an entire, 4-inch silicon wafer by  $\text{Fe}^0$  SI-ATRP. The brush thickness measured by VASE across the surface is reported in the inset. A SEC trace from detached PMPC brushes is also shown.

More than 150 nm-thick POEGMA brushes could be grown in just one hour of polymerization when 2.5-5 mM  $\text{Fe}^{\text{III}}\text{Cl}_3$ -EDTA were added to the

aqueous reaction mixture (**Figure 6.2d** and **Figure S6.1**), whereas just ~ 5 nm-thick brushes were grafted after the same time using DMF as solvent, and no appreciable brush growth could be recorded in anisole.

The presence of 5 mM EDTA alone enabled the synthesis of significantly thinner films, which initially grew following relatively slow kinetics. This was presumably due to the time required by Fe<sup>II</sup>/Fe<sup>III</sup>-EDTA adducts to diffuse from the Fe plate to the initiator-bearing substrate <sup>[289]</sup>.

Using 5 mM Fe<sup>III</sup>Cl<sub>3</sub>-EDTA, a range of bio-relevant polymer brushes could be grafted by polymerizing 2-methacryloyloxyethyl phosphorylcholine (MPC, 3 M), N-isopropylacrylamide (NIPAM, 2 M) and 2-hydroxyethyl methacrylate (HEMA, 4 M), obtaining extremely thick PMPC (250 ± 7 nm), PNIPAM (219 ± 12 nm) and PHEMA (137 ± 5 nm) films just after 45 min of reaction (**Figure 6.3a**). Aqueous Fe<sup>0</sup> SI-ATRP could be further applied for growing similar brush films from large substrates, as demonstrated in the case of PMPC brushes, which could be grown from 4-inch silicon wafers, forming ~ 200 nm-thick films with homogeneous thickness and morphology after 30 min of polymerization (**Figure 6.3c** and **Figure S6.3**). Detachment of PMPC grafts <sup>[300-302]</sup> enabled their characterization by size-exclusion chromatography (SEC), yielding a  $M_n$  of 600 kDa and a  $\mathcal{D}$  of 1.34 (corresponding to a surface coverage of 0.23 chains nm<sup>-2</sup>) <sup>[303]</sup>, and suggesting a well-controlled polymerization process (inset in **Figure 6.3c**).

In order to test the applicability of Fe<sup>0</sup> SI-ATRP within cell cultures, we subsequently analyzed the growth of PMPC brushes using Dulbecco's modified Eagle's medium (DMEM) as a solvent, and simultaneously tested the cytocompatibility of the polymerization conditions employed towards ACs.

PMPC brushes are especially relevant in the design of biointerfaces due to their biocompatibility and inertness towards unspecific protein and cell contamination <sup>[304-306]</sup>. As a result of their pronounced hydration, the growth

of PMPC grafts from substrates previously cultured with cells would directly translate into an evident variation in the strength of cell attachment, leading to the progressive detachment of ACs when the thickness and density of the underlying brushes reached sufficiently high values [307].

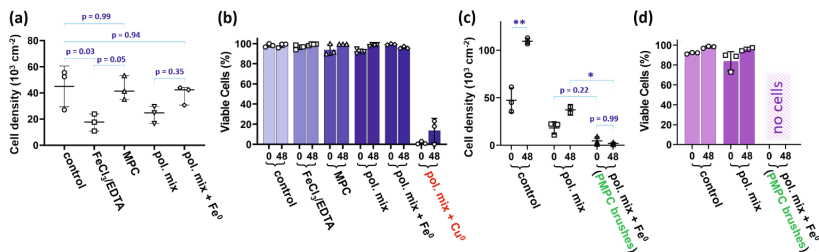


**Figure 6.4** (a) Density of ACs estimated after 24 h of culture on TCPS, followed by exposure for 1 h to different media, including DMEM (indicated as control), 5 mM Fe<sup>III</sup>Cl<sub>3</sub> in DMEM (indicated as EDTA/FeCl<sub>3</sub>), 0.3 M MPC in DMEM (indicated as MPC), 0.3 M MPC with 5 mM Fe<sup>III</sup>Cl<sub>3</sub>-EDTA and 10 mM NaCl (indicated as pol. mix), and the latter mixture covered by a Fe<sup>0</sup> plate (indicated as pol. mix + Fe<sup>0</sup>). Statistical analysis was conducted by one-way analysis of variance (ANOVA) with a Dunnett's post-hoc-Test; \* indicates p < 0.05. (b) Cell viability estimated by live-dead staining on AC cultures subjected for 1 h to the solutions indicated above, and a polymerization mixture including 0.3 M MPC, 5 mM CuBr<sub>2</sub>-tris(2-pyridylmethyl)amine (TPMA), 10 mM NaBr, and covered with a Cu<sup>0</sup> plate. (c) Density of ACs estimated after 24 h of culture on ATRP initiator-functionalized SiO<sub>2</sub> substrates and subjected to 1 h of exposure to different mixtures, and after the growth of PMPC brushes (pol. mix + Fe<sup>0</sup>). Statistical analysis was conducted by two-way ANOVA with Tukey's multiple comparisons test; \* indicates p < 0.05, \*\* indicates p < 0.001. (d) Cell viability estimated by live-dead staining for AC cultures on ATRP initiator-bearing SiO<sub>2</sub> surfaces subjected for 1 h to different mixtures.

Fe<sup>0</sup> SI-ATRP of a diluted, 0.3 M MPC solution in DMEM using 5 mM Fe<sup>III</sup>Cl<sub>3</sub>-EDTA resulted in a slow but notable growth of brushes, which reached ~ 15 nm after 60 min of reaction (Figure 6.3b). Relevantly, the slower polymer-brush thickening rate compared to those recorded using pure water as solvent (Figure 6.3a) was mainly due to the relatively low monomer concentration employed (Figure S6.4). When ACs were cultured for 24 h on tissue culture polystyrene wells (TCPS), and subsequently exposed for 1 hour to a 0.3 M DMEM solution of MPC, the cell density did not significantly vary (from 45000 ± 12700 to 43200 ± 7500 cells cm<sup>-2</sup>, p = 0.99) (Figure 6.4a), while cell viability was higher than 90% just after exposure to monomer

solution, and increased to 98% after 48 h of additional culture in standard DMEM-based medium (**Figure 6.4b**). Incubation for 1 h in 5 mM DMEM solution of  $\text{Fe}^{\text{III}}\text{Cl}_3$ -EDTA resulted in a significant reduction in cell density ( $17500 \pm 5300 \text{ cells cm}^{-2}$ ) both with respect to the control ( $p = 0.03$ ), and compared to the substrates treated with just 0.3 M MPC ( $p = 0.05$ ) (**Figure 6.4a**).

Partial cell detachment after treatment with  $\text{Fe}^{\text{III}}\text{Cl}_3$ -EDTA was presumably due to complexation of  $\text{Ca}^{\text{II}}$  within membrane proteins by residual amounts of unbound ligand, which influenced integrin-mediated ACs adhesion [308-309]. A comparable result was observed when ACs were incubated in the complete polymerization mixture (0.3 M MPC + 5 mM  $\text{Fe}^{\text{III}}\text{Cl}_3$ -EDTA), while a slight increment in cell density was recorded when  $\text{Fe}^0$ -coated plates were additionally placed in contact with the cultures, reproducing the reaction setup typically employed during  $\text{Fe}^0$  SI-ATRP of MPC ( $p = 0.35$ , **Figure 6.4a**). In these samples, additional  $\text{Fe}^{\text{II}}/\text{Fe}^{\text{III}}$  species leaking from the iron plates were probably complexed by the residual, unbound EDTA, finally preventing complexation of  $\text{Ca}^{\text{II}}$  from cell proteins.

It is important to emphasize that, despite the observed variations in cell density after exposure to the different monomer/ligand mixtures, AC viability was in all cases higher than 90%, and comparable to that measured for the controls. Even when the oxygen dissolved in the culture media was rapidly consumed by exposure to  $\text{Fe}^0$ , the tolerance of chondrocytes towards anaerobic conditions [310] guaranteed their remarkably high viability, while AC densities were similar to those recorded for the control samples ( $39000 \pm 6000$  and  $45000 \pm 12700 \text{ cells cm}^{-2}$ , respectively, in **Figure 6.4a**,  $p = 0.94$ ). The cytocompatibility of the polymerization mixtures employed during  $\text{Fe}^0$  SI-ATRP was further highlighted by comparing the viability of ACs exposed to a corresponding Cu-based catalytic system, which was previously reported to enable the rapid growth of polymer brushes by  $\text{Cu}^0$  SI-ATRP [287, 289, 311-316]. In this latter case, AC viability was nearly 0% after 1 h of exposure, and

increased just to ~ 10% following 48 h of further culture in standard medium (**Figure 6.4b** and **Figure S6.5**), confirming the toxicity towards mammalian cells of mixtures typically employed during Cu-based ATRP.

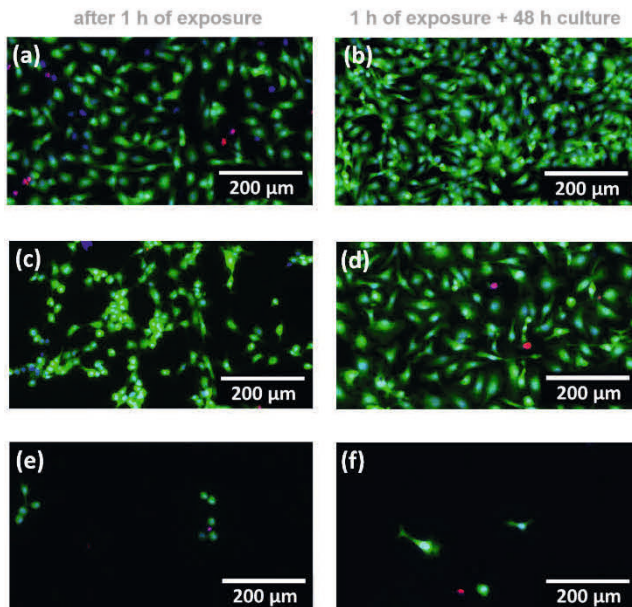


**Figure 6.5** Immunofluorescence micrographs displaying ACs stained with calcein AM (green), Hoechst 33342 (blue), and propidium iodide (red) after 1 h of exposure to the different polymerization mixtures (a, c, e) and following 48 h of further culture (b, d, f).

When TCPS substrates were replaced by ATRP-initiator-bearing  $\text{SiO}_x$  surfaces, the effect of PMPC brush growth on AC adhesion was analyzed.

Also in these experiments, ACs were initially cultured on the substrates for 24 h, followed by exposure to different mixtures for 1h, followed by additional 48 h of culture.

Cell density significantly decreased after 1 h of exposure to the polymerization mixture (0.3 M MPC, 5 mM  $\text{Fe}^{\text{III}}\text{Cl}_3$ -EDTA) compared to that measured when ACs were simply incubated in DMEM-based medium,

from  $47400 \pm 11000$  to  $18300 \pm 12700$  cells  $\text{cm}^{-2}$  ( $p < 0.05$ ). Nevertheless, cell viability remained relatively high ( $83 \pm 15\%$ ). As highlighted in the immunofluorescence micrographs reported in **Figure 6.5c**, ACs exhibited a more rounded morphology as a result of partial inhibition of cell-cell and cell-substrate adhesion through  $\text{Ca}^{\text{II}}$  complexation by EDTA. However, it is remarkable that following a further 48 h of culture in standard medium an increment in cell density from  $18300 \pm 12700$  to  $37300 \pm 6900$  cells  $\text{cm}^{-2}$  ( $p = 0.08$ ) was observed, due to AC proliferation, basically attaining cell densities similar to those recorded before exposure to the polymerization medium. This result confirmed the cytocompatibility of the polymerization conditions applied during  $\text{Fe}^0$  SI-ATRP. In addition, a well-spread cell morphology was completely recovered (**Figure 6.5d**), indicating that ACs strongly adhered to the substrate after an additional 48 h of culture.

When  $\text{Fe}^0$ -coated plates were applied together with the polymerization mixtures on AC cultures, the rapid growth of PMPC brushes led to the formation of a highly hydrated, and cell-repellent interface, which substantially weakened AC attachment and lead to a nearly complete detachment of cells ( $4700 \pm 4300$  cells  $\text{cm}^{-2}$ , after 1 h of exposure). Relatively few, rounded cells remained on the substrates, adhering to surface defects where polymer grafting did not occur due to the adventitious, mechanical removal of ATRP initiator, and were surrounded by a uniform film of PMPC brushes, as evidenced by atomic force microscopy (AFM) (**Figure 6.6**). Selective deposition of ATRP initiator on just one side of a silicon substrate additionally proved that  $\text{Fe}^0$  SI-ATRP could be easily applied to spatially control the growth of biopassive polymer brushes, and trigger cell detachment specifically on the areas of the substrate where polymer grafting could be initiated (**Figure S6.6**).



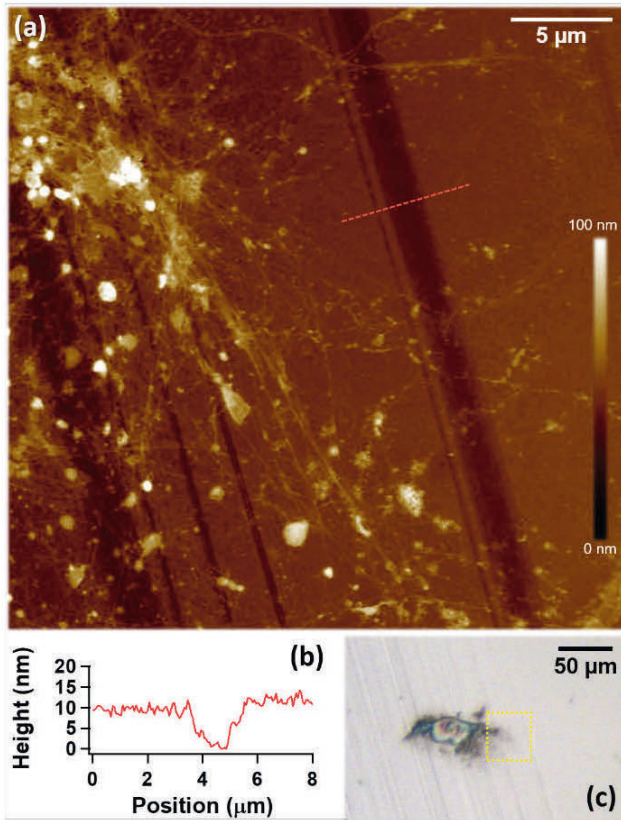


**Figure 6.6** (a) AFM tapping mode micrographs displaying cellular components of ACs extending on surface defects where PMPC brushes did not grow following  $\text{Fe}^0$  SI-ATRP, due to mechanical removal of ATRP initiator layer. In (b) a cross section highlighting the height of PMPC brushes around a mechanically scratched area on the substrate is provided. The optical micrograph (c) displays how ACs remained attached on areas where PMPC brushes could not be grown due to the removal of ATRP initiator layer by mechanical scratching.

These results collectively indicated that PMPC-brush growth by  $\text{Fe}^0$  SI-ATRP could be performed from AC cultures, substantially altering the interfacial physicochemical properties of the supporting substrates, and thus strongly influencing cell attachment. The observed release of cells was clearly



not due to the polymerization conditions applied during culturing, as confirmed by the tolerance of ACs towards the reaction mixtures, their markedly high viability and tendency to proliferate in such media.

The growth of bio-repellent brushes, mediated by  $\text{Fe}^0$ , emerges as the main phenomenon leading to a critical shift in the characteristics of the surrounding environment, to which ACs respond by weakening their affinity towards the substrates, ultimately being released from a surface that is no longer bio-adhesive.

It is noteworthy to mention that ATRP methods were already demonstrated to be applicable within cell cultures while maintaining viable cells <sup>[317]</sup>. However, polymer growth was tested in the presence of yeast cells, which are known to be extremely resilient, and which, similarly to bacteria, are protected by strong cell walls and can survive greater stresses than mammalian cells <sup>[318]</sup>.

### 6.3 Conclusions

Due to its tolerance to ambient conditions and scalability,  $\text{Fe}^0$  SI-ATRP emerges as a versatile method to synthesize chemically diverse polymer brushes for a variety of materials formulations. Its highly confined nature enables the generation of uniform brush films over very large areas, without the need of previous deoxygenation of the reaction mixtures or the presence of an inert atmosphere, and by employing just few microliters of monomer/catalyst solutions. These unique features, which are highlighted through a comprehensive analysis of its mechanistic aspects, make  $\text{Fe}^0$  SI-ATRP a very promising technique for translating SI-RDRP processes into technologically relevant surface fabrications.

Thanks to its cytocompatibility towards mammalian cells,  $\text{Fe}^0$  SI-ATRP could be easily applied to biomaterials and within tissue engineering constructs, dynamically tuning the physicochemical properties of cell microenvironments.

---

## Bibliography

- [1] M. Kragl, D. Knapp, E. Nacu, S. Khattak, M. Maden, H. H. Epperlein, E. M. Tanaka, *Nature* **2009**, 460, 60.
- [2] S. Roy, S. Gatién, *Experimental gerontology* **2008**, 43, 968.
- [3] S. R. Voss, H. H. Epperlein, E. M. Tanaka, *Cold Spring Harbor Protocols* **2009**, 2009, pdb. emo128.
- [4] C. Castells-Sala, M. Alemany-Ribes, T. Fernández-Muiños, L. Recha-Sancho, P. López-Chicón, C. Aloy-Reverté, J. Caballero-Camino, A. Márquez-Gil, C. E. Semino, *Journal of Biochips & Tissue Chips* **2013**, 1.
- [5] A. Shafiee, A. Atala, *Annual review of medicine* **2017**, 68, 29.
- [6] J. P. Vacanti, R. Langer, *The lancet* **1999**, 354, S32.
- [7] C. Mason, P. Dunnill, *Regen Med* **2008**, 3, 1.
- [8] A. Atala, *Journal of tissue engineering and regenerative medicine* **2007**, 1, 83.
- [9] L. G. Griffith, G. Naughton, *science* **2002**, 295, 1009.
- [10] F. Starnecker, F. Koenig, C. Hagl, N. Thierfelder, *Journal of Biomedical Materials Research Part B: Applied Biomaterials* **2018**, 106, 153.
- [11] A. H. Reddi, *Tissue engineering* **2000**, 6, 351.
- [12] A.-M. Freyria, F. Mallein-Gerin, *Injury* **2012**, 43, 259.
- [13] P. A. Netti, in *Regenerative Medicine Applications in Organ Transplantation*, Elsevier **2014**, p. 137.
- [14] A. Salerno, P. Netti, E. Di Maio, S. Iannace, *Journal of cellular plastics* **2009**, 45, 103.
- [15] V. Guarino, F. Causa, A. Salerno, L. Ambrosio, P. Netti, *Materials Science and Technology* **2008**, 24, 1111.
- [16] C. M. Murphy, F. J. O'Brien, *Cell adhesion & migration* **2010**, 4, 377.
- [17] M. Ventre, F. Causa, P. A. Netti, *Journal of the Royal Society Interface* **2012**, 9, 2017.
- [18] A. K. A. Silva, C. Richard, M. Bessodes, D. Scherman, O.-W. Merten, *Biomacromolecules* **2009**, 10, 9.
- [19] E. S. Place, N. D. Evans, M. M. Stevens, *Nature materials* **2009**, 8, 457.

## Bibliography

---

- [20] F. Causa, E. Battista, R. Della Moglie, D. Guarnieri, M. Iannone, P. A. Netti, *Langmuir* **2010**, 26, 9875.
- [21] C. Borselli, O. Oliviero, S. Battista, L. Ambrosio, P. A. Netti, *Journal of Biomedical Materials Research Part A* **2007**, 80, 297.
- [22] R. Gruber, H. Koch, B. A. Doll, F. Tegtmeier, T. A. Einhorn, J. O. Hollinger, *Experimental gerontology* **2006**, 41, 1080.
- [23] D. Clark, M. Nakamura, T. Miclau, R. Marcucio, *Current osteoporosis reports* **2017**, 15, 601.
- [24] K. L. Moffat, R. A. Neal, L. E. Freed, F. Guilak, in *Principles of tissue engineering*, Elsevier **2014**, p. 237.
- [25] H. H. Lu, S. F. El-Amin, K. D. Scott, C. T. Laurencin, *Journal of Biomedical Materials Research Part A*: **2003**, 64, 465.
- [26] P. D. Benya, J. D. Shaffer, *Cell* **1982**, 30, 215.
- [27] K. Von Der Mark, V. Gauss, H. Von Der Mark, P. Müller, *Nature* **1977**, 267, 531.
- [28] O. W. Petersen, L. Rønnev-Jessen, A. R. Howlett, M. J. Bissell, *Proceedings of the National Academy of Sciences* **1992**, 89, 9064.
- [29] D. Wu, Z. Wang, Z. Zheng, Y. Geng, Z. Zhang, Q. Li, Q. Zhou, Y. Cao, Z.-Y. Zhang, *Journal of translational medicine* **2018**, 16, 1.
- [30] F. Jakob, R. Ebert, A. Ignatius, T. Matsushita, Y. Watanabe, J. Groll, H. Walles, *Maturitas* **2013**, 75, 118.
- [31] E. B. Hunziker, K. Lippuner, M. Keel, N. Shintani, *Osteoarthritis and cartilage* **2015**, 23, 334.
- [32] G. Knutsen, J. O. Drogset, L. Engebretsen, T. Grøntvedt, V. Isaksen, T. C. Ludvigsen, S. Roberts, E. Solheim, T. Strand, O. Johansen, *JBJS* **2007**, 89, 2105.
- [33] B. A. Bunnell, B. T. O'Donnell, C. J. Ives, *Frontiers in bioengineering and biotechnology* **2019**, 7, 95.
- [34] Y. Jiang, D. Wang, A. Blocki, R. S. Tuan, in *Principles of Tissue Engineering*, Elsevier **2020**, p. 883.
- [35] B. Dionigi, D. O. Fauza, in *StemBook [Internet]*, Harvard Stem Cell Institute **2012**.
- [36] C. E. Murry, G. Keller, *Cell* **2008**, 132, 661.
- [37] M. H. Lee, J. A. Arcidiacono, A. M. Bilek, J. J. Wille, C. A. Hamill, K. M. Wonnacott, M. A. Wells, S. S. Oh, *Tissue Engineering Part B: Reviews* **2010**, 16, 41.

- [38] T. Togo, A. Utani, M. Naitoh, M. Ohta, Y. Tsuji, N. Morikawa, M. Nakamura, S. Suzuki, *Laboratory investigation* **2006**, 86, 445.
- [39] M. F. Pittenger, A. M. Mackay, S. C. Beck, R. K. Jaiswal, R. Douglas, J. D. Mosca, M. A. Moorman, D. W. Simonetti, S. Craig, D. R. Marshak, *science* **1999**, 284, 143.
- [40] T. Amos, M. Gordon, *Cell transplantation* **1995**, 4, 547.
- [41] J. Y. Lee, Z. Qu-Petersen, B. Cao, S. Kimura, R. Jankowski, J. Cummins, A. Usas, C. Gates, P. Robbins, A. Wernig, *The Journal of cell biology* **2000**, 150, 1085.
- [42] R. Tevlin, G. Walmsley, O. Marcic, M. S. Hu, D. Wan, M. Longaker, *Drug delivery and translational research* **2016**, 6, 159.
- [43] E. Hunziker, T. Quinn, H.-J. Häuselmann, *Osteoarthritis and Cartilage* **2002**, 10, 564.
- [44] T. Quinn, H.-J. Häuselmann, N. Shintani, E. B. Hunziker, *Osteoarthritis and cartilage* **2013**, 21, 1904.
- [45] F. Shapiro, S. Koide, M. J. Glimcher, *The Journal of bone and joint surgery. American volume* **1993**, 75, 532.
- [46] E. B. Hunziker, *Osteoarthritis and cartilage* **2002**, 10, 432.
- [47] L. Zhang, J. Hu, K. A. Athanasiou, *Critical Reviews™ in Biomedical Engineering* **2009**, 37.
- [48] S. M. Hussain, Y. Wang, F. M. Cicuttini, J. A. Simpson, G. G. Giles, S. Graves, A. E. Wluka, presented at Seminars in arthritis and rheumatism **2014**.
- [49] R. K. Chaganti, N. E. Lane, *Current reviews in musculoskeletal medicine* **2011**, 4, 99.
- [50] J. R. Steadman, W. G. Rodkey, S. B. Singleton, K. K. Briggs, *Operative techniques in orthopaedics* **1997**, 7, 300.
- [51] C. Hoemann, J. Sun, M. McKee, A. Chevrier, E. Rossomacha, G.-E. Rivard, M. Hurtig, M. Buschmann, *Osteoarthritis and Cartilage* **2007**, 15, 78.
- [52] H. Chen, J. Sun, C. D. Hoemann, V. Lascau-Coman, W. Ouyang, M. D. McKee, M. S. Shive, M. D. Buschmann, *Journal of Orthopaedic Research* **2009**, 27, 1432.
- [53] T. Furukawa, D. Eyre, S. Koide, M. Glimcher, *J Bone Joint Surg* **1980**, 62, 79.
- [54] J. L. Koh, K. Wirsing, E. Lautenschlager, L.-O. Zhang, *The American journal of sports medicine* **2004**, 32, 317.
- [55] N. B. Kock, G. Hannink, A. van Kampen, N. Verdonshot, J. L. van Susante, P. Buma, *Knee Surgery, Sports Traumatology, Arthroscopy* **2011**, 19, 1962.

## Bibliography

---

- [56] C. Tibesku, T. Szuwart, T. Kleffner, P. Schlegel, U. Jahn, H. Van Aken, S. Fuchs, *Journal of orthopaedic research* **2004**, 22, 1210.
- [57] K. Baumbach, J.-P. Petersen, P. Ueblacker, J. Schröder, C. Göpfert, A. Stork, J. M. Rueger, M. Amling, N. M. Meenen, *Archives of orthopaedic and trauma surgery* **2008**, 128, 1255.
- [58] D. Kolker, M. Murray, M. Wilson, *The Journal of bone and joint surgery. British volume* **2004**, 86, 521.
- [59] C. Vinatier, J. Guicheux, *Annals of physical and rehabilitation medicine* **2016**, 59, 139.
- [60] C. Jones, C. Willers, A. Keogh, D. Smolinski, D. Fick, P. Yates, T. Kirk, M. Zheng, *Journal of Orthopaedic Research* **2008**, 26, 292.
- [61] P. C. Kreuz, R. H. Kalkreuth, P. Niemeyer, M. Uhl, C. Erggelet, *Cartilage* **2019**, 10, 305.
- [62] E. B. Hunziker, *Clinical Orthopaedics and Related Research*® **1999**, 367, S135.
- [63] E. B. Hunziker, *Osteoarthritis and Cartilage* **1999**, 7, 15.
- [64] S. V. Murphy, A. Atala, *Nat Biotechnol* **2014**, 32, 773.
- [65] R. Bracci, E. Maccaroni, S. Cascinu, *New England Journal of Medicine* **2013**, 368, 2043.
- [66] M. Nakamura, S. Iwanaga, C. Henmi, K. Arai, Y. Nishiyama, *Biofabrication* **2010**, 2, 014110.
- [67] J. Groll, T. Boland, T. Blunk, J. A. Burdick, D.-W. Cho, P. D. Dalton, B. Derby, G. Forgacs, Q. Li, V. A. Mironov, *Biofabrication* **2016**, 8, 013001.
- [68] J. Malda, J. Visser, F. P. Melchels, T. Jüngst, W. E. Hennink, W. J. Dhert, J. Groll, D. W. Hutmacher, *Advanced materials* **2013**, 25, 5011.
- [69] J. Li, M. Chen, X. Fan, H. Zhou, *Journal of translational medicine* **2016**, 14, 271.
- [70] F. Pati, J. Jang, J. W. Lee, D.-W. Cho, in *Essentials of 3D biofabrication and translation*, Elsevier **2015**, p. 123.
- [71] A. McCormack, C. B. Highley, N. R. Leslie, F. P. Melchels, *Trends in Biotechnology* **2020**.
- [72] T. Bhattacharjee, S. M. Zehnder, K. G. Rowe, S. Jain, R. M. Nixon, W. G. Sawyer, T. E. Angelini, *Science advances* **2015**, 1, e1500655.
- [73] T. Jiang, J. G. Munguia-Lopez, S. Flores-Torres, J. Kort-Mascort, J. M. Kinsella, *Applied Physics Reviews* **2019**, 6, 011310.
- [74] C. B. Highley, C. B. Rodell, J. A. Burdick, *Advanced Materials* **2015**, 27, 5075.

- [75] T. J. Hinton, Q. Jallerat, R. N. Palchesko, J. H. Park, M. S. Grodzicki, H.-J. Shue, M. H. Ramadan, A. R. Hudson, A. W. Feinberg, *Science advances* **2015**, 1, e1500758.
- [76] A. Lee, A. Hudson, D. Shiwarski, J. Tashman, T. Hinton, S. Yerneni, J. Bliley, P. Campbell, A. Feinberg, *Science* **2019**, 365, 482.
- [77] O. Jeon, Y. B. Lee, H. Jeong, S. J. Lee, D. Wells, E. Alsborg, *Materials Horizons* **2019**, 6, 1625.
- [78] A. M. Compaan, K. Song, Y. Huang, *ACS applied materials & interfaces* **2019**, 11, 5714.
- [79] S. Duchi, C. Onofrillo, C. D. O'Connell, R. Blanchard, C. Augustine, A. F. Quigley, R. M. Kapsa, P. Pivonka, G. Wallace, C. Di Bella, *Scientific reports* **2017**, 7, 1.
- [80] S. H. Ahn, H. J. Lee, J.-S. Lee, H. Yoon, W. Chun, G. H. Kim, *Scientific reports* **2015**, 5, 13427.
- [81] C. D O'Connell, C. Di Bella, F. Thompson, C. Augustine, S. Beirne, R. Cornock, C. J. Richards, J. Chung, S. Gambhir, Z. Yue, *Biofabrication* **2016**, 8, 015019.
- [82] Y. Zhang, Y. Yu, A. Akkouch, A. Dababneh, F. Dolati, I. T. Ozbolat, *Biomaterials science* **2015**, 3, 134.
- [83] I. T. Ozbolat, W. Peng, V. Ozbolat, *Drug discovery today* **2016**, 21, 1257.
- [84] M. Costantini, S. Testa, P. Mozetic, A. Barbetta, C. Fuoco, E. Fornetti, F. Tamiro, S. Bernardini, J. Jaroszewicz, W. Świąszkowski, *Biomaterials* **2017**, 131, 98.
- [85] S. Benedikt, J. Wang, M. Markovic, N. Moszner, K. Dietliker, A. Ovsianikov, H. Grützmacher, R. Liska, *Journal of Polymer Science Part A: Polymer Chemistry* **2016**, 54, 473.
- [86] H. Shih, C. C. Lin, *Macromolecular rapid communications* **2013**, 34, 269.
- [87] C. Bahney, T. Lujan, C. Hsu, M. Bottlang, J. West, B. Johnstone, *European cells & materials* **2011**, 22, 43.
- [88] R. Holmes, X.-B. Yang, A. Dunne, L. Florea, D. Wood, G. Tronci, *Polymers* **2017**, 9, 226.
- [89] L. A. Sawicki, A. M. Kloxin, *Biomaterials science* **2014**, 2, 1612.
- [90] B. D. Fairbanks, M. P. Schwartz, C. N. Bowman, K. S. Anseth, *Biomaterials* **2009**, 30, 6702.
- [91] C. M. O'Brien, B. Holmes, S. Faucett, L. G. Zhang, *Tissue Engineering Part B: Reviews* **2015**, 21, 103.
- [92] M. Guvendiren, J. Molde, R. M. Soares, J. Kohn, *ACS biomaterials science & engineering* **2016**, 2, 1679.

## Bibliography

---

- [93] A. Skardal, A. Atala, *Annals of biomedical engineering* **2015**, 43, 730.
- [94] B. Grigoryan, S. J. Paulsen, D. C. Corbett, D. W. Sazer, C. L. Fortin, A. J. Zaita, P. T. Greenfield, N. J. Calafat, J. P. Gounley, A. H. Ta, *Science* **2019**, 364, 458.
- [95] P. E. Watson, I. D. Watson, R. D. Batt, *The American journal of clinical nutrition* **1980**, 33, 27.
- [96] A. S. Hoffman, *Advanced drug delivery reviews* **2012**, 64, 18.
- [97] B. D. Ratner, A. S. HOFFMAN, ACS Publications **1976**.
- [98] K. Y. Lee, D. J. Mooney, *Chemical reviews* **2001**, 101, 1869.
- [99] O. Wichterle, D. Lim, *Nature* **1960**, 185, 117.
- [100] *Zeitschrift für Chemie und Industrie der Kolloide* **1907**, 1, 213.
- [101] S. J. Buwalda, K. W. Boere, P. J. Dijkstra, J. Feijen, T. Vermonden, W. E. Hennink, *Journal of controlled release* **2014**, 190, 254.
- [102] R. Censi, P. Di Martino, T. Vermonden, W. E. Hennink, *Journal of Controlled Release* **2012**, 161, 680.
- [103] W. E. Hennink, C. F. van Nostrum, *Advanced drug delivery reviews* **2012**, 64, 223.
- [104] E. Ruel-Gariepy, J.-C. Leroux, *European Journal of Pharmaceutics and Biopharmaceutics* **2004**, 58, 409.
- [105] M. A. Ward, T. K. Georgiou, *Polymers* **2011**, 3, 1215.
- [106] N. Broguiere, E. Cavalli, G. M. Salzmann, L. A. Applegate, M. Zenobi-Wong, *ACS Biomaterials Science & Engineering* **2016**, 2, 2176.
- [107] I. W. Velthoen, J. Van Beek, P. J. Dijkstra, J. Feijen, *Reactive and Functional Polymers* **2011**, 71, 245.
- [108] Y. Okuyama, R. Yoshida, K. Sakai, T. Okano, Y. Sakurai, *Journal of Biomaterials Science, Polymer Edition* **1993**, 4, 545.
- [109] F. Martellini, L. H. Mei, J. L. Baliño, M. Carenza, *Radiation Physics and Chemistry* **2003**, 66, 155.
- [110] H. Yang, W. J. Kao, *Pharmaceutical research* **2006**, 23, 205.
- [111] Y. S. Zhang, A. Khademhosseini, *Science* **2017**, 356, eaaf3627.
- [112] P. W. Rothemund, *Nature* **2006**, 440, 297.
- [113] S. Zhang, *Nature biotechnology* **2003**, 21, 1171.



- [114] M. F. Perutz, J. T. Finch, J. Berriman, A. Lesk, *Proceedings of the National Academy of Sciences* **2002**, 99, 5591.
- [115] G. Liu, Q. Yuan, G. Hollett, W. Zhao, Y. Kang, J. Wu, *Polymer Chemistry* **2018**, 9, 3436.
- [116] C. B. Rodell, A. L. Kaminski, J. A. Burdick, *Biomacromolecules* **2013**, 14, 4125.
- [117] L. S. M. Teixeira, J. Feijen, C. A. van Blitterswijk, P. J. Dijkstra, M. Karperien, *Biomaterials* **2012**, 33, 1281.
- [118] U. P. Shinde, B. Yeon, B. Jeong, *Progress in polymer science* **2013**, 38, 672.
- [119] A. S. Sawhney, C. P. Pathak, J. A. Hubbell, *Macromolecules* **1993**, 26, 581.
- [120] P. A. Levett, F. P. Melchels, K. Schrobback, D. W. Huttmacher, J. Malda, T. J. Klein, *Acta biomaterialia* **2014**, 10, 214.
- [121] K. Yue, G. Trujillo-de Santiago, M. M. Alvarez, A. Tamayol, N. Annabi, A. Khademhosseini, *Biomaterials* **2015**, 73, 254.
- [122] H. Shirahama, B. H. Lee, L. P. Tan, N.-J. Cho, *Scientific reports* **2016**, 6, 1.
- [123] S. K. Hahn, J. K. Park, T. Tomimatsu, T. Shimoboji, *International journal of biological macromolecules* **2007**, 40, 374.
- [124] K. A. Smeds, A. Pfister-Serres, D. L. Hatchell, M. W. GRINSTAFF, *Journal of Macromolecular Science—Pure and Applied Chemistry* **1999**, 36, 981.
- [125] B. Baroli, *Journal of Chemical Technology & Biotechnology: International Research in Process, Environmental & Clean Technology* **2006**, 81, 491.
- [126] S. Lu, K. S. Anseth, *Journal of controlled release* **1999**, 57, 291.
- [127] L. Xu, N. Sheybani, W. A. Yeudall, H. Yang, *Biomaterials science* **2015**, 3, 250.
- [128] C. G. Williams, A. N. Malik, T. K. Kim, P. N. Manson, J. H. Elisseeff, *Biomaterials* **2005**, 26, 1211.
- [129] D. Liang-Chang, Y. Qi, A. S. Hoffman, *Journal of controlled release* **1992**, 19, 171.
- [130] J.-Y. Sun, X. Zhao, W. R. Illeperuma, O. Chaudhuri, K. H. Oh, D. J. Mooney, J. J. Vlassak, Z. Suo, *Nature* **2012**, 489, 133.
- [131] P. Matricardi, C. Di Meo, T. Coviello, W. E. Hennink, F. Alhaique, *Advanced Drug Delivery Reviews* **2013**, 65, 1172.
- [132] A. Sionkowska, *Progress in polymer science* **2011**, 36, 1254.
- [133] Z. A. Schnepf, R. Gonzalez-McQuire, S. Mann, *Advanced Materials* **2006**, 18, 1869.

## Bibliography

---

- [134] H. Li, D. Q. Wang, H. L. Chen, B. L. Liu, L. Z. Gao, *Macromolecular Bioscience* **2003**, 3, 720.
- [135] Y. Yue, J. Han, G. Han, A. D. French, Y. Qi, Q. Wu, *Carbohydrate polymers* **2016**, 147, 155.
- [136] M. Müller, E. Öztürk, Ø. Arlov, P. Gatenholm, M. Zenobi-Wong, *Annals of biomedical engineering* **2017**, 45, 210.
- [137] S. Bhattacharyya, S. Guillot, H. Dabboue, J.-F. Tranchant, J.-P. Salvetat, *Biomacromolecules* **2008**, 9, 505.
- [138] N. Annabi, J. W. Nichol, X. Zhong, C. Ji, S. Koshy, A. Khademhosseini, F. Dehghani, *Tissue Engineering Part B: Reviews* **2010**, 16, 371.
- [139] T. Billiet, M. Vandenhaute, J. Schelfhout, S. Van Vlierberghe, P. Dubruel, *Biomaterials* **2012**, 33, 6020.
- [140] Y. Jiang, J. Chen, C. Deng, E. J. Suuronen, Z. Zhong, *Biomaterials* **2014**, 35, 4969.
- [141] Y. Du, E. Lo, S. Ali, A. Khademhosseini, *Proceedings of the National Academy of Sciences* **2008**, 105, 9522.
- [142] L. Riley, L. Schirmer, T. Segura, *Current Opinion in Biotechnology* **2019**, 60, 1.
- [143] A. C. Daly, L. Riley, T. Segura, J. A. Burdick, *Nature Reviews Materials* **2019**, DOI: 10.1038/s41578-019-0148-6.
- [144] N. F. Truong, E. Kurt, N. Tahmizyan, S. C. Lesher-Perez, M. Chen, N. J. Darling, W. Xi, T. Segura, *Acta Biomater* **2019**, 94, 160.
- [145] C. B. Highley, K. H. Song, A. C. Daly, J. A. Burdick, **2019**, 6, 1801076.
- [146] S. J. Xin, D. Chimene, J. E. Garza, A. K. Gaharwar, D. L. Alge, *Biomater Sci-Uk* **2019**, 7, 1179.
- [147] S. Xin, O. M. Wyman, D. L. Alge, *Advanced healthcare materials* **2018**, 7, 1800160.
- [148] D. Guzman-Villanueva, H. D. Smyth, D. Herrera-Ruiz, I. M. El-Sherbiny, *Journal of nanomaterials* **2011**, 2011.
- [149] Y. Xin, G. Chai, T. Zhang, X. Wang, M. Qu, A. Tan, M. Bogari, M. Zhu, L. Lin, Q. Hu, *Biomedical reports* **2016**, 5, 723.
- [150] A. Townsend-Nicholson, S. N. Jayasinghe, *Biomacromolecules* **2006**, 7, 3364.
- [151] T. P. Lagus, J. F. Edd, *Journal of Physics D: Applied Physics* **2013**, 46, 114005.
- [152] T. S. Kaminski, O. Scheler, P. Garstecki, *Lab on a Chip* **2016**, 16, 2168.

- 
- [153] Z. Zhang, N. Xu, D. T. Chen, P. Yunker, A. M. Alsayed, K. B. Aptowicz, P. Habdas, A. J. Liu, S. R. Nagel, A. G. Yodh, *Nature* **2009**, 459, 230.
- [154] G. M. Conley, P. Aebischer, S. Nöjd, P. Schurtenberger, F. Scheffold, *Science advances* **2017**, 3, e1700969.
- [155] C. B. Highley, K. H. Song, A. C. Daly, J. A. Burdick, *Advanced Science* **2019**, 6, 1801076.
- [156] S. Xin, D. Chimene, J. E. Garza, A. K. Gaharwar, D. L. Alge, *Biomaterials science* **2019**, 7, 1179.
- [157] D. R. Griffin, W. M. Weaver, P. O. Scumpia, D. Di Carlo, T. Segura, *Nature materials* **2015**, 14, 737.
- [158] T. C. Hales, *arXiv preprint math/9811071* **1998**.
- [159] A. S. Caldwell, G. T. Campbell, K. M. T. Shekiri, K. S. Anseth, *Advanced Healthcare Materials* **2017**, 6.
- [160] A. Sheikhi, J. de Rutte, R. Haghniaz, O. Akouissi, A. Sohrabi, D. Di Carlo, A. Khademhosseini, *Biomaterials* **2019**, 192, 560.
- [161] J. DeSimone, M. Parrott, A. Murphy, R. A. Petros, Google Patents, 2015.
- [162] A. J. Krüger, J. Köhler, S. Cichosz, J. C. Rose, D. B. Gehlen, T. Haraszti, M. Möller, L. De Laporte, *Chemical Communications* **2018**, 54, 6943.
- [163] J. P. Rolland, B. W. Maynor, L. E. Euliss, A. E. Exner, G. M. Denison, J. M. DeSimone, *Journal of the American Chemical Society* **2005**, 127, 10096.
- [164] A. J. Krüger, O. Bakirman, L. P. Guerzoni, A. Jans, D. B. Gehlen, D. Rommel, T. Haraszti, A. J. Kuehne, L. De Laporte, *Advanced Materials* **2019**, 31, 1903668.
- [165] H. Rogan, F. Ilagan, X. Tong, C. R. Chu, F. Yang, *Biomaterials* **2020**, 228, 119579.
- [166] F. Jiang, H. Hörber, J. Howard, D. J. Müller, *Journal of structural biology* **2004**, 148, 268.
- [167] A. Sinclair, M. B. O'Kelly, T. Bai, H. C. Hung, P. Jain, S. Jiang, *Advanced Materials* **2018**, 30, 1803087.
- [168] Y. Li, C. T. Poon, M. Li, T. J. Lu, B. Pingguan-Murphy, F. Xu, *Advanced Functional Materials* **2015**, 25, 5999.
- [169] W. Peng, P. Datta, Y. Wu, M. Dey, B. Ayan, A. Dababneh, I. T. Ozbolat, in *Cell Biology and Translational Medicine, Volume 3*, Springer **2018**, p. 53.
- [170] T. Sato, H. Clevers, *Science* **2013**, 340, 1190.
- [171] G. Rossi, A. Manfrin, M. P. Lutolf, *Nature Reviews Genetics* **2018**, 19, 671.

## Bibliography

---

- [172] L. Moroni, J. A. Burdick, C. Highley, S. J. Lee, Y. Morimoto, S. Takeuchi, J. J. Yoo, *Nature Reviews Materials* **2018**, 3, 21.
- [173] F. Khan, M. Tanaka, *International journal of molecular sciences* **2018**, 19, 17.
- [174] J. Kundu, F. Pati, Y. H. Jeong, D.-W. Cho, in *Biofabrication*, Elsevier **2013**, p. 23.
- [175] R. G. Wells, *Hepatology* **2008**, 47, 1394.
- [176] R. Fan, M. Piou, E. Darling, D. Cormier, J. Sun, J. Wan, *Journal of biomaterials applications* **2016**, 31, 684.
- [177] J. Berg, T. Hiller, M. S. Kissner, T. H. Qazi, G. N. Duda, A. C. Hocke, S. Hippenstiel, L. Elomaa, M. Weinhart, C. Fahrenson, *Scientific reports* **2018**, 8, 1.
- [178] S. Gunderson, R. Schiavone, *JOM* **1989**, 41, 60.
- [179] W. M. Kier, *Journal of Experimental Biology* **2012**, 215, 1247.
- [180] M. F. Hsueh, A. Khabut, S. Kjellstrom, P. Onnerfjord, V. B. Kraus, *J Proteome Res* **2016**, 15, 374.
- [181] C. Chung, J. A. Burdick, *Adv Drug Deliv Rev* **2008**, 60, 243.
- [182] E. A. Makris, A. H. Gomoll, K. N. Malizos, J. C. Hu, K. A. Athanasiou, *Nat Rev Rheumatol* **2015**, 11, 21.
- [183] A. R. Armiento, M. J. Stoddart, M. Alini, D. Eglin, *Acta Biomater* **2018**, 65, 1.
- [184] C. K. Kuo, P. X. Ma, *Biomaterials* **2001**, 22, 511.
- [185] S. J. Bidarra, C. C. Barrias, P. L. Granja, *Acta Biomater* **2014**, 10, 1646.
- [186] J. J. Rice, M. M. Martino, L. De Laporte, F. Tortelli, P. S. Briquez, J. A. Hubbell, *Adv Healthc Mater* **2013**, 2, 57.
- [187] R. O. Hynes, *Science* **2009**, 326, 1216.
- [188] C. B. Knudson, W. Knudson, *Semin Cell Dev Biol* **2001**, 12, 69.
- [189] C. C. Rider, B. Mulloy, *Molecules* **2017**, 22.
- [190] I. Freeman, A. Kedem, S. Cohen, *Biomaterials* **2008**, 29, 3260.
- [191] W. Xiao-feng, X. Ya-xiang, S. Guo-xin, K. Kaeko, T. Ryo, H. Saburo, *Journal of Zhejiang University-SCIENCE A* **2003**, 4, 86.
- [192] S. E. Sakiyama-Elbert, *Acta Biomater* **2014**, 10, 1581.
- [193] S. Liekens, D. Leali, J. Neyts, R. Esnouf, M. Rusnati, P. Dell'Era, P. C. Maudgal, E. De Clercq, M. Presta, *Mol Pharmacol* **1999**, 56, 204.

- [194] T. H. Nguyen, S. H. Kim, C. G. Decker, D. Y. Wong, J. A. Loo, H. D. Maynard, *Nat Chem* **2013**, 5, 221.
- [195] E. Ozturk, O. Arlov, S. Aksel, L. Li, D. M. Ornitz, G. Skjak-Braek, M. Zenobi-Wong, *Adv Funct Mater* **2016**, 26, 3649.
- [196] R. Mhanna, A. Kashyap, G. Palazzolo, Q. Vallmajo-Martin, J. Becher, S. Moller, M. Schnabelrauch, M. Zenobi-Wong, *Tissue Eng Part A* **2014**, 20, 1454.
- [197] A. Kerschenmeyer, O. Arlov, V. Malheiro, M. Steinwachs, M. Rottmar, K. Maniura-Weber, G. Palazzolo, M. Zenobi-Wong, *Biomater Sci* **2017**, 5, 1756.
- [198] D. D. Allison, K. J. Grande-Allen, *Tissue Eng* **2006**, 12, 2131.
- [199] M. W. Holmes, M. T. Bayliss, H. Muir, *Biochem J* **1988**, 250, 435.
- [200] J. R. E. Fraser, T. C. Laurent, U. Laurent, *Journal of internal medicine* **1997**, 242, 27.
- [201] M. K. Cowman, T. A. Schmidt, P. Raghavan, A. Stecco, *F1000Res* **2015**, 4, 622.
- [202] R. J. Peach, D. Hollenbaugh, I. Stamenkovic, A. Aruffo, *J Cell Biol* **1993**, 122, 257.
- [203] W. Knudson, C. Knudson, *Current Opinion in Orthopaedics* **2004**, 15, 369.
- [204] R. A. Bly, A. D. Bhrany, C. S. Murakami, K. C. Sie, *Facial Plast Surg Clin North Am* **2016**, 24, 577.
- [205] C. C. Breugem, K. J. Stewart, M. Kon, *J Craniofac Surg* **2011**, 22, 1367.
- [206] E. C. Bingham, *An investigation of the laws of plastic flow*, US Government Printing Office, **1917**.
- [207] P. Bajaj, R. M. Schweller, A. Khademhosseini, J. L. West, R. Bashir, *Annu Rev Biomed Eng* **2014**, 16, 247.
- [208] L. Moroni, T. Boland, J. A. Burdick, C. De Maria, B. Derby, G. Forgacs, J. Groll, Q. Li, J. Malda, V. A. Mironov, C. Mota, M. Nakamura, W. Shu, S. Takeuchi, T. B. F. Woodfield, T. Xu, J. J. Yoo, G. Vozzi, *Trends Biotechnol* **2018**, 36, 384.
- [209] G. Sworn, in *Handbook of hydrocolloids*, Elsevier **2009**, p. 204.
- [210] H. Grasdalen, O. Smidsrød, *Carbohydrate Polymers* **1987**, 7, 371.
- [211] G. Sworn, G. Sanderson, W. Gibson, *Food Hydrocolloids* **1995**, 9, 265.
- [212] I. Norton, D. Jarvis, T. Foster, *International Journal of Biological Macromolecules* **1999**, 26, 255.
- [213] U. D. o. Health, H. Services, *Washington, DC: US Food and Drug Administration* **2012**.

## Bibliography

---

- [214] D. Chimene, K. K. Lennox, R. R. Kaunas, A. K. Gaharwar, *Ann Biomed Eng* **2016**, 44, 2090.
- [215] O. Arlov, F. L. Aachmann, A. Sundan, T. Espevik, G. Skjak-Braek, *Biomacromolecules* **2014**, 15, 2744.
- [216] M. Kesti, C. Eberhardt, G. Pagliccia, D. Kenkel, D. Grande, A. Boss, M. Zenobi-Wong, *Advanced Functional Materials* **2015**, 25, 7406.
- [217] J. Malda, J. Groll, P. R. van Weeren, *Nature Reviews Rheumatology* **2019**, 1.
- [218] Y. S. Zhang, A. Arneri, S. Bersini, S.-R. Shin, K. Zhu, Z. Goli-Malekabadi, J. Aleman, C. Colosi, F. Busignani, V. Dell'Erba, C. Bishop, T. Shupe, D. Demarchi, M. Moretti, M. Rasponi, M. R. Dokmeci, A. Atala, A. Khademhosseini, *Biomaterials* **2016**, 110, 45.
- [219] T. Bhattacharjee, S. M. Zehnder, K. G. Rowe, S. Jain, R. M. Nixon, W. G. Sawyer, T. E. Angelini, **2015**, 1, e1500655.
- [220] A. Habib, V. Sathish, S. Mallik, B. Khoda, *Materials (Basel)* **2018**, 11.
- [221] S. A. Wilson, L. M. Cross, C. W. Peak, A. K. Gaharwar, *Acs Appl Mater Inter* **2017**, 9, 43449.
- [222] A. Lee, A. R. Hudson, D. J. Shiwerski, J. W. Tashman, T. J. Hinton, S. Yerneni, J. M. Bliley, P. G. Campbell, A. W. Feinberg, **2019**, 365, 482.
- [223] J. Yin, M. Yan, Y. Wang, J. Fu, H. Suo, *ACS Appl Mater Interfaces* **2018**, 10, 6849.
- [224] W. Liu, M. A. Heinrich, Y. Zhou, A. Akpek, N. Hu, X. Liu, X. Guan, Z. Zhong, X. Jin, A. Khademhosseini, Y. S. Zhang, *Adv Healthc Mater* **2017**, 6.
- [225] A. Hiller, K. Borchers, G. E. M. Tovar, A. Southan, *Additive Manufacturing* **2017**, 18, 136.
- [226] A. Hiller, K. Borchers, G. E. Tovar, A. Southan, *Additive Manufacturing* **2017**, 18, 136.
- [227] H. Onoe, T. Okitsu, A. Itou, M. Kato-Negishi, R. Gojo, D. Kiriya, K. Sato, S. Miura, S. Iwanaga, K. Kuribayashi-Shigetomi, Y. T. Matsunaga, Y. Shimoyama, S. Takeuchi, *Nature Materials* **2013**, 12, 584.
- [228] Y. Cheng, Y. Yu, F. Fu, J. Wang, L. Shang, Z. Gu, Y. Zhao, *Acs Appl Mater Inter* **2016**, 8, 1080.
- [229] L. P. B. Guerzoni, J. C. Rose, D. B. Gehlen, A. Jans, T. Haraszti, M. Wessling, A. J. C. Kuehne, L. De Laporte, **2019**, 15, 1900692.
- [230] J. C. Rose, M. Fölster, L. Kivilip, J. L. Gerardo-Nava, E. E. Jaekel, D. B. Gehlen, W. Rohlf, L. De Laporte, *Polymer Chemistry* **2019**.

- [231] F. J. O'Brien, B. A. Harley, I. V. Yannas, L. J. Gibson, *Biomaterials* **2005**, 26, 433.
- [232] J. Zeltinger, J. K. Sherwood, D. A. Graham, R. Mueller, L. G. Griffith, *Tissue Engineering* **2001**, 7, 557.
- [233] Q. L. Loh, C. Choong, *Tissue Eng Part B-Re* **2013**, 19, 485.
- [234] G. Huang, F. Li, X. Zhao, Y. Ma, Y. Li, M. Lin, G. Jin, T. J. Lu, G. M. Genin, F. Xu, *Chemical reviews* **2017**, 117, 12764.
- [235] M. Dinkgreve, J. Paredes, M. M. Denn, D. Bonn, *Journal of Non-Newtonian Fluid Mechanics* **2016**, 238, 233.
- [236] A. Ribeiro, M. M. Blokzijl, R. Levato, C. W. Visser, M. Castilho, W. E. Hennink, T. Vermonden, J. Malda, *Biofabrication* **2017**, 10, 014102.
- [237] T. G. Mezger, *The rheology handbook: for users of rotational and oscillatory rheometers*, Vincentz Network GmbH & Co KG, **2006**.
- [238] S. Xiao, T. Zhao, J. Wang, C. Wang, J. Du, L. Ying, J. Lin, C. Zhang, W. Hu, L. Wang, K. Xu, *Stem Cell Rev Rep* **2019**, 15, 664.
- [239] J. Li, B. Yang, Y. Qian, Q. Wang, R. Han, T. Hao, Y. Shu, Y. Zhang, F. Yao, C. Wang, *J Biomed Mater Res B Appl Biomater* **2015**, 103, 1498.
- [240] A. A. M. Shimojo, A. M. B. Pires, R. Lichy, M. H. A. Santana, *J Brazil Chem Soc* **2015**, 26, 506.
- [241] N. Nakajima, Y. Ikada, *Bioconjug Chem* **1995**, 6, 123.
- [242] P. Mohammadi, M. S. Toivonen, O. Ikkala, W. Wagermaier, M. B. Linder, *Sci Rep* **2017**, 7, 11860.
- [243] J. L. McWhirter, H. Noguchi, G. Gompper, *Proceedings of the National Academy of Sciences* **2009**, 106, 6039.
- [244] T. Papanthasiou, D. C. Guell, *Flow-induced alignment in composite materials*, Woodhead publishing, **1997**.
- [245] L. Moroni, J. A. Burdick, C. Highley, S. J. Lee, Y. Morimoto, S. Takeuchi, J. J. Yoo, *Nat Rev Mater* **2018**, 3, 21.
- [246] N. D. Evans, E. Gentleman, *Journal of Materials Chemistry B* **2014**, 2, 2345.
- [247] T. S. Karande, J. L. Ong, C. M. Agrawal, *Annals of biomedical engineering* **2004**, 32, 1728.
- [248] A. D. Murdoch, L. M. Grady, M. P. Ablett, T. Katopodi, R. S. Meadows, T. E. Hardingham, *Stem cells* **2007**, 25, 2786.
- [249] B. S. Kim, J.-S. Lee, G. Gao, D.-W. Cho, *Biofabrication* **2017**, 9, 025034.

## Bibliography

---

- [250] M. Zhou, J. Hou, Y. Li, S. Mou, Z. Wang, R. E. Horch, J. Sun, Q. Yuan, *Scientific reports* **2019**, 9, 1.
- [251] E. Wattrang, P. Wallgren, L. Fuxler, M. Lindersson, C. Fossum, *Veterinary immunology and immunopathology* **1997**, 56, 133.
- [252] C. Clarke, C. Short, E. Usenik, R. Rawls, *Research in veterinary science* **1989**, 47, 195.
- [253] B. Ermeling, E. Steffen, R. Fish, R. Hook Jr, *Laboratory animal science* **1992**, 42, 402.
- [254] R. A. Clarke, R. G. Pauley, R. S. Hill, J. H. Brauker, S. Sternberg, D. R. Boggs, Google Patents, 1994.
- [255] A. N. Morritt, S. K. Bortolotto, R. J. Dilley, X. Han, A. R. Kompa, D. McCombe, C. E. Wright, S. Itescu, J. A. Angus, W. A. Morrison, *Circulation* **2007**, 115, 353.
- [256] S. Hak, N. K. Reitan, O. Haraldseth, C. de Lange Davies, *Angiogenesis* **2010**, 13, 113.
- [257] J. Hall, B. Wishaw, R. Stokes, *Journal of the American Chemical Society* **1953**, 75, 1556.
- [258] R. Trindade, T. Albrektsson, P. Tengvall, A. Wennerberg, *Clinical implant dentistry and related research* **2016**, 18, 192.
- [259] J. M. Anderson, A. Rodriguez, D. T. Chang, presented at Seminars in immunology **2008**.
- [260] C. Stewart, B. Akhavan, S. G. Wise, M. M. Bilek, *Progress in Materials Science* **2019**, 100588.
- [261] S. B. Goodman, Z. Yao, M. Keeney, F. Yang, *Biomaterials* **2013**, 34, 3174.
- [262] M. B. Gorbet, M. V. Sefton, *Biomaterials* **2004**, 25, 5681.
- [263] Y. Su, C. Luo, Z. Zhang, H. Hermawan, D. Zhu, J. Huang, Y. Liang, G. Li, L. Ren, *Journal of the mechanical behavior of biomedical materials* **2018**, 77, 90.
- [264] R. A. Gittens, T. McLachlan, R. Olivares-Navarrete, Y. Cai, S. Berner, R. Tannenbaum, Z. Schwartz, K. H. Sandhage, B. D. Boyan, *Biomaterials* **2011**, 32, 3395.
- [265] J. E. Davies, E. Ajami, R. Moineddin, V. C. Mendes, *Biomaterials* **2013**, 34, 3535.
- [266] K. Rechendorff, M. B. Hovgaard, M. Foss, V. Zhdanov, F. Besenbacher, *Langmuir* **2006**, 22, 10885.
- [267] E. M. Blanco, M. A. Horton, P. Mesquida, *Langmuir* **2008**, 24, 2284.
- [268] G. Morgese, E. Cavalli, J. G. Rosenboom, M. Zenobi-Wong, E. M. Benetti, *Angewandte Chemie International Edition* **2018**, 57, 1621.



- [269] B. Zappone, G. W. Greene, E. Oroudjev, G. D. Jay, J. N. Israelachvili, *Langmuir* **2008**, 24, 1495.
- [270] P. Sengupta, B. L. Prasad, *Regenerative Engineering and Translational Medicine* **2018**, 4, 75.
- [271] V. D'Britto, H. Kapse, H. Babrekar, A. Prabhune, S. Bhoraskar, V. Premnath, B. Prasad, *Nanoscale* **2011**, 3, 2957.
- [272] M. Yamaguchi, T. Shinbo, T. Kanamori, P.-c. Wang, M. Niwa, H. Kawakami, S. Nagaoka, K. Hirakawa, M. Kamiya, *Journal of Artificial Organs* **2004**, 7, 187.
- [273] J. E. Babensee, J. M. Anderson, L. V. McIntire, A. G. Mikos, *Advanced drug delivery reviews* **1998**, 33, 111.
- [274] S. Franz, S. Rammelt, D. Scharnweber, J. C. Simon, *Biomaterials* **2011**, 32, 6692.
- [275] A. Crupi, A. Costa, A. Tarnok, S. Melzer, L. Teodori, *European journal of immunology* **2015**, 45, 3222.
- [276] M. Mumme, A. Wixmerten, S. Miot, A. Barbero, A. Kaempfen, F. Saxer, S. Gehmert, A. Krieg, D. J. Schaefer, M. Jakob, *Swiss Medical Weekly* **2019**, 149.
- [277] J. R. Yu, J. Navarro, J. C. Coburn, B. Mahadik, J. Molnar, J. H. Holmes IV, A. J. Nam, J. P. Fisher, *Advanced healthcare materials* **2019**, 8, 1801471.
- [278] E. S. Fioretta, L. Von Boehmer, S. E. Motta, V. Lintas, S. P. Hoerstrup, M. Y. Emmert, *Experimental gerontology* **2019**, 117, 1.
- [279] R. Pilliar, *Clinical orthopaedics and related research* **1983**, 42.
- [280] R. Tejero, E. Anitua, G. Orive, *Progress in Polymer Science* **2014**, 39, 1406.
- [281] K. Zhang, W. Yan, R. Simič, E. M. Benetti, N. D. Spencer, *ACS Applied Materials & Interfaces* **2020**.
- [282] Y. Lin, L. Wang, J. Zhou, L. Ye, H. Hu, Z. Luo, L. Zhou, *Polymer* **2019**, 162, 80.
- [283] J. Yeow, R. Chapman, A. J. Gormley, C. Boyer, *Chemical Society Reviews* **2018**, 47, 4357.
- [284] S. Shanmugam, J. Xu, C. Boyer, *Macromolecules* **2014**, 47, 4930.
- [285] K. Matyjaszewski, H. Dong, W. Jakubowski, J. Pietrasik, A. Kusumo, *Langmuir* **2007**, 23, 4528.
- [286] L. A. Navarro, A. E. Enciso, K. Matyjaszewski, S. Zauscher, *Journal of the American Chemical Society* **2019**, 141, 3100.
- [287] W. Yan, M. Fantin, S. Ramakrishna, N. D. Spencer, K. Matyjaszewski, E. M. Benetti, *ACS applied materials & interfaces* **2019**, 11, 27470.

## Bibliography

---

- [288] M. Divandari, J. Pollard, E. Dehghani, N. Bruns, E. M. Benetti, *Biomacromolecules* **2017**, 18, 4261.
- [289] M. Fantin, S. N. Ramakrishna, J. Yan, W. Yan, M. Divandari, N. D. Spencer, K. Matyjaszewski, E. M. Benetti, *Macromolecules* **2018**, 51, 6825.
- [290] Y. Wang, Y. Zhang, B. Parker, K. Matyjaszewski, *Macromolecules* **2011**, 44, 4022.
- [291] Y. Wang, K. Matyjaszewski, *Macromolecules* **2011**, 44, 1226.
- [292] M. Teodorescu, S. G. Gaynor, K. Matyjaszewski, *Macromolecules* **2000**, 33, 2335.
- [293] D. Zhou, X. Gao, W.-j. Wang, S. Zhu, *Macromolecules* **2012**, 45, 1198.
- [294] R. Lanigan, T. Yamarik, *International journal of toxicology* **2002**, 21, 95.
- [295] H. Bergenudd, M. Jonsson, D. Nyström, E. Malmström, *Journal of Molecular Catalysis A: Chemical* **2009**, 306, 69.
- [296] G. Wang, M. Lu, H. Wu, *Polymer bulletin* **2012**, 69, 417.
- [297] G. Coullerez, A. Carlmark, E. Malmström, M. Jonsson, *The Journal of Physical Chemistry A* **2004**, 108, 7129.
- [298] D. M. Jones, W. T. Huck, *Advanced Materials* **2001**, 13, 1256.
- [299] D. Konkolewicz, P. Krysz, J. R. Góis, P. c. V. Mendonça, M. Zhong, Y. Wang, A. Gennaro, A. A. Isse, M. Fantin, K. Matyjaszewski, *Macromolecules* **2014**, 47, 560.
- [300] R. R. Patil, S. Turgman-Cohen, J. i. Stogel, D. Kiserow, J. Genzer, *ACS Macro Letters* **2015**, 4, 251.
- [301] E. M. Benetti, C. Kang, J. Mandal, M. Divandari, N. D. Spencer, *Macromolecules* **2017**, 50, 5711.
- [302] C. Kang, S. N. Ramakrishna, A. Nelson, C. V. Cremmel, H. Vom Stein, N. D. Spencer, L. Isa, E. M. Benetti, *Nanoscale* **2015**, 7, 13017.
- [303] S. T. Milner, T. Witten, M. Cates, *Macromolecules* **1988**, 21, 2610.
- [304] Y. Chang, Y. J. Shih, C. J. Lai, H. H. Kung, S. Jiang, *Advanced Functional Materials* **2013**, 23, 1100.
- [305] Z. Zhang, T. Chao, S. Chen, S. Jiang, *Langmuir* **2006**, 22, 10072.
- [306] S. Jiang, Z. Cao, *Advanced materials* **2010**, 22, 920.
- [307] W. Feng, J. L. Brash, S. Zhu, *Biomaterials* **2006**, 27, 847.
- [308] B.-H. Luo, C. V. Carman, T. A. Springer, *Annu. Rev. Immunol.* **2007**, 25, 619.
- [309] B. M. Gumbiner, *Nature reviews Molecular cell biology* **2005**, 6, 622.

- 
- [310] R. E. Marcus, L. Sokoloff, *Arthritis & Rheumatism: Official Journal of the American College of Rheumatology* **1973**, 16, 646.
- [311] T. Zhang, Y. Du, F. Müller, I. Amin, R. Jordan, *Polymer Chemistry* **2015**, 6, 2726.
- [312] T. Zhang, Y. Du, J. Kalbacova, R. Schubel, R. D. Rodriguez, T. Chen, D. R. Zahn, R. Jordan, *Polymer Chemistry* **2015**, 6, 8176.
- [313] E. S. Dehghani, Y. Du, T. Zhang, S. N. Ramakrishna, N. D. Spencer, R. Jordan, E. M. Benetti, *Macromolecules* **2017**, 50, 2436.
- [314] Y. Che, T. Zhang, Y. Du, I. Amin, C. Marschelke, R. Jordan, *Angewandte Chemie International Edition* **2018**, 57, 16380.
- [315] T. Zhang, E. M. Benetti, R. Jordan, ACS Publications, 2019.
- [316] W. Yan, M. Fantin, N. D. Spencer, K. Matyjaszewski, E. M. Benetti, *ACS Macro Letters* **2019**, 8, 865.
- [317] J. Y. Kim, B. S. Lee, J. Choi, B. J. Kim, J. Y. Choi, S. M. Kang, S. H. Yang, I. S. Choi, *Angewandte Chemie International Edition* **2016**, 55, 15306.
- [318] G. Sprague, J. Thorner, *The Molecular and Cellular Biology of the Yeast Saccharomyces Gene Expression* **1992**, 2, 657.



## Acknowledgments

The end of my time as a PhD student also marks the end of an important chapter of my life. It is time to look back and acknowledge the help and support I received during this period. I want to thank everyone directly or indirectly involved in helping me complete this four-year-long project. I want to thank all my fellow researchers and colleges for their feedback, time and hands-on support at various occasions. All the good talks and fun times in and around the lab, work and not-work related trips and adventures in Switzerland and all around the world. Even though not everyone can be listed here, I want to mention some people that played a special role in my PhD directly.

I want to express my gratitude to:

Marcy, for giving me the opportunity to work as a PhD candidate in your lab. For making it possible to attend many conferences and events all over the world. For leaving me the freedom to explore the world of hydrogels and find my own projects. Without you I would have not been the scientist I am today.

Martin, for being in my committee and for always finding some time and the good mood you spread around. For being there and supportive when I needed it and the good advices in difficult times. For your honest suggestions and giving me insight into the life of a supervisor.

Steffen, for being in my committee and your helpful suggestions. For your open and clear communication and the opportunity to see my own work from a different perspective. Your cheerful character made the last phase of my PhD easier.

Eddy and Amine, for the fruitful collaboration and an excursion into real chemistry. For demonstrating me how fast things can progress. For being demanding but always contributing your own share.

The whole TEB lab, for being great colleagues and good times in and around the lab.

The ISG D-HEST, for the little excursions into problems that can be solved with pure logic (mostly). Especially Jochen and Jean-Claude for the help with getting new things working and the support when nobody knew the answer.

Anina, for great talks, on and off-topic, during many occasions that helped so much in getting a clear perspective.

Philipp and Alvar, for the help with tricky polymer spectra and showing me Switzerland's biggest magnet field.

Michelle, for fun collaborations and hilarious meetings at the hospital and campus.

Dominic, for your inspiring eagerness and dedication to science.

Luca, for the occasional but deep conversations.

Ricardo, for having completely different approaches but still being open to help.

Yann, for being a great student and your harmonic way of just doing things.

Florian, for all the music and absurdities.

Philipp, for your willingness to help at every time of the day (except in the mornings). The good times we had on travels and conferences. The many occasions in which drinks were served and the party was starting.

Ingrid, for the great times at various events and Boardgame sessions.

Sarah (Ara), for the spontaneous and chaotic visits into my life. For living in a completely different world but always trying to drag me in and let me participate. For also being respectful and appreciative of my ideology.

Felix, for being supportive and understanding of the highs and lows of the PhD. For the many evenings via skype and for always listening and giving honest opinions, even when they are antithetic to what I want to hear.

Nina, for all the important memories we share and the trips and adventures around the world (mostly Europe, though ;-).

Die Tübinger: Hannah, Jan, Vicky und Daniel, für die vielen spontanen Treffen und guten Zeiten.

Jana und Frank, für die viele schöne Zeit die wir zusammen verbracht haben. Dafür, dass ihr immer Verständnis für unser chaotisches Leben hattet und wir an eurem teilhaben durften.

Meine Schwester Sarah, für die vielen Besuche und Karten. Dafür, dass du dich immer über Anrufe freust auch wenn du nie Zeit zu telefonieren hast. Für die nette Gastfreundschaft auf Reisen und die schöne Zeit die wir zusammen hatten.

Mein Bruder Fabian, für tolle Zeiten im hohen Norden in denen der PhD nicht wichtig war. Für deine Neugierde und den Drang wirklich zu verstehen was ich da mache.

Meine Eltern Gabi und Wolfgang, für die Unterstützung und das Verständnis in schwierigen Zeiten. Für die vielen Fahrten und das leckere Essen. Dafür, dass ihr eine gute Balance gefunden habt für ein unaufdringliches Kümmern. Dafür das ihr immer an mich geglaubt habt und auf meiner Seite wart.

Martine, my love, for being the best and cutest support there is. 🐱 For all the adventures around the world, all those special weekends, your understanding and the countless flights. For the walk on the wild sides, the ocean breeze, all the things I would have never dared to do without you, your willingness to accept me as I am and your courage to explore worlds. For reading stories, cooking lasagna (and other delicacies), your trust, faith, loyalty and so much more. Listing everything would fill a thesis of its own. <3





